Progress in Materials Science 151 (2025) 101421

Contents lists available at ScienceDirect

Progress in Materials Science

journal homepage: www.elsevier.com/locate/pmatsci

Electrorheological fluids: A living review

Lenka Munteanu [a], Andrei Munteanu [a], Michal Sedlacik [a,b,*]

[a] Centre of Polymer Systems, University Institute, Tomas Bata University in Zlín, Trida T. Bati 5678, 760 01 Zlín, Czech Republic
[b] Department of Production Engineering, Faculty of Technology, Tomas Bata University in Zlín, Vavreckova 275, 760 01 Zlín, Czech Republic

A B S T R A C T

Electrorheological (ER) materials have attracted considerable attention over the decades, owning to their unique ability to rapidly change their rheological properties upon exposure to an electric field. Such feature enables these materials in numerous applications. This paper reviews the general aspects of electrorheological fluids (ERFs), and introduces the most often used ER materials. Liquid carriers are briefly compared and numerous dispersed dielectric particles are represented from both, inorganic and organic categories, along with a wide range of composites. A selection of reviewed ERF particles characteristics (their type, geometry, size, conductivity and ER efficiency) is summarized in tables. Advantages and drawbacks of state-of-the-art ERFs are outlined, along with their general requirements. Additionally, an open living online document is attached and meant to keep a summary of the key characteristics of ER particles covered in future ERF-focused publications and create a rich online resource for the scientific community over time. Fellow researchers are therefore welcomed to contact the authors for their published data to be included (the open living table is to be updated regularly).

1. Introduction

Electrorheological (ER) systems are smart materials with an ability to reversibly and instantly change their rheological properties when exposed to an electric field. Such electrorheological fluids (ERFs) consist of polarizable particles (dispersed phase) and non-conductive liquid carrier. The particles are polarized upon the exposure to the electric field, consequently they orient into chain-like structures, as visualized in Fig. 1a.

In short, the on-field structure formation the interactions between the particles lead to an increased yield stress and alters the other rheological properties with the relative increase of the shear stress/viscosity being referred to as the ER effect [1]. In publications, the most common method to characterize ERFs is usually demonstrated firstly through rotational tests through flow curves, depicting the shear stress, or viscosity, over shear rate, as illustrated in Fig. 1b.

In particular, when the electric field is not activated (also referred as the off-field state) the specific ERF suspension usually exhibits nearly a Newtonian behaviour; however, in reality ERFs can also exhibit shear thinning or shear thickening behaviour, as the shear stress increases proportionally to increasing shear rate. When the electric field is applied (the so-called on-field state), the shear stress value steeply increases, with the material becoming a yield stress fluid. The shear stress can further climb with increasing the higher electric field as depicted in Fig. 1b however, eventually the particles are saturated and the stress is not increased anymore. A number of models were presented over time to describe the ER behaviour of fluids [2], such as Bingham model [3], Cho, Choi, and Jhon model [4], Seo-Seo model [5], and more; however, the details of these exceed the framework of this particular review. Secondly, when the electric field is removed the reversibility of the ERF instantly transitions back to the off-state which effect is often shown during a step-wise increase of the electric field over time at constant shear rate as shown in Fig. 1c. Finally, oscillatory measurements are often used

* Corresponding author at: Centre of Polymer Systems, University Institute, Tomas Bata University in Zlín, Trida T. Bati 5678, 760 01 Zlín, Czech Republic.
E-mail address: msedlacik@utb.cz (M. Sedlacik).

https://doi.org/10.1016/j.pmatsci.2024.101421
Received 14 June 2024; Received in revised form 28 November 2024; Accepted 7 December 2024
Available online 11 December 2024

to show the data of storage and loss moduli with varying frequencies for further complement the rheological characterization (Fig. 1d). Usually, during the off-state the ERF will show a Maxwell behaviour while in the on-state both moduli are usually being increased and constant throughout the entire experimental window.

Ever since the first recognition of these smart fluids in 1949 by Winslow [1], the research has been pushing the ER systems forward; exploring possibilities of different materials, searching for specific properties for individual applications, and pursuing ways of overcoming their drawbacks. In comparison to hydraulic or electric devices, the ER effect-based equipment performs faster, safer, and often more efficiently.

A brief attention should be paid to ER-based applications. It should be considered that for extensive use of ERFs during the on-state, materials able to operate in lower power consumption (which usually means lower fields) with high enough ER efficiency are preferred. Firstly, the most notorious are electrically controlled devices which transform the electrical to a mechanical energy such as dampers, valves, absorbers, clutches, brakes, actuators [6–13]. Tactile display and haptic devices based on ER technology were also proposed [14,15]. In terms of vibration damping, ERFs may potentially offer their potential as seismic control systems [16,17]. Electrorheological fluids are further promising in the field of soft-robotics, small-scale robots, or designs of robotic arms, these devices are essential for instance in the space industry; however, their use is not limited to this particular field [18,19]. Hwang et al. [20] proposed a haptic master device meant to be applied to a robot-assisted surgery. The authors also empathized the device controllability of the repulsive forces and accuracy of the cutting device. Electrorheological actuator for endoscopy was also proposed [21]. In terms of mobility aid and rehabilitation, a few devices were proposed, such as an actuator-based soft, lightweight gel spats with variable stiffness for walking assistance [22] or a rehabilitation device with incorporated ER clutches, which is expected by the authors to serve as a more affordable through the use of ER technology in comparison to the similar concurrent medical aids [23]. Next, electro-rheological polishing has gained a note-worthy attention, as a mixture of ER particles and abrasive particles shows significant polishing performance. Additionally, the force acting on the abrasive particles gets higher with the increasing ER effect, improving the removal rate and efficiency [24,25]. Furthermore, ER-polishing device was proposed with ability to both, polish and grind on a micron scale [26]. Another notable field benefiting from ER technology is oil transport. In particular, ERFs enable a more efficient cold flow and so the transportation of crude oils [27,28]. Lastly, a not very common use of ERFs includes the increasement of the conductivity during

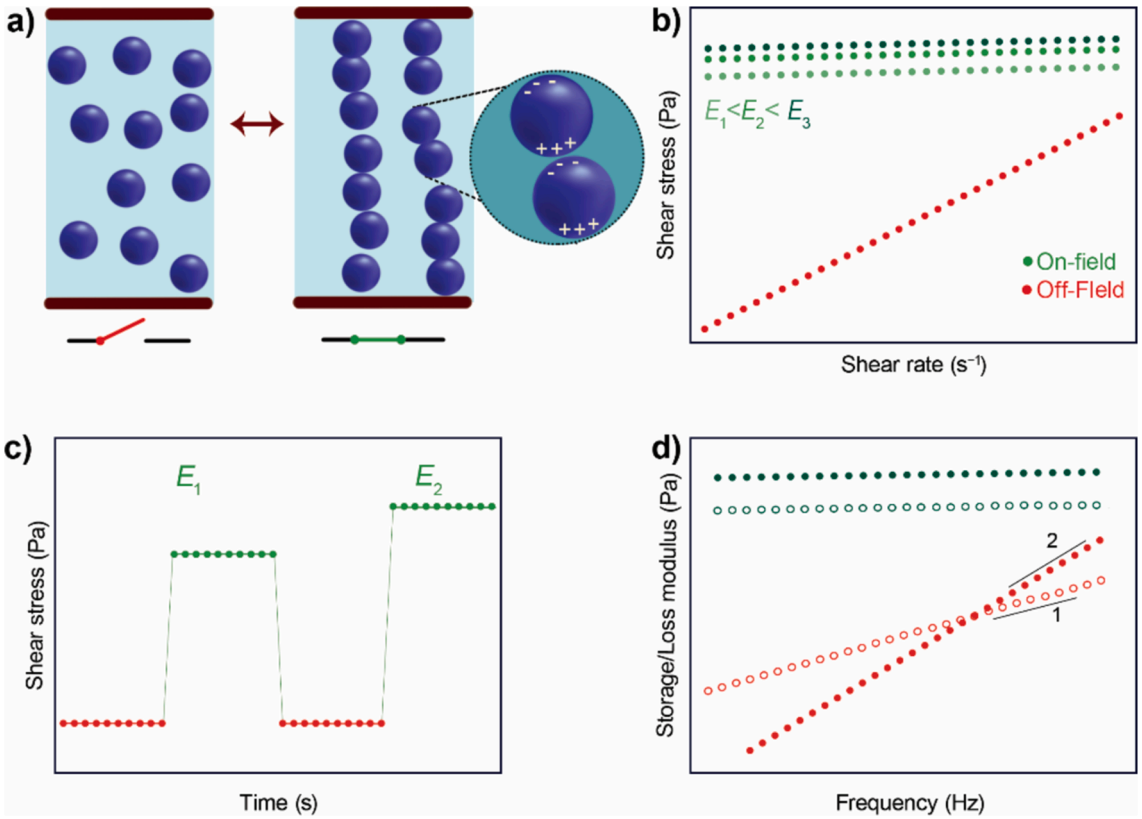

Fig. 1. a) Demonstration of the erf during the on- and off-state. Upon the field activation, the particles become polarized and orient into chain-like structure (right) while a random distribution is generated when the field is deactivated (left). b) Typical flow curve for a Newtonian based ERF during the off- (red points) and on-state (green points) for increasing fields. c) Typical step-wise test with the electric field activated periodically while being increased at a constant shear rate. Red points correspond to the off-state while the green points represent the on-state. d) Typical frequency sweep in a log–log scale for an ERF with the closed symbols representing the storage modulus G' and open symbols loss modulus G''. Red points represent the ERF during the off-state and the green data representing the on-state, with the off-state slope indicated by the numbers 1 and 2.

the on-state [29].

As such, ERFs have received a considerable attention, as can be seen in Fig. 2. The graph presents the amount of scientific publication entries per keyword 'electrorheolog*' in the Web of Science database for the last three decades [30]. As presented, even though the main boom of the ER topic was around the first decade of the 21th century (with the maximum peak of 351 entries in 2005), the amount of research is up to date active, with at least 100 new per year.

However, to fully commercialize the ERFs for wider applications in the industry, particular requirements should be met, which sometimes bring certain challenges.

Firstly, a high ER efficiency and ER performance; this includes ideally low viscosity in the off-state (when the electrical field is inactive), and high in the on-state (active electrical field) paired with an increased yield stress. The ER efficiency *e* (relative to a given shear rate value) is generally defined as:

$$\mathrm{e} = \frac{\tau_\mathrm{e} - \tau_0}{\tau_0} \mathrm{or} \frac{\eta_\mathrm{e} - \eta_0}{\eta_0} \tag{1}$$

where τ_e and τ_0 represent the values of shear stress in the on-state and off-state, respectively. Likewise, η_e is the viscosity in the on-state and η_0 stand for the off-state viscosity.

Secondly, a good sedimentation stability is required as the ERF should stay as homogenized as possible without agglomerating. Other key parameters include proper chemical stability, wide range of working temperature, long life-time, being non-toxic, non-corrosive and in a non-abrasive nature. Furthermore, the reversible change between the on- and off-state should be possible in a short experimental window (milliseconds). In addition, the conductivity of the dispersed phase should be in an appropriate range, often recommended between $10^{-6} - 10^{-9}$ S m^{-1} [31]. Although such values may seem minor (especially if compared to conductor materials, such as copper), this range is sufficient to enable the ER effect, while not causing short circuit or otherwise endangering the ER device.

In general, doping can be applied as a way to tailor the conductivity into the ER-convenient range and so it is often used in regards to many types of ER particles. Conductivity contributes to the electrostatic forces between the particles consequently affecting the toughness of the on-field formed chain-like structures [32]. Thus, the doping can increase the amount of charge carriers, consequently effectively increasing the structures' toughness and the material's conductivity when the target electric field intensity is applied [33] (however a reasonable balance is needed, as too high amount of leaking currents may result in a short circuit). As such, doping improves ER performance as well as dielectric and electric properties of the material [34].

Despite the uniqueness and potential of ERFs, they also possess certain drawbacks that should be addressed. Following the above-mentioned requirements, in reality the ER efficiency used to be often rather low in proportion to the required resources. For that reason, enhancement of ER efficiency has received considerable attention in the recent years (as can be seen in detail in numerous later-mentioned studies). Furthermore, the long–term sedimentation stability tends to decline which hinders the ERF's performance (decreased particle mobility when creating the chain-like structures in a field). However, several studies have addressed this issue through various means, such as through lowering the particles density through porous structure [35], or hollowing particles [36–39], and other modifications of material and morphology [40] (described in detail in the 'Particle morphology' section). Last but not least, the necessity to generate a medium electrical field (mostly ranging between $0.5 - 3$ kV mm^{-1} or higher) may limit the options for specific applications and possibly require a costly energy consumption, depending on the effective value of electrical field generated.

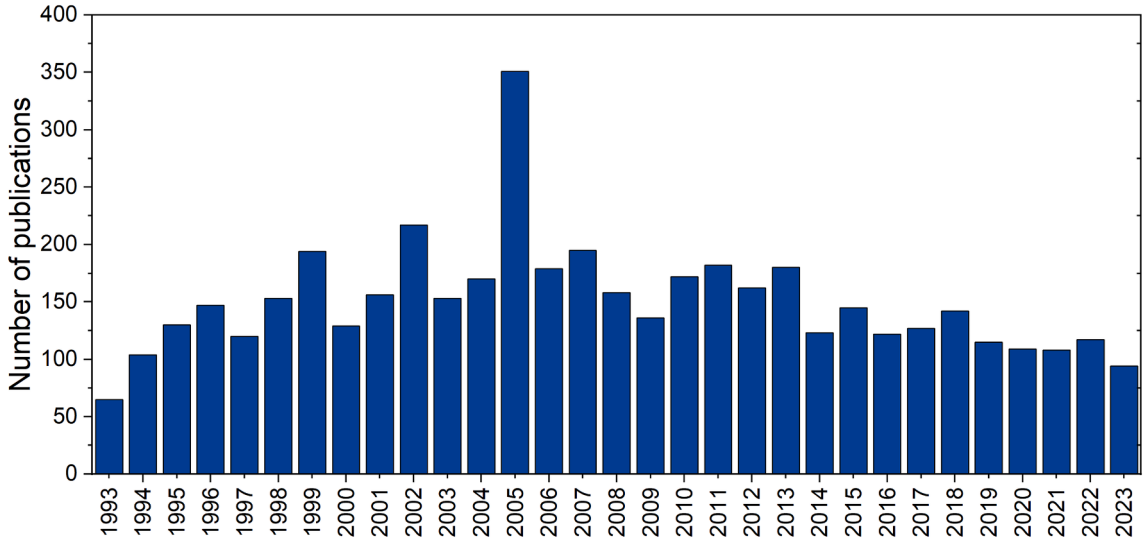

Fig. 2. Visualization of all types of scientific publications available by a keyword 'electrorheolog*' in the Web of Science database published between 1993 and 2023 [30].

For the reasons above, most of the up-to-date research in this field aims to either improve the ER properties and efficiency or to address their above-mentioned weak points. Consequently, a wide range of materials has been researched. This review will explore both common and unique materials used in ERFs and will address their viability.

2. Varieties of the ER effect

In total, three types of ERFs have been reported so far. Firstly, the most researched and applied type, so far, is the positive ER effect, meaning the rheological properties of the fluid are enhanced by the influence of an external electrical field. Secondly, the less known negative ER effect refers to ERFs whose properties diminish upon the application of the electric field [41]. Finally, photo-ER effect should be mentioned. Although limited research has been concluded towards this effect so far, UV illumination can contribute to enhancing the ER effect in both, positive or negative directions [42,43]. Kelbysheva et al. [44] introduced a device to study simultaneously photo effect in an active electrical field. In particular, ERF samples of colloidal polyimide in silicone oil and other carriers were investigated. Minor changes in shear stress values were visible for both polyimide samples, the first containing SO_3H groups showed gradient decrease in shear stress over UV radiation time, the other, possessing SO_3Na groups, on the other hand showed increase after 30 min of radiation and then gradually dropped.

As noted, the negative ERFs have not seen as much research spotlight as their positive counter-part, thus they are so far not as explored. Certain proposed explanations of achieving this effect are expressed. First theory implies that the solid particles may have a tendency to segregate and form a zone of high concentration of particles, and then second zone which is nearly free of particles, resulting in decreasing the viscosity of the latter [41]. Second explanation suggests that the polarized particles may migrate towards the electrodes, thus leading to a similar zone-separation [45]. In contrast, the polarized positive ERF particles align into chain-like structures resulting in an increased viscosity, as was afore-mentioned. The resulting changes in particle motion is represented in Fig. 3, as a comparison between the positive and negative ER effects. However, the main limitation of negative ERFs is a long recovery time after removal of the electric field, resulting in a prolonged retaining of low viscosity. Secondly, the changes between the on- and off-state in the rheological properties are often not significant enough for wider applications, concurrently. Nevertheless, they may be convenient in the industry if a controllable decrease of the viscosity or nearly Newtonian behaviour is desired.

Reports of negative ERFs first started to emerge towards the end of 20th century [41,46]. A negative ER effect was also reported in swollen silicone/$BaTiO_3$ gels [47,48]. Furthermore, Ko et al. [49] observing ER effect of alginic acid and alginate salt-based systems reported the first bio-molecules-based negative ERF. In particular, the study indicates that the type of ER effect is depended on the salt type. Particularly, calcium alginate-based sample showed a negative ER effect while other studied alginates showed its counterpart.

A number of studies reported possibilities of reversing the two types of ER effect. Such transitions offer a new insight into controlling the desired viscosity which might become part of specific applications. Plachy et al. [50] reported a transition of a negative ER behaviour based on graphitic carbon nitride suspended in silicone oil to the positive ER as a result of copper ions doping. Other studies were focused on using case-specific fillers leading to changes of the ER effect. For instance, Agafonov et al. [51] reported an occurring ER effect change of tungsten oxide suspension, from positive to negative. This was caused by changing the type of adsorbed surfactant of solid inorganic filler particles. Similarly, Cetin et al. [52] studied an ERF with colemanite and polyindene/colemanite composites and observed that an addition of Triton-X and glycerol surfactants converts the negative ER effect to positive while enhancing the ER effect. Ramos-Tejada et al. [53] focused primarily on goethite particles in silicone oil reaching similar result by an addition of aerosol particles. Do et al. [54] used an electromigration technique to design negative ER materials and aimed to expand their possibilities of manufacture. Their research demonstrated that bare polyacrylonitrile (PAN) particles modified with amino groups on their surface along with a coupling reaction of other polymers led to both positive and negative ER effect, depending on the coupled polymer. Shortly after, the same group reported that, aside other factors, the operating temperature and thermal treatment of the examined PAN particles also affect the ER effect. In particular, while bare PAN particles showed positive ER behaviour, the negative ER effect was apparent for those particles which were heat-treated (in a temperature range from 100 to 250 °C). The negative ER effect was likely a result of an increased crystallinity of the treated particles [55]. And finally, a recent study by Yang et al. [56] focused on an a negative

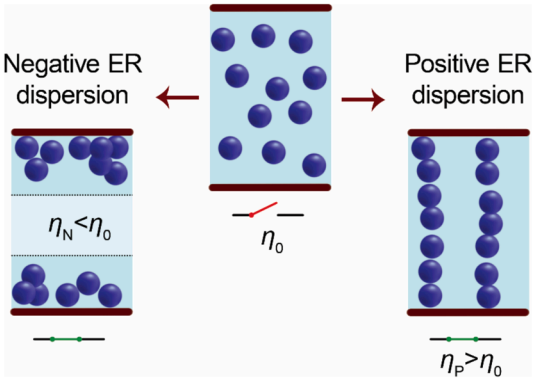

Fig. 3. Schematic comparison of particle migration in negative and positive ERFs.

ER application in a dual-mode switching electrophoretic display device. The group tested fumed silica particles as electronic ink at various concentrations with an addition of 0.6 wt% polyisobutylene as a thickener. The electronic ink performance was also demonstrated on a fabricated prototype of flexible e-paper film. As mentioned above, shear stress and viscosity are not the only properties being increased when an electric field is applied. Bica et al. [57,58] used ERFs to tune the conductivity and capacitance of their fluid using electric and/or magnetic fields. In short, when an electric field is applied, the particles arrange in chain-like structures allowing the current to pass easier through the neighbouring particles. The group has studied several types of ERFs and described the mechanism in detail together with the theory behind it and modelling this behaviour.

3. Liquid carrier

The liquid carrier is a substance in which the dispersed phase of ERFs is distributed. Although liquids are generally used as medium carriers for ER fluids, it is note-worthy that solid substances are also regularly used. Such examples would include ER elastomers which eliminate the sedimentation problem; however, their ER efficiency is orders of magnitude lower, depending on the modulus difference of the carriers, matrix composition, and particle concentration [59–61]. In terms of usual ERFs, the carrier is a non-conductive liquid of low viscosity and low dielectric constant, possessing good chemical and thermal stability in a wide range of working temperatures. Furthermore, the carrier should be non-toxic, have a relatively appropriate density to the utilized dispersed phase material, and low moisture absorption [45]. Last but not least, a low viscosity can be efficient in enabling particles movement and, consequently, the chain-like structure formation, thus leading to an increased ER effect. However, this should not be generalized, as it may be affected by a specific dispersed phase [62]. It is also noteworthy that Roman et al. [62] observed a rather apparent viscosity hysteresis of a polyaniline (PANI)-graphene sample in 20 cSt silicone oil after the field was repeatedly deactivated, suggesting the reversibility of the ER behaviour can be affected. The viscosity of the carrier also affects the sedimentation stability of the ERF. If the viscosity is too low, the ERF particles could be prone to sediment faster [63] (as can be seen in Fig. 4a) [64]. In summary, the performance and properties of ER systems are influenced by the liquid carrier, as such it can be attention-worthy to consider various carriers when pushing towards

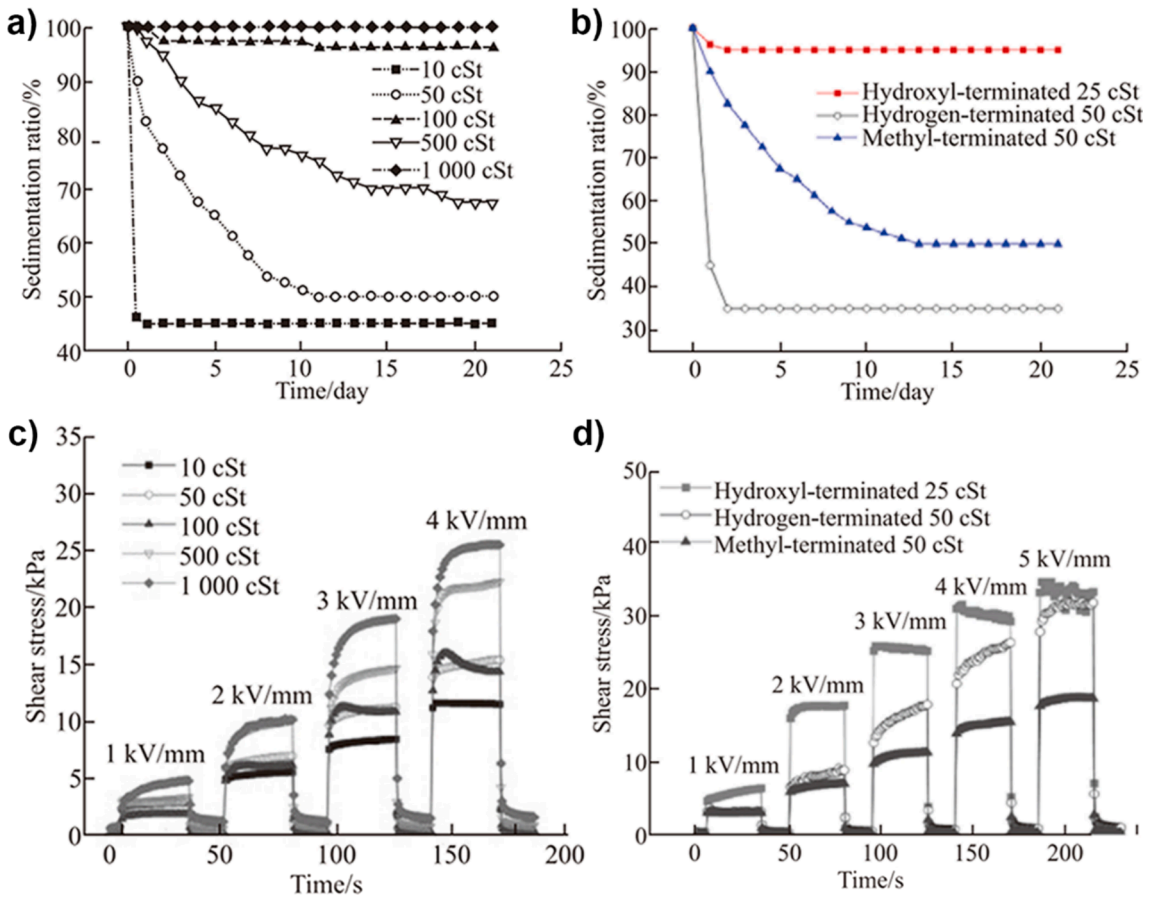

Fig. 4. Ma and Dong [64]: Assessment of various liquid carries of ERF based on modified TiO_2 particles. Sedimentation evaluation of the ERFs with dimethyl silicone oil as liquid carrier of various viscosities (a) and their ER performance under square voltage pulses (c). Sedimentation ratio of ERFs containing silicone oils with different terminal groups (b) and their ER performance under square voltage pulses (d). Re-printed from Ref. [64] with a permission of SAGE Publications.

the limits of a particular ERF.

Concurrently, a considerable range of mediums fitting into the abovementioned conditions is available, but mostly silicone or mineral oils are used, as they showcase good oxidative and thermal stability [65]. Hong et al. [66] confirmed the superiority of silicone oil over corn and soybean oils in regards to yield stress. Furthermore, Ma and Dong [64] evaluated the behaviour of various silicone oil carriers of different viscosities and terminal groups on ER performance of oxalate group-modified TiO_2 ERFs in DC field. In particular, five kinds of dimethyl silicone oil with different kinematic viscosities (10, 50, 100, 500, and 1000 cSt) were compared, as well as three types of silicone oil with different terminal groups (hydroxyl 25 cSt, hydrogen 50 cSt, and methyl 50 cSt, as presented in Fig. 4. The Figure shows the data differences in sedimentation stability of the ERF samples (a, b) and their shear stress values in the field, ranging from 0 to 5 kV mm^{-1} (c, d). As can be seen, the sample dispersed in hydroxyl-terminated group showed the highest ER effect, although comparable with the hydrogen-terminated alternative in higher fields, and the highest sedimentation stability ratio. Furthermore, the study also highlights its higher ER efficiency, but also the current leakage density. However, it should be reminded that the sedimentation is influenced by other properties and factors connected to the dispersed phase. At first sight, the numerical difference in the ER effect might not seem as too significant, but it may be valuable addition to consider when designing an ERF with tailored properties.

Additionally, numerous plant-based oils have been tested as they carry particular advantages, namely, bio-degradability and biocompatibility. As such, these are important for eco-friendly applications, and potentially in applications related to the medical field. For instance, Davies at al. [67] compared ER response of microcrystalline cellulose in oils suitable for controllable drug delivery system at low electric field below 1 kV mm^{-1}, namely almond, apricot, peanut, safflower, sesame seed, and soybean oils. The study concluded that little difference in the yield stress value was observed between the properties of almond oil in comparison to silicone oil. Similarly, an evaluation of vegetable oils (olive, canola, grapeseed, and soybean oil) was concluded by Park et al. [68] in regards to ER behaviour of Mg-doped silica/titania ERFs. The study proved that, out of the above-selected oils, the dispersion in olive oil reached the highest shear stress in an active field. Furthermore, the authors confirmed an overall good sedimentation stability of dispersed particles in all tested oils, with canola oil showing slightly inferior results to the rest.

Similarly, Hong and Wen [69], evaluated ER samples based on urea-coated barium titanyl oxalate particles in various liquid media. In total, six different kinds of carrier were tested (dimethyl terminated silicone oil, hydrogenated silicone oil, white mineral oil, liquid

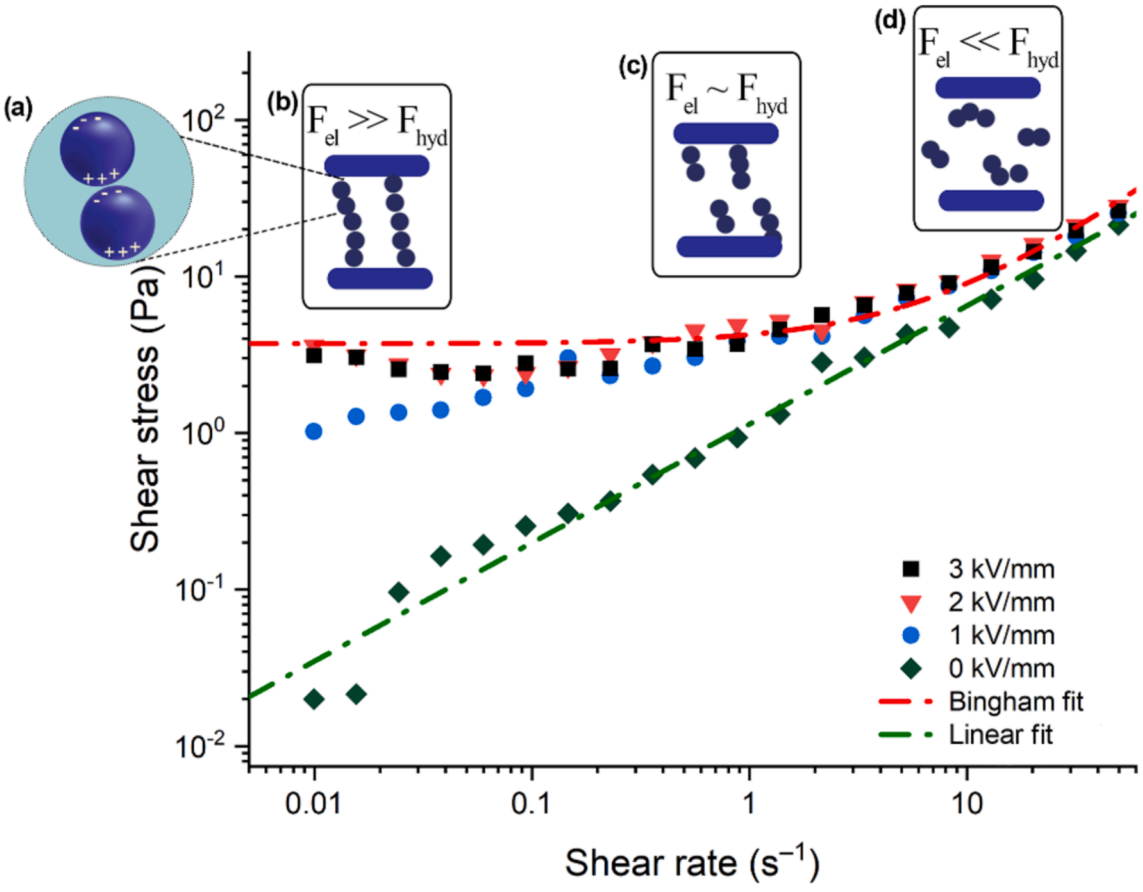

Fig. 5. Sample flow curve, adjusted from a reference [88]. Polarization of particles in insert (a), chain-like structures stability illustration starting in a low shear rate region – insert (b), increased shear rate region insert (c), and finally high shear rate region in the right insert (d). Re-printed from Ref. [88] with a permission of Elsevier.

paraffin, sunflower seed oil, and corn oil). Especially hydrogenated silicone oil reached considerable yield stress values (although at higher field voltage, the off-state viscosity also increased); however, the authors attribute this to the hydrogen bonding interaction.

As discussed, numerous carriers are available and can be suitable for specific applications. Silicone oils may offer the most versatile option; however, the other oils should be considered, for instance, for bio-compatible purposes. Furthermore, certain liquid carriers might lead to specific interactions with the dispersed phase, which should be also taken into consideration.

4. Dispersed phase

4.1. Introduction to dispersed phase

The second essential component of ERFs includes the dispersed phase which is composed of solid particles, with many examples described in detail in the following sections. As illustrated in the introduction, the dispersed phase is responsible for the ER effect, the particles form internal chain–like structures when exposed to an electric field [70]. In short, this leads to an increased yield stress in the low shear rate region, as the electrostatic forces influencing the chain-like structures compete and up to a certain point withstand hydrodynamic forces [71]. This is further illustrated in the flow curve and inserts in Fig. 5. As can be seen, the shear stress values in the on-field can be easily fit by a Bingham plastic model (or other models for yield stress fluids [72,73]) meaning that the electric forces dominate. The estimated chain-like structures are illustrated in the insert (b). Further, insert (c) shows the estimated structure as the interparticle forces start competing with the hydrodynamic ones and eventually, the chain-like columns collapse when the hydrodynamic forces overcome the electrostatic at a higher shear rate [74], as shown further in the most right part of graph and insert (d). From this point onwards, the shear stress values both in the active field and in the deactivated field tend to follow a nearly Newtonian fluid trend. Therefore, it is also desirable to design systems whose formed internal structures in the on-field prove a stability across a broad shear rate range (some remain stable even around 1000 s^{-1}) [75,76].

As a whole, the ER performance is further affected by many factors and as such, the chosen particles for ER system should fulfil the following criteria:

- Appropriate size and morphology, as described in their specific chapters later.
- Good sedimentation stability, following the general above-mentioned ER fluids requirements (proper chemical stability, wide range of working temperature, long life-time, non-toxic, non-corrosive, non-abrasive properties, and short dielectric relaxation time). Furthermore, any potential agglomerates should be easily re-dispersed.
- Appropriate particle wettability and interactions with the carrier are also impactful factors. A poor wettability leads to a dispersed phase that tends to form agglomerates [68,77].
- Appropriate composition. The volume or mass fraction is also a key factor, as more concentrated systems lead to an enhanced ER effect and efficiency, up to a certain limit [78]. On the other hand, an excessively concentrated ERF results in a poor particle mobility and consequently in an inability to properly align, due to high friction forces [79]. Certain studies [80–85] paid attention to considerably low-concentrated ERFs (1 % or lower – weight or volume proportion of the dispersed phase to the liquid carrier), providing cost-efficient systems in terms of the used material without compromising ER performance.
- Finally, a high electric polarizability is needed, because the interfacial polarization of particles contributes to the ER effect [86] (as presented in the insert (a) in Fig. 5). Additionally, the particles of higher polarizability seem to reach a viscosity plateau at higher shear rate [87].

Therefore in general, the ERF particles require certain properties to exhibit the ER behaviour through their reorganization in an active electric field. Such characteristic further require an appropriate dielectric character (as further explained in a later section ‘Dielectric properties’), namely an optimal dielectric relaxation strength and relaxation time, possibly in an accordance to Maxwell-Wagner polarization [89]. Hao at al. [90] proposed a correlation between the dielectric properties of the ERF particles and their orientation into the chain-like structures was also suggested. In particular, a large dielectric loss was expected to contribute to the particles’ ability to orient in the electric field, while a considerable dielectric constant was assumed to improve the thermal and mechanical stability of the created chain-like structures. Similar to the conductivity, the dielectric properties need to be within a certain balance, on one hand to exhibit an effective ER effect, on the other not to overload the system and possibly cause a short-circuit or otherwise endanger the ER device polarization (ionic or molecular polarization may shift the conductivity too much). Many types of the dispersed phase have been researched or applied and each material brings further advantages and drawbacks in terms of their structure and individual properties which influence their behaviour both on-field (such as formation of the chain-like structures, their stability in higher shear rate regions) and off-field (sedimentation stability and re-dispersibility).

4.2. Particle structure and ER properties

Additionally, it should be noted that a particle structure can highly influence the resulting ER properties and consequently the ER performance of an ERF, including the durability of chain-like structures in an active field. Numerous authors compared either the same or very similar materials as dispersed phase and reported diverse results, as will be seen through various examples mentioned in the following sections. This should serve at the very least as an inspiration when designing potential ERF particles, since many modern materials can utilize specific ways how to post-treat particles after their synthesis and tailor their properties. In terms of a particle geometry; shape, size, and surface area should be highlighted (and are also further discussed in a detail in the section ‘Particle

morphology').

A few base shapes can be recognized; sphere particles, rod-like or fibrous, plate-like or flakes, as presented in Fig. 6. Furthermore, the shearing on-field is illustrated in the inserted schema in the figure, namely for spheres, rods, and tube structures. The structures of the ER fluid are known for a long time with Tang et al. [91] presenting the both the structural evolution and the equilibrium state under various electric fields and shearing conditions for 3 types of geometries including parallel plates, slit and pipe flow.

Considering spherical particles, the assumption that the ER fluid form chain-like structures was validated very early by Gonor et al.

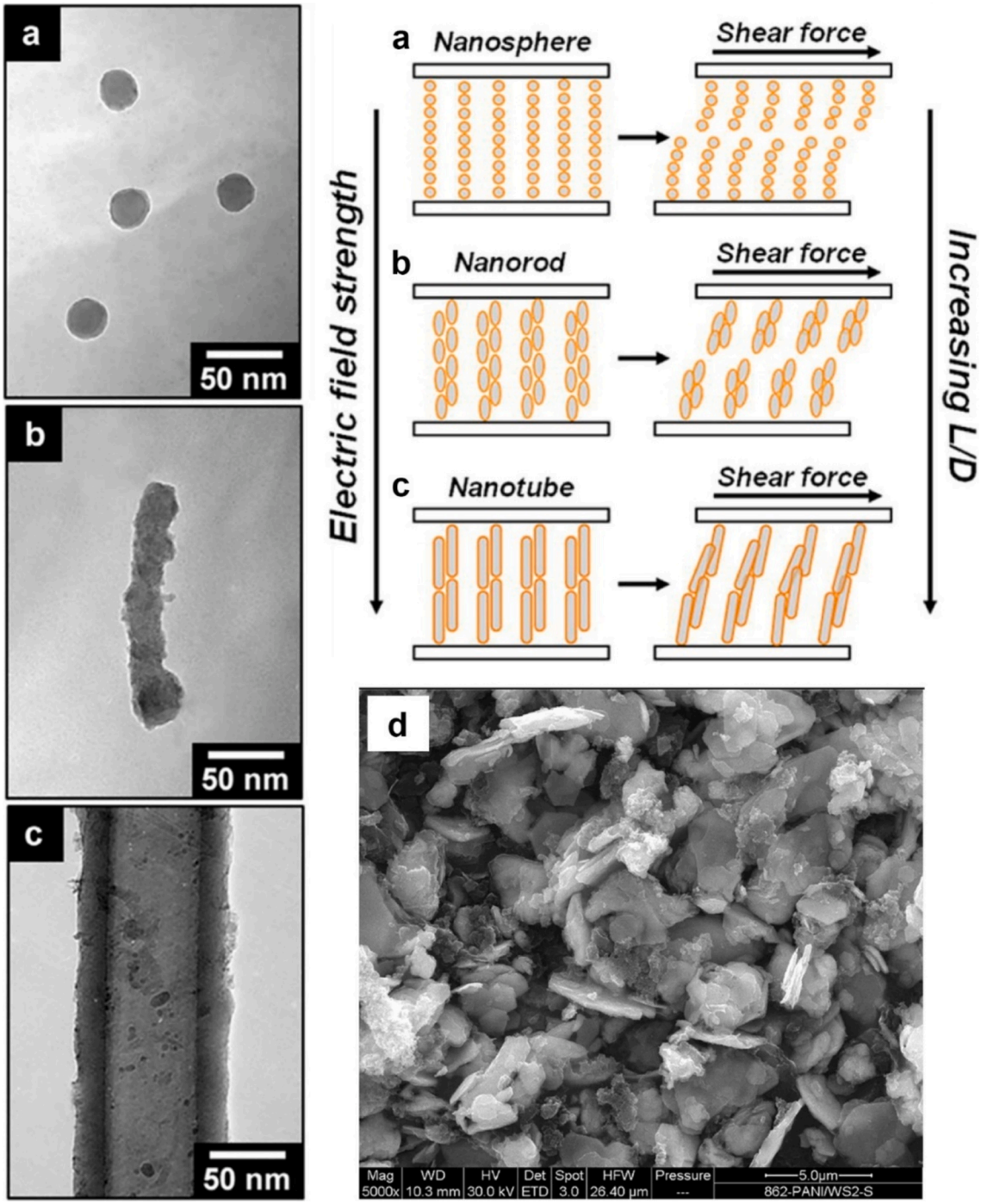

Fig. 6. Base morphology of ER particles. Hong et al. [92]: Transmission electron microscopy of titania/silica spheres (a), rods (b), and nanotubes with a higher aspect ratio (c), along with a schema of ER effect of the geometries. Stejskal et al. [93]: Scanning electron microscopy of flake-like PANI/tungsten sulphides particles (d). Re-printed from Refs. [92,93] with a permission of Elsevier.

[94] who proposed a simple model that took into account only interparticle interactions in column-like structures while neglecting any interactions between the chains. In general, spherical particles tend to exhibit lower ER performance than their rod- or tube-like counterparts [92]. This is a result of the enhanced aspect ratio (or also called length-diameter *(L/D)* ratio) of rods, tubes, or fibrous particles. As can be seen in the Fig. 6, the higher aspect ratio particles tend to form a strong geometrical construction, as noted by Hong et al. [92]. Consequently, the higher *L/D* ratio enlarges the particles' specific surface area, and also the inter-particle friction occurring during orientation of the particles. The polarizability and deformation of the chain-like structure is also affected [95,96]. Further, Jin at al. [97] noted the orientation changes through an increasing electrical field in ERF based on attapulgite nanorods. In particular, the nanorod particles' orientation was rather random and the formation of the typical chain-like structures was not clear in the 50 V mm^{-1} field. Then at 150 V mm^{-1}, the orientation of the particles was still nonunified, although the chain-like formation was apparent and finally, the particles formed visibly robust structures and showed a mostly parallel orientation to the electrical field [97].

However, different variant of rod-like particles' orientation was also reported, specifically, Kuznetsov et al. [98] observed the rod-like particles' orientation in situ by X-ray scattering. While one variation of their ERF sample showed a parallel trend in low shear rate, another variation of the particles exhibited perpendicular-oriented structures (similar to a 'deck of cards', as noted by the authors). Additionally, the authors note that a transition between both types of structures may be possible [98]. In most cases, particles with fibrous geometry were reported to elongate into more complex branched network of chain-like structures on-field with superior durability in comparison to those based on spherical particles [99–101], However, an increased aspect ratio is not always ensured in superior performance as the ER effect depends on many other conditions, as per conclusion of Qi et al. [102], who reported an opposite tendency from comparison of microspheres and microrods of various dimensions. Also, Yoon et al. [39] reported higher aggregation for 6 *L/D* ratio rods, in comparison to their 3 *L/D* analogue.

Additionally, crystalline structure plays an important role. The same material can result in varying ER effect, if the crystalline structure is manipulated, for instance, by synthesis conditions [103–106]. Crystalline structure also can influence the rod-shaped particle orientation in field [107]. Similarly, porous surface can be highly beneficial in terms of ER properties as porous structure enables larger specific active surface area. Consequently, such surface can further contribute to an enhanced ER effect [108–111]. Various commercial zeolite types of diverse crystalline structure were compared by Cho et al. [112], and in particular 13A type zeolite-based sample showed the highest static yield stress and fastest relaxation time, which the authors concluded resulted from the largest pore size. Various materials can also take advantage of surface modifications, as can be later seen in the subsections of the individual materials.

Finally, combined multiple materials can be combined to create composite particles, or core–shell particles. These particles are generally composed of two distinguishable components: inner core and outer coated shell. Very often the composite structure beneficially contributes the ER effect and depending on the material combination [113–118], unique properties may arise [119–121].

4.3. Types of dispersed phase particles

The two main groups of the dispersed phase can be distinguished, namely inorganic and organic particles, followed by a wide range of composite particles, which can be also inorganic, organic, or hybrid. Inorganic particles should possess an appropriate dielectric dipole moment, while the organic, namely conducting or semiconducting polymers, have conjugated π bonding which enables the electron mobility through the polymer chains. Natural polymers (cellulose, chitin, chitosan, to name a few) are estimated to reach an ER effect because of their electro-responsive polar groups [122,123].

Additionally, the systems can be differentiated as hydrous and anhydrous ERFs (also known as wet-based and dry-based). The former type contains adsorbed water on the particles surface. Consequently, in the wet-based systems, the particle polarization is initiated by the migration of ions in the adsorbed water. In the case of dry-based alternatives, the polarization is caused by movement of electrons in the particle. While the presence of water in wet-based systems increases the intensity of ER performance, it causes certain limitations, such as narrow working temperature, and erosion of the device. Also, an excessive amount of moisture may result in high current and eventually can cause a short circuit, endangering the safety of the device [31], and further decrease in the sedimentation stability due to lower compatibility of water-containing ER particles with oil-based carrier liquid. Due to these drawbacks, eventually the dry-based systems, such as conductive polymers, were put in the spotlight. Certain studies also paid attention to introduce modified dry-based particles of materials that are typically wet-based (such as cellulose) [81,122,124]. Composite and core–shell particles are significantly attention-worthy, as they tend to offer superior ER properties compared to their pure counterpart. In addition, the material weaknesses, often apparent in its pure form, can be neglected in the composite, while maintaining its specific advantages. Nevertheless, their disadvantages dwell within polarization mismatch between the core and the shell [125], often poor durability, and complex multi-step preparation which can become too complicated and time-consuming thus a possible obstacle for commercial production.

4.4. Inorganic dispersed phase

4.4.1. Titania

Titanium dioxide (TiO_2) possess convenient qualities such as, high dielectric constant, conductivity, good thermal stability and eco-

friendly properties. Commercially, the material has been explored in a wide range of fields. Photo-ER effect was also observed in Titania-based ERF [126]. It is also important to consider its general rheological properties (similarly, the same should be noted to any material) and in what ways they can be influenced or understood [127].

However, pure TiO_2 exhibits little ER effect at DC fields. Therefore, various methods have been developed to utilize its strengths while overcoming this weakness. These includes adjusting the geometry of particles, applying surface modifications, and finally doping with rare-earth ions (such as niobium [33] or cerium [128]) and other elements [110]. For instance, Yin and Zhao [129] introduced mesoporous titania particles doped by cerium, and later with a similar study regarding usage of chromium [130]. In both cases the doping considerably enhanced the ERFs yield stress in comparison to pure TiO_2-based samples. Another example of Cr-doping, Almajdalawi et al. [131] applied it to titania nanorods with nanocavities and in particular, a sample of TiO_2 doped by 0.7 mol % Cr of 0.5 wt% concentration dispersed in silicone oil exhibited the best suitable ER performance.

In terms of surface modification, a number of examples can be listed: sodium dodecyl sulfate (SDS) [132] modification, diammonium phosphate [133], or ionic liquid (IL) modification [134]. Additionally, SDS surfactant can be used to manipulate rheological properties of titanium oxide-based suspension in the off-field [135]. For instance, enabling a control over pH of the suspensions, and depending on the pH value and working temperature, the samples showed either shear-thinning or Newtonian behaviour [136]. Succinic acid modification was also recently reported [137]. Zhao et al. [138] introduced dual-modified TiO_2 nanoparticles with IL and acetic acid. Albeit the latter addition slightly hindered the ER effect, in exchange, the current density of the particles was significantly lowered, thus enabling their potential in a wider range of applications.

As for composite formation, combination with silica is not a rare occurrence [39]. Noh et al. [139] introduced mica/titania particles which were coated with various dyes. From hybrid compositions, Sun et al. [118] reported C_3N_4/TiO_2 core–shell composite. Yoon et al. [34] combined both approaches introducing alkaline metal doped silica/titania composite.

4.4.2. Titanate

After discussing titanium dioxide-based dispersion phase particles, similar titanate materials should be noted. In particular, barium titanate ($BaTiO_3$) attracted attention due to its great dielectric and ferroelectric properties, as well as porous structure [104]. Although its ER effect diminishes under high DC fields [140] and can show electrophoretic effect, further weakening its ER response, this weakness can be overcome by doping [141] or through its incorporation into a composite structure. Lastly, the titanate-based material attracts attention as nano-based applications. Namely, urea-coated $BaTiO_3$ nanoparticles were recently utilized as an additive to high-frequency supercapacitors to reduce their discharge [142].

Strontium titanate ($SrTiO_3$) possesses similar desirable qualities, making it also attention-worthy as an ER material. Jiang et al. [106] emphasised a facile method to synthesise these crystalline particles of various nanostructures through an ultrasound irradiation approach. Hybrid composite options were also reported [143,144].

4.4.3. Silica

Similarly to TiO_2, silica dispersions have been investigated as a promising ER material. The ER properties of silica particles are significantly affected by adsorbed water on their surface both in positive and negative way [145]. On the other hand, what makes this material attractive, is its easily adjustable morphology by various surfactants [96,146,147] as well as its porous structure. An example of surface modification can be also seen in Fig. 7. For these reasons, silica represents a convenient template material for composite particles [95,148]. Additionally, drag reduction can sometimes be important for applications at high shear rates to avoid turbulent flow. For these cases, an addition of silica nanoparticles to polyacrylamide-based ERFs are reported to have an advantage [149].

Drag reduction can sometimes be important for applications at high shear rates to avoid turbilant flow. For these cases,

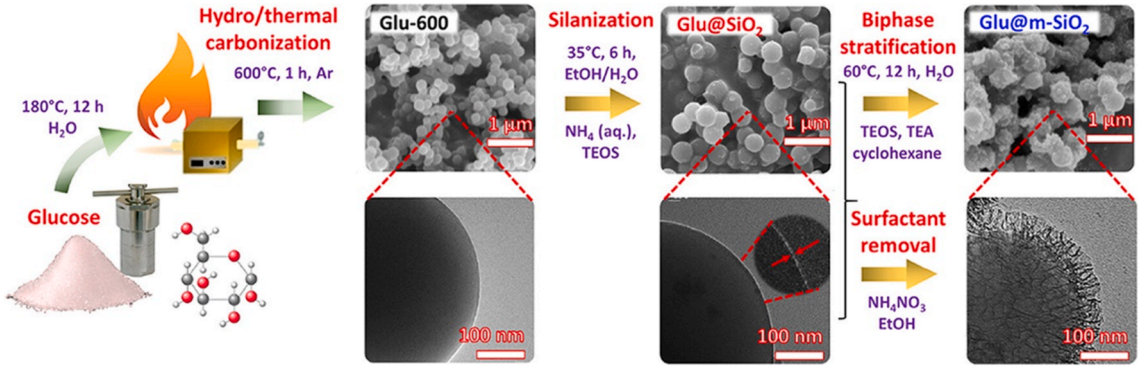

Fig. 7. Pavlikova et al [154]: Schematic illustration of glucose/mesoporous silica composite synthesis, with SEM photos of the particles (top row) and TEM (bottom row). Re-printed with the permission from {Pavlikova E, Plachy T, Urbanek M, Cvek M. Engineering Conductivity and Performance in Electrorheological Fluids Using a Nanosilica Grafting Approach. ACS Applied Nano Materials; 6: 9768-76; 2023}. Copyright 2023 American Chemical Society..

polyacrylamide and similarly silica-based ERFs are reported to have an advantage.

Therefore, pure silicon oxide is not commonly used nowadays, rather it is preferred modified; for instance, with metallic cations [111], or as a part of composite particles. Both hybrid [150] and inorganic [151] composite combinations are frequent choices. Kim et al. [152] utilized both, core–shell formation and surface modification, suggesting the particles' potential also in bio-medical field. Yoon et al. [35] utilized graphene oxide-coated silica spheres to evaluate the investigate the influence of particle density on the ER behaviour and sedimentation stability of the ERF. The density was possible to manipulate due to porous silica core and various pore size of individual samples. As a result, the sample with the least density exhibited the best ER performance as well as the sedimentation stability. Chen et al. [153] synthesised $H_2Ti_2O_5/MoS_2/SiO_2$ core–shell nanoparticles taking an advantage of the morphology and the high conductivity of the molybdenum disulfide with silicon dioxide to control the conductivity to a desired level, overall exhibiting an acceptable ER effect and dielectric properties. Pavlikova et al. [154] reported composite particles combining carbonized glucose and mesoporous silica coating by dual-step coating. Fig. 7 illustrates the full procedure while showing the morphological changes of the particles after each step by scanning electron microscopy (SEM) and transmission electron microscopy (TEM). Carbonization process enables enhancing conductivity of various organic materials [155–157]. Additionally, by adjusting the conditions of the process, namely the time and temperature, it is possible to control conductivity range of the carbonized material [158,159]. As a result, the glucose/mesoporous silica composite particles gained tailored conductivity as well as a reasonable level of long-term sedimentation.

4.4.4. Clay

Clay-based particles have also been researched as a potential ER dispersed phase, especially due to their widely accessible, low-cost, and abundant nature as a resource with high variety of crystalline structures. They offer interface with a large specific surface, options of facile chemical modifications through surfactants. Often these particles can prove to be great host material for polymers, which can even be intercalated into the clay structure or exfoliated [160–163]. In fact, such clay-polymer materials are focused in these review articles [164,165].

Montmorillonite (MMT) has received attention as an inexpensive ER material featuring the above-mentioned advantages with a particular structure and interlayer structure, which is convenient for above-mentioned intercalated composite designs. Starting with MMT/TiO_2, Xiang et al. [166] explored the nanocrystal-shaped particles and their ERF showcased improvement in terms of temperature and sedimentation stability, as well as reaching exceptional ER effect. The group later further adjusted the MMT/TiO_2 particles layer clay structure enclosed with titania nanorods, also resulting in considerable ER effect [167]. Kim et al. [168] introduced PANI-MMT enriched with Na^+ cations, this combination enabled stable ER performance even at high shear rates and lowered the current density. Composites consisting of intercalated polyethylene oxide within MMT were also studied, proving favourable ER properties as well as improved thermal stability due to the polymer intercalation [169].

Kaolite is another low-cost alternative, offering a unique layered structure of interstratified $AlO_2(OH)_4$ octahedral sheets and SiO_4 tetrahedral sheets [170]. Such structure makes it an attention-worthy material for intercalated composite engineering [171]. Wang and Zhao [172] explored various ERFs based on intercalated dimethyl sulfoxide/kaolinite and glycerol/kaolinite composites. Compared to pure kaolinite, both alternatives improved their sedimentation stability and dielectric properties.

Other clay-origin particles offer similar qualities. Ramos-Tejada et al. [173] compared ERFs based on isotropic and elongated particles of goethite and hematite and confirmed that the anisotropic particles exhibited a more efficient ER behaviour. The same group later followed this research, further analysing the effects of the clay particles' size and shape, plus comparing diverse clay-based particles and their mixed systems. In particular, coated and bare montmorillonite K30, sepiolite (SEP), and laponite (LAP) of various geometries were investigated, additionally cetyltrimethylammonium bromide (CTAB) was used to coat selected samples and especially treated with SEP gaining a steep increase in static yield stress. Additionally, both LAP and SEP appeared to reinforce the pure MMT structures, raising particularly their storage modulus. However, mixing together LAP into Org-SEP resulted in a weaker ER response [174]. Kutalkova et al. [175] analysed the ER behaviour of fiber-shaped SEP particles. The highest particle concentration sample (15 % wt) resulted into a gel-like structure while steeply enhancing the sedimentation stability, although the ER efficiency proved to be inferior to the other examined samples (5 %wt exhibited the best ER efficiency).

Kim et al. [176] coated polystyrene (PS) core by LAP, creating nanocomposite though Pickering emulsion. A similar approach to create PANI/attapulgite was reported by Han et al [116]. Furthermore, PANI-coated SEP particles were analysed by Jang and Choi [177].

4.4.5. Zeolites

Zeolites represent a low-density crystalline material with a regular structure. These aluminosilicates are widely used in chemical industry (especially as catalysts), in addition, their porous structure offers a large active area. Recently, their synthesis aiming for a specific particle size control has gained an attention [178].

Zeolites belong to the wet-based ERFs and compared to other alternatives of the group, they show better thermal stability [112]. Adsorbed water increases the mobility of cations inside the pores which leads to an increase in the dielectric loss and improves the turning ability of the particles [179]. Sun et al. [180] reported silicon/titanium zeolite combined with titanium oxide into core–shell particles (TS-1/TiO_2) and the composite particles showed improvement of ER performance.

4.4.6. Graphene-based materials

Graphene, in the form of strictly 2D crystals [181], has attracted noteworthy attention in a wide range of fields and applications. Its unique properties differ it from other carbon-based materials, namely: accessibility, extraordinary carrier mobility, large active surface area, good dispersion stability. As such, graphene is a compatible host for polymers [182].

Pristine graphene's extraordinary conductivity might not be ideal as an ER material, as it is likely to cause a short circuit. In contrast, its oxidized form – graphene oxide (GO), is believed to be more suitable for ER applications due to its lower conductivity. Furthermore, its functional groups enable further facile modifications and consequently ER effect enhancement [183] as well as notable stability in both aqueous and organic solvents [184]. As such, it is usable without post-treatment, but its ER effect without modifications is not as impressive. In its pure form the yield stress is estimated to be rather low in comparison to other ER particle types, thus both surface modification or composite formation are suggested to achieve a greater ER effect for both graphene [185] and GO [186,187]. Additionally, silica-coated graphene was demonstrated to respond well to AC field (the authors note that majority of GO-based ERFs are more suitable for DC fields) [188].

An alternative way to improve GO properties was proposed by Hong and Jang [189]. The authors introduced a dispersion method based on solvent exchange, unlike the usual drying method, resulted in improved ER performance as well as sedimentation stability. A schema in Fig. 8a describes the differences between these two methods. Furthermore, the other parts of Fig. 8 (b, c, and d) compare the ER response of ERF dispersions based on solvent exchange method particles and drying method-obtained particles. As such, the figure demonstrates the above-mentioned improvement of yield stress, and sedimentation stability, respectively. The authors emphasize that high active surface area and other unique properties remain once the GO is re-dispersed in silicon oil after the solvent exchange method. In contrast, when the initial solvent is dried, the π–π attractions in stacked GO sheets become dominant and lead to aggregation. Consequently, not only this inhibits unique properties of the sheets, but also make the full re-dispersion in silicon oil challenging [189,190].

The conductivity of GO can be further adjusted through chemical, thermal, or other procedures, in a reduced GO (rGO) form. Yin et al. [191] evaluated rGO/polypyrrole (PPy) nanosheet composite particles, confirming an enhanced ER performance in comparison to pure PPy.

A number of studies further compare the ER properties of diverse graphene-based options. Yuan et al. [117] compared GO-supported PANI and rGO-supported PANI nanoplates ERFs and confirmed the ER performance of the former was superior in both

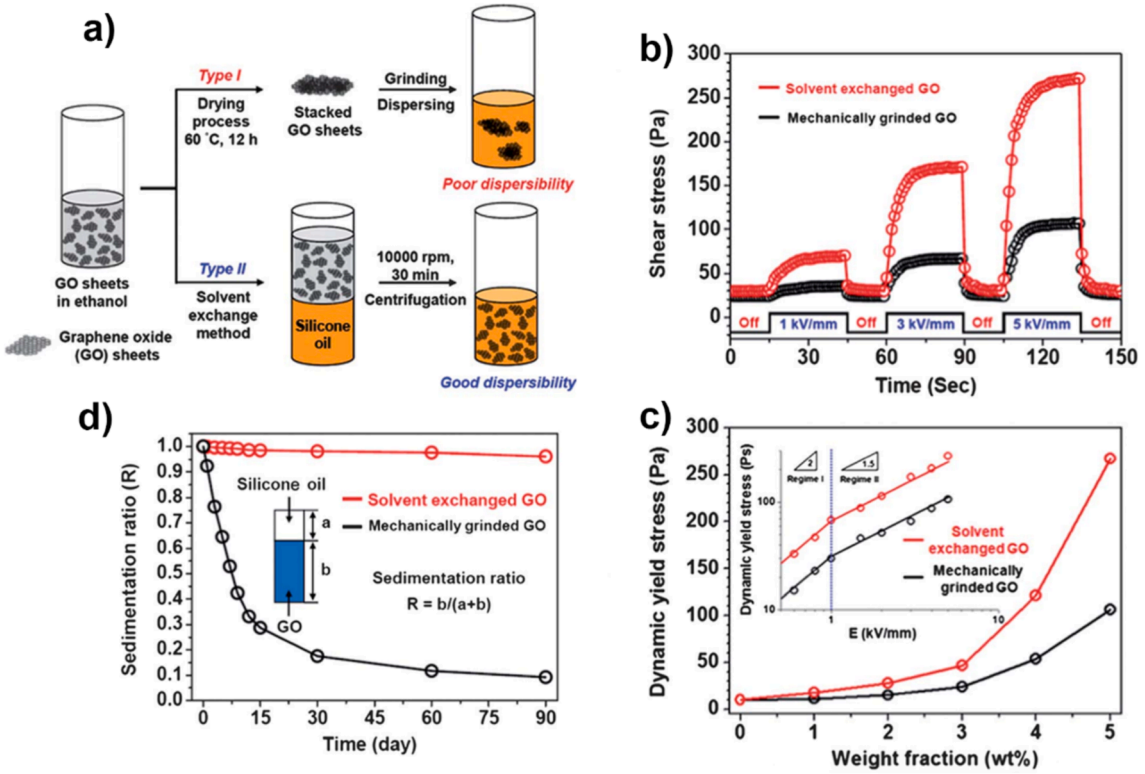

Fig. 8. Hong and Jang [189]: Illustration of solvent exchange method and drying method of GO sheets (a). Evaluation GO sheets-based ERFs, the shear stress values over time on-field and off-field (b). Dynamic yield stress over weight fraction at 5 kV mm^{-1} (c). Comparison of sedimentation stability of both GO sheets-based dispersions (d). Re-printed from Ref. [189] with a permission from the Royal Society of Chemistry

alternating current AC and DC field (unlike rGO, GO/PANI degraded in AC field). Furthermore, Shin et al. [192] studied GO morphology modification through the ball-milling method. As the study concludes, an ERF based on particles adjusted through this facile method exhibited superior dispersity and ER performance, compared to regular GO particles. As another example, Ilčíková et al. [193] introduced GO particles modified with types of betaine moieties. In particular, the modification with carboxybetaine ester of a 5 %wt concentration-based ERF reached the highest yield stress; however, the sulfobetaine moiety sample showed higher ER efficiency. Similarly, Mrlik et al. [194] modified rGO with poly(butyl methacrylate) (PBMA) chains and compared its ER performance to other GO-based ERFs. Furthermore, Li et al. [187] introduced polyhedral oligomeric silsesquioxane (POSS)-decorated GO (POSS-GO), providing an enhancement of ER effect in comparison to pure GO. Zhang et al. [195] synthesised colloidal-GO/PANI nanocomposites, with the PANI being responsible for enhanced thermal stability and the colloidal-GO enabling facile dispersion in aqueous media.

As can be seen, there is a considerable variety of inorganic materials, able to adequately fulfil the role of a dispersed phase. Most of these are wet-based systems. Multiple groups of inorganic materials possess great dielectric properties and generally. In comparison to organic particles, the inorganic materials tend to offer a higher dielectric relaxation strength (especially titania and titanate materials). This is estimated to improve the toughness of the chain-like structures during the on-field (more details about dielectric properties are available in the respective section 'Other material's factors influencing the ER effect'). Their prior disadvantage is their rather high density which may lead to a low sedimentation stability. Each of the mentioned category offers additional benefits too, namely: titania – various morphology options and great stability properties; silica – porous surface, morphology variety and convenient template for composite formation; clays and zeolites – porous surface and rich variety of crystalline structure, low cost materials; rGO – facile modification possibilities and overall great stability. Even though it is possible to use them in their pure form, exploring the possibilities of material combinations as a part of a composite-based system is highly encouraged. Composite particles are mostly reported to exceed the ER performance of their pure counterparts. The downside of composites dwells within the time and resources needed to obtain the optimal material parameters as their synthesis involves multiple steps and longer (and at times complicated) procedures. It is important to establish a better theoretical background in terms of predicting the best synthesis parameters.

The majority of the cited references of inorganic-based particles (and similarly other types in the later sections) were used to extract crucial information in terms of materials and selected properties. In total, the extracted information is presented in four tables in the supplementary information. Each of them is focused on a specific type of particles, starting with pure or modified inorganic particles in Table 1, followed by pure or modified organic particles in Table 2. Composites (inorganic, organic and hybrid) are summarized in Table 3. Lastly, Table 4 briefly enriches giant electrorheological fluids particles. As can be seen, aside particle geometry, material, the liquid carried used, other key details are presented. These include the particle concentration, the DC conductivity; (The AC

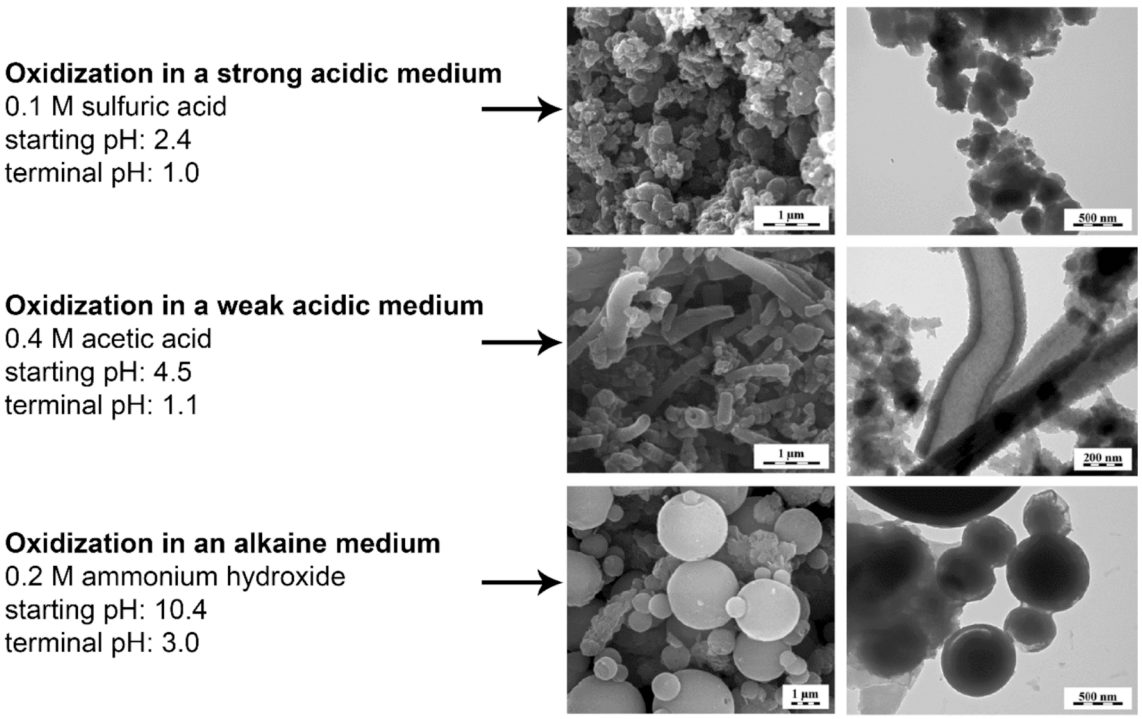

Fig. 9. Stejskal et al. [210]: Control of PANI morphology, confirmed by SEM (left photos column) and TEM (right photos column). Adapted with a permission from {J. Stejskal, I. Sapurina, M. Trchová and E. N. Konyushenko. Oxidation of aniline: Polyaniline granules, nanotubes, and oligoaniline microspheres. Macromolecules, 2008, 41, 3530–3536.}. Copyright 2008 American Chemical Society.

conductivity is not compared in the table, although it may be available in a publication. Therefore, if the AC conductivity is available but the DC conductivity could not be determined, the data summary field will be marked as NA, as not available) and the ER efficiency. Usually, the ER efficiency shows a linear behaviour with the shear rate ($\dot{\gamma}$) until the hydrodynamic forces overcome the electric ones. Thus, the ER efficiency is divided into two columns, using different shear rates values (in particular, 0.1 and 100 s^{-1}, unless stated otherwise in brackets), with the electric field value given in the later. Most of the ER efficiency values were calculated from the corresponding graphs or tables (usually either flow curve or step-wise graphs) if available in the referenced publications using equation (1). It should be noted that some of the properties and their corresponding data had to be omitted, depending on their availability in the published articles, in which case NA in noted instead. However, in these cases, it is often possible to find other supplementary data for detailed understanding of the particular material (for instance, the dielectric properties are standardly evaluated). In case multiple samples are compared in a given research paper, the extracted data may be simplified to include only the more relevant values (i. e. the highest or the most optimal, or a range). These criteria apply to all summary tables of this review.

4.5. Organic materials – conductive polymers

Although the initial studies had mostly focused on the inorganic particles, certain limitations were recognised. For instance, a large density variation between the dispersed particles and the liquid carrier may result in poor dispersion stability, and, potentially, the inorganic particles may be too hard and potentially be abrasive to the ER device [196,197]. Consequently, especially anhydrous polymeric materials gained attention, owning to their high polarization due to their conjugated π bonding, as afore-mentioned, and lower density, resulting in improved sedimentation stability. As such, conductive polymers were put into the spotlight.

4.5.1. Polyaniline

Firstly, PANI should be mentioned as an extensively investigated polymer, and sometimes it is considered to be an essential ER material candidate, especially in the anhydrous group. That is due its appropriate conductivity, exceptional electrochemical performance, environmental stability, facile synthesis, and low production cost [198]. Polyaniline also offers notable thermal and sedimentation stability [199,200].

Its high conductivity requires control to avoid a possibility of short circuit or current leakage. Nevertheless, the conductivity can be reasonably modified through processes, such as afore-mentioned doping, or in contrast dedoping to decrease the conductivity into the desired range, or protonation [201]. In the context of conductive polymers, a chemical dopant is a substance which is able to drastically change properties of the polymer, even if used in a very small amount. Multiple forms of doping can be further distinguished (for instance primary doping, protonation, de-doping, secondary doping) [202]. In the case of protonation, the conductivity is further affected by the solvent acidity and degree of protonation [203], and similarly, specific dopants are able to further affect the thermal stability or other properties [204,205]. Another minor drawback of PANI is overall rather low yield stress in pure form [198,206]. What is interesting, the polymer does not have a regular morphology and in fact, the particles' shape and size can be controlled by synthesis process [207–209]. As afore-mentioned, control of particle morphology may be used as an advantage in ERF applications. For this reason, a shape-flexible material as PANI can be well-utilized to fulfil specific requirements. For instance, Stejskal et al. [210] demonstrated options to control the PANI morphology thought oxidization of aniline in different degrees of acidity, as visualized in Fig. 9. As can be seen, granular particles resulted from oxidation in strongly acidic solution, nanotubes were a result of mildly acidic solution and spheres when alkaline solution was used.

Furthermore, nano-fibrous PANI-based ERF was proposed by Yin et al. [99] showing superior ER performance when compared to granular PANI. The nano-fibrous particles also showcased extraordinary sedimentation stability. Sung et al. [36] introduced an approach to create hollow PANI nanospheres with rough surface, enhancing the dispersion stability. Lastly, carbonization can be used to alter PANI's properties [211]. Beneficial changes were reported in aniline oligomers prepared via the carbonization under alkaline conditions [212]. In this study, particle morphology changed from spherical to two-dimensional plates. This resulted in a significant enhancement of the ER efficiency of the respective ERF suspension. Carbonized PANI was also utilized by Yin et al. [213] as an initial material to create carbonaceous nanotubes (CT) which were grafted with silica on their surface as the next step. The resulting silicone-grafted CT particles exhibited enhanced dispersion stability and ER efficiency.

Although the pure or carbonized polymer PANI is applicable as ERF dispersion phase [113], often it offers more advantages as a part of core–shell composite particles, provided a suitable material is used to produce a core.

Many of both, inorganic and organic, co-materials have been analysed and evaluated as suitable for ERFs. To name a few hybrid composites: Yin et al. [214] combined PANI with titania into nanocable-like core–shell particles. Marins et al. [198] followed the study of PANI-based system and developed sepiolite particles coated with PANI through two methods; denoted bulk and slurry polymerization. The best results were achieved through the latter method. Notable ER effect and sedimentation stability was also confirmed in an ERF based on PANI/montmorillonite (MMT) composites by Lu and Zhao [215]. Stejskal et al. [93] complemented the polymer with molybdenum and tungsten sulphides. Last but not least, these results confirm the superiority of anisotropic particles in terms of achieved yield stress values. The same material composition was tested by Li et al. [216], while examining various ratios of both materials, and the composite sample based on 4:1 PANI to MoS_2 proved the best ER performance. Zhang et al. [120] acquired a unique particle shape using exfoliated MoS_2 nanosheets to enable a growth of PANI nanoneedles. The composite particles lead not only to

enhanced dielectric properties and ER performance, but also to excellent electromagnetic microwave absorption properties.

Further, multiple iron oxide/PANI were reported. Sim et al. [217] introduced PANI-coated Fe_3O_4 particles featuring dual ER and magnetorheological (MR) response. Tian et al. [218] synthesised flower-shaped PANI/Fe_2O_3 composites. Alike, but flake-shaped PANI/Fe_2O_3 were prepared and analysed by Zhu et al. [219], showing a high yield stress reaching from about 800 Pa to over 10 kPa at 4.3 kV mm^{-1}. Jeong et al. [220] introduced particles of manganese ferrite coated with PANI, exhibiting dual ER and MR response. The dual performance was also reported with the utilization of zinc ferrite (ZF) particles, for instance, Kim et al. [221,222] introduced variations of ZF/PANI-based particles a dual performance. Similarly, PANI derivate poly(diphenylamine) (PDPA), was reported as a PDPA/ZF core–shell with similar dual ER and MR behaviour [223]. Additionally, ZF/PANI (with PANI dedoped in benzoic acid) composite particles were proved to be ER responsive as well as having protective anti-corrosion properties [88].

4.5.2. *Polyelectrolytes and polymer electrolytes*

The earliest polyelectrolytes-based ER systems have seen attention since 1980 s, starting with poly(lithium methacrylate), poly (sodium styrene sulfonate), highly sulfonated poly(styrene-co-divinylbenzene), ion-exchange resin and more [224,225]. These traditional polyelectrolytes belong to the wet-based systems; thus, their ER effect is rather minor in dry state and their working temperature is narrow. Further, ERFs based on metal salts dissolved in polyurethane matrix [226] or polyacrylonitrile complexes with inorganic salts were introduced [227], greatly reducing the ERFs affinity to moisture, reducing the abrasiveness and widening the operating temperature. Recently, polyethylene oxide was intercalated into MMT, replacing water in the layered structure and leading

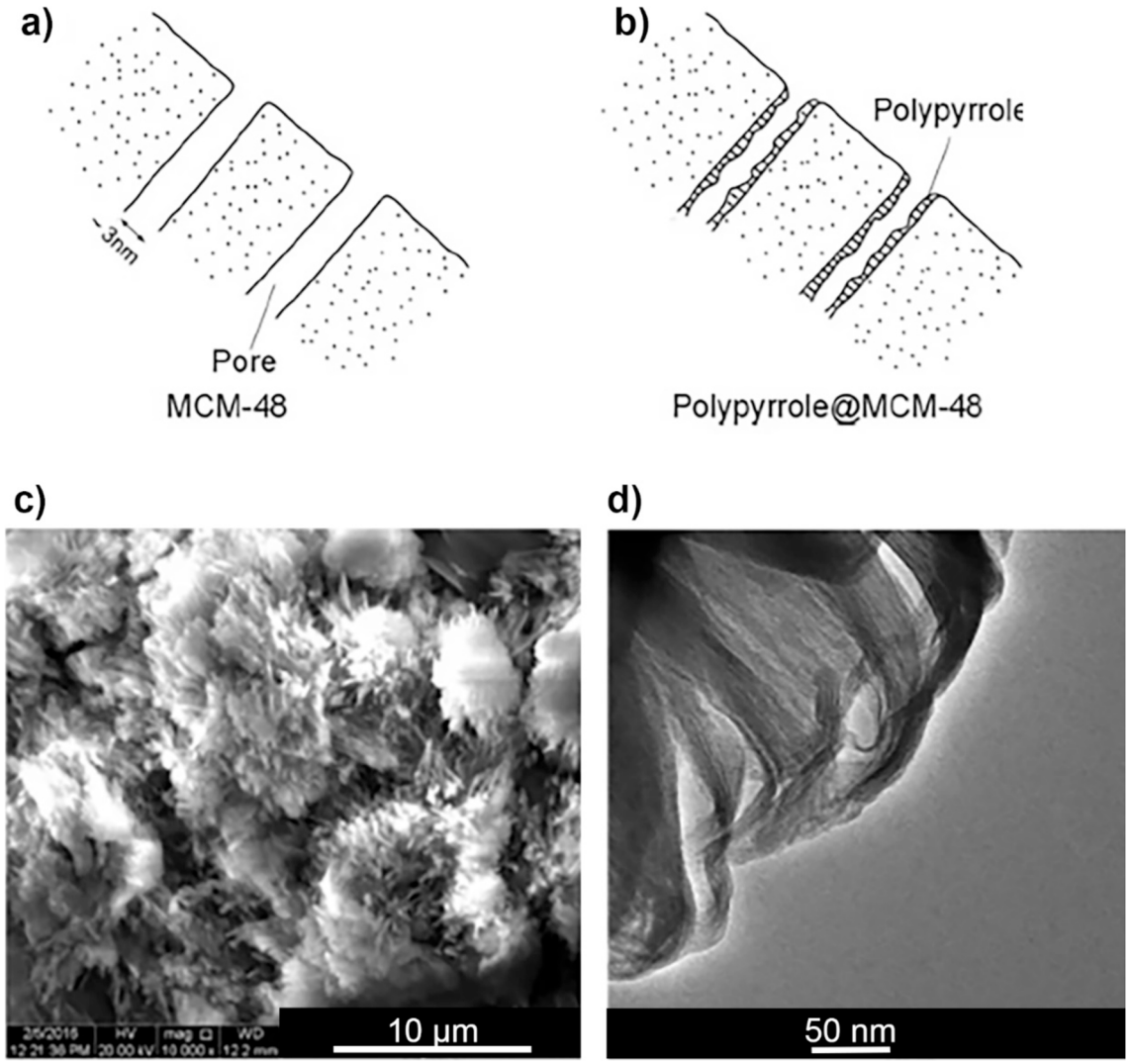

Fig. 10. Wysocka–Zolopa et al. [251]: Scheme of MCM-48 and PPy growth (a and b). Extracted polypyrrole morphology after silica dissolvement confirmed by SEM (c) and TEM (d). Re-printed from Ref. [251] with a permission of Springer.

to improved ER effect [169].

Finally, polymeric ionic liquids, or poly(ionic liquid)s, (PILs) have been introduced and concurrently are the research-dominating material of this class. Unlike their afore-mentioned predecessors, PILs contain polyatomic fluorinated component ions, enabling a large interfacial polarization, while staying hydrophobic, coupled with desirable properties [228,229] (convenient conductivity, thermal stability, tuneable solution properties, chemical stability) and a variety of morphology control options [230]. Additionally, in terms of particle design on molecular level, the PILs-based ERFs' properties can differ if they are synthesised with different length of side-substituent alkyl chains [231] or with varied tethered countercations attached to backbone [232].

Additionally, PILs can also be utilized as modification (for instance, titania-based particles) [134,138], or in a form of a composite particles. To name a few examples, PIL/PANI composites were evaluated by Zheng et al. [115] improving the ER response and decreasing the current leakage in comparison to pure PIL. Wang et al. [233] introduced polymerized ionic liquid/doubly polymerized ionic liquid core–shell particles which increased the ER effect by more than one magnitude and enhanced temperature stability in comparison to a regular PIL-based ERF.

4.5.3. Polypyrrole

Alike PANI, PPy has also gained considerable attention not only as another promising ER candidate, but also in a variety of other fields. Similarly to the formerly mentioned polymer, PPy also possess an appropriate conductivity, a good environmental stability [234], and an easy synthesis through either electrochemical polymerization or oxidative polymerization [235–239]. Additionally, the conductivity of PPy can be controlled by the used amount of oxidant and surfactant [236], or by the doping process (which can also lead to adjusting other properties). The synthesis of this polymer can be easily tailored, resulting in adjusting the surface properties [240] as well as giving access to multiple morphologies [241]. For instance, Xia et al. [242] used thermo-oxidative treatment in air to produce PPy nanofibers and confirmed its superiority in ER performance in comparison to a dispersed phase based on granular-shaped PPy. Similarly, Almajdalawi et al. [243] additionally compared the performance after treatments with ammonium hydroxide to reduce the conductivity. As mentioned, the polymeric material can be used as pure particles, or as a part of composite to further enhance the particles' properties. Recently, Seo et al. [244] analysed and compared previously reported PPy, PPy-coated silica and nanocomposite of PPy and mesoporous silica (MCM-41) using various models. Furthermore, Kim and Hong fabricated PPy-silica nanocomposite [245]. Later, Kim and Yoon [82] followed by introducing PPy-tin oxide nanocomposite particles with reasonable ER efficiency. Mrlik et al. [246] researched PPy-coated titania rod-like particles, confirming enhancement of the ER behaviour in comparison to pure TiO_2 particles.

The dual coating technique can be also utilized, for instance, Chen at al. [247] introduced dual-coated GO particles using nanosheets of PPy and PIL, as a single coating layer may not be able to sufficiently decrease the conductivity of GO. The PPy and PIL layers significantly improved the ER effect and available electric field strength in comparison to pure GO or the single layer GO/PPy. Polypyrrole also facilitated the formation of PIL layer. Additionally, Fang et al. [248], rather than the common coating method, enabled an intercalated growth of PPy chains inside silica pores (MCM-41 type) and reported an enhanced ER behaviour in comparison to other reported MCM-41-based systems. Similarly, other material combinations were also introduced through intercalated polymer composites [169,249,250]. Following, a similar approach was utilized by Wysocka–Zolopa et al. [251] and tested on silica MCM-48 (although their research was not directed towards ER applications, the results could be very beneficial for the field, as a further direction of intercalated polymers). After the synthesis and intercalating PPy in the pores, the polymer was extracted and exhibited superior properties in comparison to regular chemically-bulk produced PPy. The initial PPy-pore growth scheme as well as the PPy morphology after extraction are presented in Fig. 10. As can be seen, the PPy obtained nanowire-like morphology. Both the structure and resulted high surface area were determined to be responsible for the properties improvement. As above-mentioned, even though these extracted PPy particles were not further evaluated in terms of ER properties, given the enhancement of electrochemical properties and acquirement of whisker-like structure, as-extracted polymer could enhance potential ER performance.

4.5.4. Polyaniline derivates

Due to specific disadvantages of PANI, specifically originally high conductivity and low solubility in organic solvents, certain PANI derivates received attention. Gercek et al. [252] analysed the ER performance of certain derivates poly(*o*-toluidine (POT), poly(*N*-methyl aniline) (PNMA), poly(*N*-ethyl aniline) (PNEAn), and poly(2-ethyl aniline) (P2EAn) in a comparative study. The sedimentation stability of the examined derivates was sufficient for 30 days. Poly(*o*-toluidine) showed the highest conductivity, dielectric constant, and ER effect.

Poly(*o*-toluidine) also caught the attention of Yilmaz et al. [253] who synthesised POT/zinc composites. Dispersed in silicone oil, these composites showed adequate sedimentation stability for 40 days, a truly remarkable result for ERFs.

Further, PNMA should be highlighted. In comparison to PANI, besides a lower conductivity, it possesses a higher oxidation stability and a better dispersion in the carrier. In addition, its facile synthesis enables it as a good core option [254]. For instance, Moon and Choi [255] combined it with poly(methyl methacrylate) (PMMA) to create PNMA/PMMA core–shell particles, achieving exceptionally high ER efficiency (as can be seen in detail in Table 3). Furthermore, Dong et al. [256] coated PNMA particles with magnetite, similarly, Lu et al. [257] embedded poly(2-methylaniline) with magnetite, both particle types showcased a dual ER and MR response. Wang et al. [125] introduced nanoflakes composed of rGO core and poly(ethylaniline) shell, reporting results of different reduction

rate. The authors concluded that while the reduction did not change the geometry of the particles, the conductivity was altered.

Another derivate, Poly(o-anisidine) (POA), attracted an attention due to its naturally lower, and very ER-convenient, conductivity and higher reactivity in comparison to PANI. [258] Lee and Choi [259] synthesised spherical silica/POA core–shell particles, using *N*-[(3-trimethoxylsilyl)-propyl]fiblilaniline as an agent. The composite particles proved to have appropriate dispersion stability and better ER effect in comparison to reported pure silica-based or pure POA-based ERFs. Similarly, Lu et al. [121] introduced magnetite/POA composite particles, exhibiting both MR and ER response. Although the non-magnetic POA shell weakened the MR properties, the polymer addition improved not only ER performance, but also the suspension's thermal and sedimentation stability.

P-phenylenediamine (PPD) should be mentioned, has variable synthesis options, enabling its flexibility in a wide range of applications [211,260]; however, in terms of ER systems, it has received rather minor attention. The derivate's conductivity and consequently its ER effect can be enhanced by adjusting its synthesis [261]. In particular, by oxidation of PPD with *p*-benzoquinone in the presence of methanesulfonic acid. *P*-phenylenediamine can form 3 isomers (poly(*ortho*-, *meta*-, and *para*-phenylenediamine)), with the *para*-isomer exhibiting the highest conductivity and ER effect [262]. Poly(*p*-phenylenediamine)-based ERF was also tested through a carbonization process, and unlike the above-mentioned case of PANI carbonization, this derivate's ER properties decreased. The higher carbonation temperature applied, the lower ER efficiency was eventually achieved [263]. Cao et al. [264] introduced composite particles of poly(*p*-phenylenediamine) and GO. The group used facile ball-milling method in the presence of dry ice, which is suitable as an eco-friendly approach. Zhang et al. [265] reported an ERF composed of PPD-functionalized graphene oxide-*g*-polyaniline (PPDG-*g*-PANI) jellyfish-shaped fibre particles. The system demonstrated excellent suspension stability, in comparison to a regular PANI-based ERF.

4.5.5. Other conductive polymers

More polymers also offer options as potential ER materials. Polyindole (Pln) has excellent redox activity and thermal stability, as well it is less prone to hydrolytic degradation. On the other hand, its conductivity is inferior to that of both above-mentioned conductive polymers [266,267]. Phasuksom and Sirivat [268] succeeded in improving its conductivity value up to almost 15 S cm^{-1} (although this is too high for ER applications, it may be desirable in other fields) by synthesising Pln through emulsion polymerization and a doping/de-doping process. Emulsion polymerization was also utilized by Park et al. [269]. Sari et al. [270] introduced Pln/polyethylene nanocomposite particles and confirmed a further improvement of thermal stability in comparison to pure Pln. Erole et al. [271] combined this polymer into a hybrid composite with organo-MMT. Enhanced sedimentation stability of 82 % ratio after 25 days was evaluated for their 25 wt% sample. Kang and Choi [272] fabricated core–shell zinc ferrite/Pln particles exhibiting a

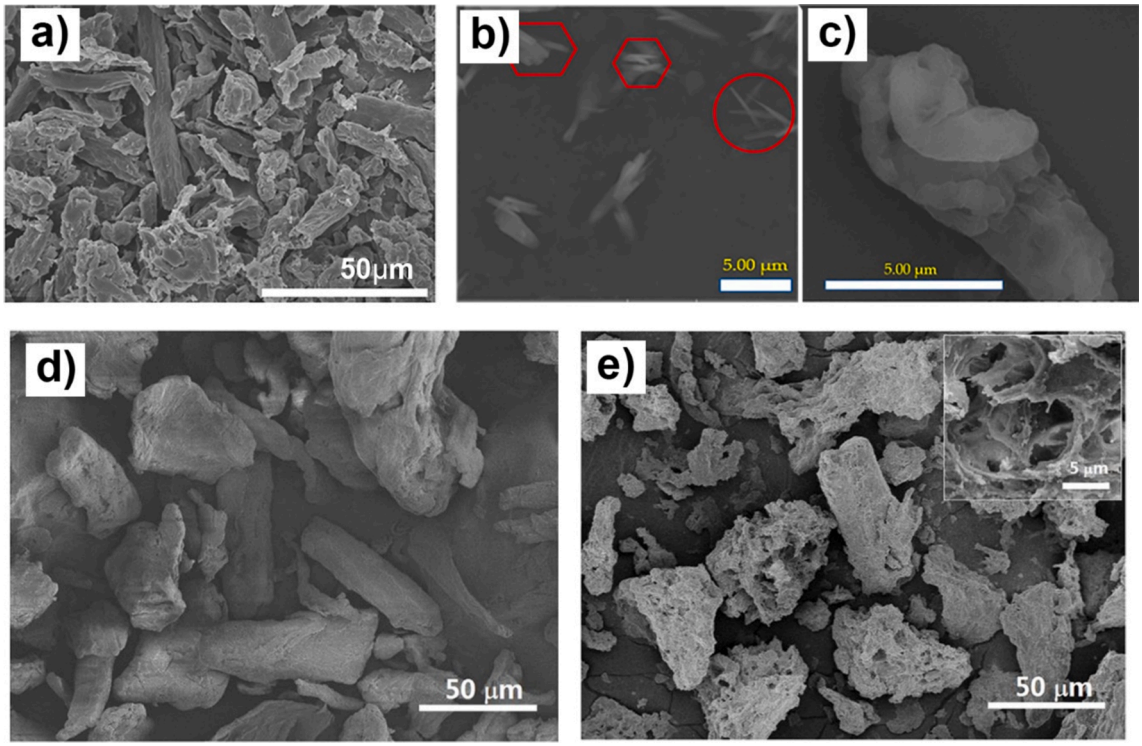

Fig. 11. Examples of cellulose derivates and modifications. Bae et al. [293]: Microcrystaline cellulose (a). Choi et al. [294]: microfibrilated cellulose low magnification (b) and high magnification (c). Liu et al. [122]: comparison of pristine cellulose (d) and cellulose modified by urea-terminated silane (e). Reproduced from Refs. [122,293,294] with a permission from Elsevier and MDPI.

dual ER and MR response. Another dual response ERF was presented by Hong et al. [273] based on iron oxide/Pln core–shell particles featuring good thermal and sedimentation stability.

From other polymers, poly(*p*-phenylene) (PPP) [274] and polythiophene (PT) along with its derivates [275] sparkled attention, although not as recently. Gumus et al. [276] investigated ER behaviour and creep recovery of PT in silicone oil and PT/borax ERFs in vibration damping experiments. Hong et al. [277] reported silica/PT nanospheres with excellent sedimentation stability for a high 30 vol% concentration, the yield stress peaked at 3.9 kPa at 3 kV mm^{-1}. Additionally, polyacrylamide polymers were studied for their drag reduction properties in turbulent flow [278,279]. Although the focus of these studies was not ER-related specifically, drag reduction could be an interesting niche in future ERFs.

As presented, many conductive or semi-conductive polymers have seen a considerable spotlight as ERF dispersed phase both in their pure form, as well as composite particles owning to their overall great stability, low density, morphology flexibility, and facile modification of conductivity and other properties.

4.5.6. *Organic materials – biopolymers*

Alternative eco-friendly materials for usage in ER substances have also received considerable attention. Due to global environmental changes, the trend of using bio-particles and eco-friendly materials has been apparent in various scientific fields and numerous ER materials studies have followed this trend. Consequently to date, the ER response has been researched in abundant eco-friendlier materials or materials that are generally seen as a mere by-product or waste. As such, natural polymers have gained significant attention, namely cellulose, chitosan, and starch. Other examples of alternative materials, which recently caught minor attention, include particles based on spent coffee grounds [280] and dispersed algae [75]. The latter study hints that the otherwise harmful algae could represent a new eco-friendly material, exhibiting ER properties of the same or close values comparable to those of a cellulose phosphate-based ERF. In addition, the algae system was reported as suitable for applications without the necessity of any additional modification. Similarly, post-treatment of particulate matter was approached by Jeong et al. [281] who evaluated a dispersion of fine dust particles and confirmed its ER behaviour and, as such, presented a possible way to reuse the captured fine dust.

Closely connected to the environmentally-friendly approach, a few examples of extraction of ER material particles from agriculture waste should be briefly mentioned. Kwon at al. [282] extracted nano-silica particles from rice-husk as a base for an ERF, by using thermal and acid treatment. Their measurements confirmed a standard ER behaviour of the suspension. Similarly a year later, rice-extracted silica was utilised as a part of core–shell particles in combination with POT coating by Bach et al. [283].

4.5.7. *Cellulose and its derivates*

This linear polymer is the most abundant organic compound which can be obtained from a wide range of plants, including a few types of agricultural waste, i.e. rice husk [284], coconut husk [285], red algae [286], and can be extracted into various forms (nanofibers [287], nanocrystals [288], nanowhiskers [289], aerogels [290], to name a few examples). Aside the abundancy, its other main advantages peak in biocompatibility and renewability. As such, cellulose meets requirements as an eco-friendly, non-toxic, and sustainable candidate for multiple applications, including that of dispersed phase of ER responsive systems. On the other hand, the pure cellulose-based materials exhibit little ER effect, in comparison to inorganic particles-based ERFs [291]. Furthermore, its ER behaviour is very dependent on the presence of water, exposing it to above-mentioned disadvantages of hydrous systems. For these reasons, its derivates are more commonly used [81]. For instance, microcrystalline [292,293] (shown in Fig. 11a) or microfibrillated [294] (as visualized in Fig. 11b, c) cellulose derivates were confirmed as suitable for ERFs.

Kim et al. [124] reported dry-based phosphate cellulose ERF. Similarly, modifications can be utilized. Liu et al. [122]studied pristine cellulose modified by urea-terminated silane (Fig. 11 d, e) and demonstrated changes in morphology, an enhancement of ER

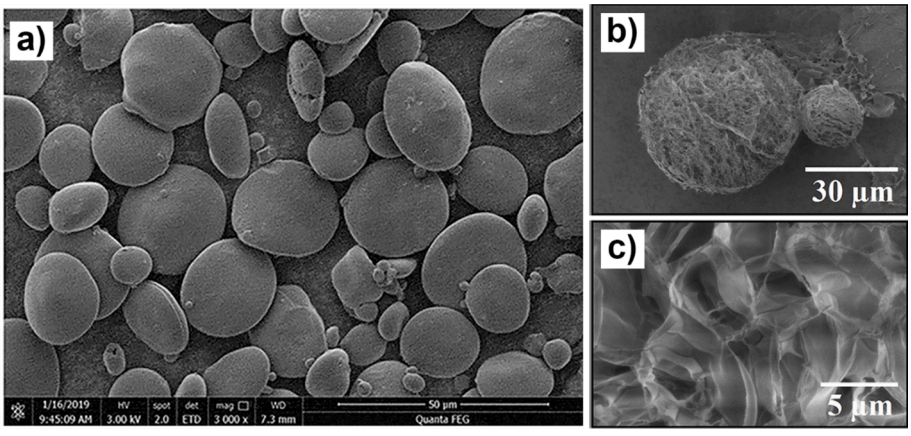

Fig. 12. Scanning electron microscopy images of selected natural organic polymers. Zhang and Zhang [300]: granular starch (a). Kuznetsov et al. [305]: Chitosan particle (b) and porous structure detail (c). Re-printed from Refs. [300,305] with a permission of Taylor & Francis and Elsevier.

properties (achieving exceptional ER efficiency). The modification is also estimated to decrease the particle's sensitivity to water. Two-step carbonization can also be used to improve the material's conductivity and ER effect [295].

In addition, the surface of this biopolymer can be relatively reactive, if given appropriate treatment, thus suitable for modification into composites or as a composite reinforcement [296]. For instance, Liu et al. [291] prepared cellulose/LAP composite particles by a facile dissolution–regeneration method, improving the ER effect and sedimentation stability.

4.5.8. Starch

Alike cellulose, starch is abundant organic material (polymeric carbohydrate), obtainable from various common food sources (such as potatoes [297], corn [298], rice [299], wheat [300]).

The starch-based ER behaviour can be enhanced by modification, for example, substituting its phosphate group through an esterification process [301] or through chlorisarine–functionalization [302], to name a few options. Hybrid feldspar-based carboxymethyl starch was reported by Saboktakin et al. [303] enabling improved control over the design as well as the structure, thus leading to optimized characterization of the material. Last but not least, a biodegradable ERF composed of modified corn starch particles dispersed in corn oil was analysed and showed an ER response with acceptable sedimentation [304]. Example of granular starch particles is presented in a SEM image, Fig. 12a.

4.5.9. Chitosan

Similarly to other previously mentioned biopolymer-based materials, chitosan and chitin-origin products have been peaking in a number of studies, for about two decades now. Its attractivity is based on its abundancy as a resource, unique porous structure, low density, safety, and biodegradability, although it suffers from low mechanical and thermal stability. The chitosan morphology can be seen in Fig. 12, in particular, Fig. 12b.

Their potential in bio-compatible applications has attracted a considerable attention and electrorheology is not an exception. One of the studies was focused on chitosan-based ERF in soybean oil and its ER characteristic [306]. Ko et al. [307] reported results of degree of deacetylation (DD) on gelation of the chitosan suspension dispersion in silicone oil and its influence on the ER effect. Multiple chitosan-based biodegradable nanocomposites have been reported by Cabuk el at. [308,309], namely chitosan/bentonite particles with enhanced viscoelastic properties as a result of the interactions between the chitosan and bentonite [308]. Futhermore the research group introduced ERF based on chitosan/organo-bentonite composites with antibacterial and antifungal properties [309]. Kuznetsov et al. [83,305] reported chitosan-based ERFs of low-volume concentrations (<1.0 wt%) with enhanced sedimentation stability and ER efficiency. The same research group later extended the research to examine α–chitin–based ERF [84] as well as composite particles containing chitosan, cellulose, and polydimethylsiloxane, both at alike-low concentrations [310].

4.5.10. Metal-organic framework

Finally, metal–organic framework materials (MOF) as a hybrid material should be mentioned as it received a considerable attention in various fields of study over the past three decades. This material contains periodic structures of metal elements joined by organic linkers [311], which is illustrated in the bottom schema part of Fig. 13a. Similarly to zeolites or chitosan-based particles, MOF offers unique porous structures and as a result, large active area coupled with low density, metal ions and rich variety of composition as well as option for further modification [312]. Compared to other ERF materials, the MOFs have higher conductivity thus current leakage and as such, they easily cause short circuit. Additionally, in the pure form they offer minor ER effect, as they offer no charge carrier for polarization. However, these drawbacks are possible to overcome by either modification or by including them in a composite particle

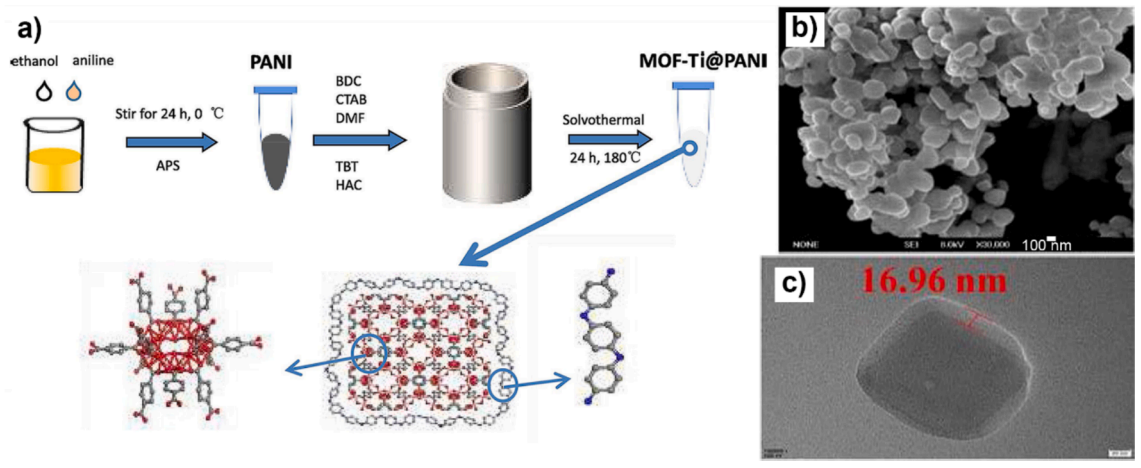

Fig. 13. Example of MOF-based nanoparticles. Wang et al. [314]: Schema of MOF-Ti/PANI synthesis process (a), SEM image of MOF-Ti/PANI-0.2 sample (b) and TEM image of MOF-Ti/PANI-0.2 (c). Re-printer from Ref. [314] with a permission of Elsevier.

[313]. To control the conductivity as well as provide other various advantages, Wen et al. [313] synthesised MOF/PANI composite. The benefits of PANI addition to MOF structure was also confirmed by Wang et al. [314] who prepared MOF-Ti/PANI nanocomposites (presented as an example of MOF-based material in Fig. 13. In this case, appropriate PANI coating was said to decrease zero-field viscosity, improve the dielectric properties, and improve the ER effect. As another example, titanium oxide addition to Ti-MOF was reported to enhance the ER properties through such composite formation, as the nanocomposite particles greatly surpassed pure modified MOF-Ti-based ER fluid performance [315]. In another study [316], MOF-Ti/SiO_2 composite was synthesised with an internal hole structure. This design enables enhanced sedimentation stability, considerable ER efficiency, and additionally, the particles showed unique double dielectric loss relaxation peaks.

Alternative approach to utilize the MOF structure was reported by Li et al. [317] who derived TiO_2 particles from the MOF acquiring hierarchical porous structure. Similarly, He et al. [318] prepared porous titania particles derived from MOF-Ti way using cetyltrimethylammonium bromide-assisted solvent method. The porous-TiO_2-based ERF, in comparison the original Ti-incorporated MOF-based ERF, proved enhanced ER performance and dielectric constant as well as lower current leakage. Extracted in a similar way, TiO_2 particles obtained from Ce-doped-MOF derived resulted in enhancement of ER performance compared to those obtained from non-doped MOF [109]. In comparison to clay particles, a study of preparation of ERF based on MOF particles of $Cu_3(BTC)_2$ confirms that this system surpasses the ER properties of zeolites, in particular 13X type zeolite [319].

4.5.11. Ionic covalent organic framework

As was mentioned, systems based on pure MOF particles possess very little room for polarization. This issue was addressed by Ma et al. [320] who instead focused on multiple ER systems based on ionic covalent organic framework (iCOF) particles, providing a strong interfacial polarization and exceptional yield stress. The same group also introduced a similar water-free system (based on ionic covalent organic polymer particles), effectively increasing the range of working temperature of the ERF [76]. However, iCOF particles as an ERF material has not been explored much and have seen an attention only recently. Nonetheless, this material might be worthy of consideration especially as a modern material, as besides its exceptional interfacial polarization and considerable ER properties, the particles can be tailored to obtain various framework structures with varied ion content [320].

To conclude, following the inorganic materials, various synthetic polymers were explored as dry-based systems, as well as wet-based biopolymer particles for ER dispersed phase. While biopolymers should be considered in regards to ecological sustainability or for biodegradable purposes, the anhydrous polymer-based systems generally offer higher ER effect alongside other desirable properties. In contrast to inorganic particles, polymers offer lower density and therefore higher sedimentation stability. However, they may not be as long-term durable in continuous mechanical load as their inorganic counterparts. In terms of dielectric properties, the organic particles tend to have a higher mobility, therefore a lower relaxation time. Overall, PANI, its derivates, and PPy should be especially considered for ER applications, also chitosan may offer great potential due to its porous nature. Similarly to inorganic section, utilization of composite-based system should be suggested, although, as afore-mentioned, they also have their downsides.

Pure or modified organic particles are summarized in Table 2, following the same criteria as stated above for Table 1. Similarly, composite particles are summarised in Table 3.

5. Giant electrorheological fluids

In relation to the traditional ERFs, giant electrorheological (GER) fluids should be noted, initially they were first mentioned as a model in 2003 by Wen at al. [321]. In comparison to regular ERFs, they differ in specific aspects. While the ER effect of the former usually reaches yield stress less than 10 kPa [322], the shear stress of the GER can achieve considerably higher values up to hundreds of kPa. The high ER effect is caused by polar molecule (PM) dominated ER (PM-ER) effect principle. As such, the GER effect origin lies in the alignment and interaction of the polar molecules with polarization charge on particles, as illustrated in Fig. 14. As the neighbouring particles orient in the electrical field, their PMs strengthen the alignment due to a high local electric field (marked as E_{local}) between two aligned polar particles, as can be seen in the insert in Fig. 14. Consequently, this particular interaction can reach notably higher ER effect than the regular ER particles dielectric interaction [323]. Additionally, Lu and Shen [324] report that even for high local fields

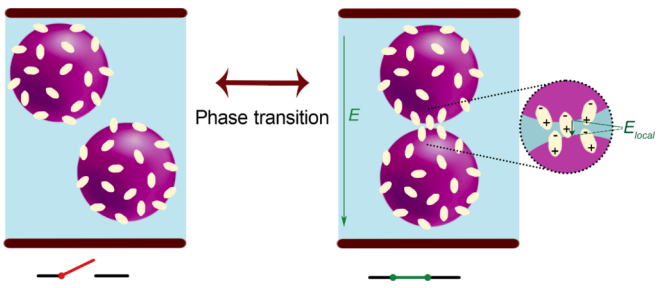

Fig. 14. Schematic illustration of PM-ER interaction between the GER particles in off-field and on-field, with the later highlighting the PM alignment in the local electric field.

which may reach up to 10^8 V m^{-1}, the probability of causing an electrical overload is very low and even if it happens, a macroscale effect should not occur. Owning to these polar molecule interactions, the GER type fluid is often also referred to as PM-ER fluid.

The high performance of GER fluids shows a great potential. For instance, GER was recently suggested to be applied in an electrostatic layer jamming [325,326], 2-degree of freedom damper [327] and in an GER actuator design proposal [326,328]. In comparison to a traditionally applied pneumatic system, the GER provided 4 times faster response, wider stiffness variation range and improved stability when exposed to a higher voltage. However, there are certain weaknesses that hinder their applications. Firstly, the GER fluid lifetime is relatively short as a consequence of the friction loss of the polar molecules [329]. The long-term stability might also be influenced by potential impurities, for instance, from electrodes [330]. Lu and Shen [324] attempted to overcome this drawback by designing a new type of PM-ER, so called PM (L)–ER, with lifetime about 5 times higher than the usual GER fluid, while keeping a reasonable yield stress at high shear rate (in particular, 300 s^{-1}). This improvement was achieved by, instead of adsorbing the polar molecules into the solid particles, the PM being dissolved into the liquid carrier.

A second issue is the thermal stability of the PM-ER fluid. As Qui et al. [329] notes, the dielectric particles with adsorbed PMs are easier to decompose at higher temperature, therefore as their research suggests, improving the thermal stability would result in enhancing its lifetime. As a solution, the research group introduced a GER fluid containing TiO_2 particles inlaid with nanocarbon clusters and dissolved in silicone oil. What is noteworthy, these clusters serve as a nanoconductor replacing the traditional PMs. The GER particles' shape is described as a jujube cake model and as shown in the study results, this novel GER fluid shows an exceptional ER performance, a longer life time, a high thermal stability in comparison to other GER fluids, in addition to a small current leakage.

Qui et al. [331] notes that the presence of water in GER fluids is closely connected to the thermal problem, as it is often used as a solvent or a reactant. Thus, water presence is unavoidable, nevertheless, it increases the current density and reduces the system's resistance to electrical breakdowns. Therefore, the GER fluids are often thermally treated to reduce the presence of water as much as possible. For these reasons, the Qiu's group further studied the effects of adsorbed water on TiO_2-based GER fluid samples of various adsorption energy at different temperatures. The study concluded that samples with low adsorption energy exhibited GER behaviour at room temperature without treatment. However, those with high adsorption energy had to be treated at high temperature, otherwise they exhibited regular ER behaviour. What is more, the high energy sample treated at 175 °C showed GER behaviour when tested at the same temperature. However, Yang et al. [332] analysed the GER dependence on degree of temperature treatment and concluded that after the fluid is treated between 160 °C and 200 °C, the yield stress value consequently decreases and disappears completely if treated at temperature higher than 200 °C. The most efficient temperature for this process was determined to be 120°C.

Thirdly, as noticed by Zhao et al. [333], in the case of alternating (AC) electric field, GER fluids are less reactive and flexible than traditional ERFs. Therefore, their potential for an application under commercial sinusoidal electric field is limited. As the research group further studied, the PM-ER response to electric field of wide range of frequency in alternate triangle and square electric field, the results suggest that the fluids still keep their high shear stress values and would be suitable for applications in the low frequency range of square electric field.

Last but not least, liquid carrier affects the ERF performance, as was previously mentioned in the respective section, and GER fluids are no exception. As previously mentioned in the Liquid carrier section, Hong and Wen [69] focused on urea-coated barium titanyl oxalate particles used as GER phase. In total, six different kinds of liquid medium were tested (dimethyl terminated silicone oil, hydrogenated silicone oil, white mineral oil, liquid paraffin, sunflower seed oil, and corn oil) and proved diverse results. The study also tested the permeability of the oils thought Washburn method and confirmed the wetting effect though a rheological analysis. Furthermore, the study suggests that the hydrogenated silicone oil is wetting perfectly with the GER particles while giving them a reasonable amplifying ratio. Additionally, the authors consider this type of GER to have the compatibility to broaden its application to microfluidics [69].

Another alternative approach to improve the measurement and application of PM-ER fluids suggested by Wang et al. [334] introduced electrodes with a modified surface for devices using GER fluids. The reason is, unlike the traditional ERF particles, the PM interactions and alignment cause slip at the interface between the fluid and electrodes. This slip consequently hinders the measurement and application. Multiple kinds of electrodes were tested for measuring the ER effect of calcium titanate nanoparticle PM-ER fluid and the best results were achieved with modified electrodes coated with diamond and aluminium grains. The same research group [335] further extended their research of GER fluids interaction with devices onto a rheometer as well, suggesting a method for a more precise measuring method of the intrinsic yield stress and shear modulus of PM-ER fluids. The newly obtained results were compared with data from a regular rheometer which resulted in considerably lower values.

Inspired by the PM effect, Xu and Tian et al. [336] modified TiO_2 particles (1,4-butyrolactone–TiO_2) with adsorbed polar molecules and reported considerable yield stress of 48.1 kPa at 5 kV mm^{-1} (with approximately 61.7 ER efficiency) and almost unnoticeable sedimentation for approximately 20 days. The authors further compare these modified TiO_2-based ERF with another GER system.

To summarize, GER fluids may offer unique areas of research. For more detailed comparison, Table 4 summarizes, alike the other tables, chosen key aspects of above-referenced GER particles; however, in these cases, ER efficiency data and conductivity were very limited, thus omitted in the table.

Table 1
Summary of inorganic-based particles.

Material and liquid carrier	Approximate size	Geometry	Concentration	DC Conductivity ($S\ cm^{-1}$)	ER efficiency — 0.1 (s^{-1})	100 (s^{-1})	Additional notes	Publication
TiO_2Silicone oil	10 nm ø, length up to several μm	Tube-like	10 vol%	NA	580.6 (1 s^{-1})	28.4 3 kV mm^{-1}	Synthesised by hydrothermal treatment of TiO_2 in alkaline solution. Extraordinary aspect ratio. Enhanced sedimentation stability; 3 wt% and 10 wt% concentrations were compared, the latter is said to retain stable dispersion stability after several months.	Yin and Zhao [40]
Oxalate group-modified TiO_2Various silicone oils	200–500 nm	Amorphous	30 vol%	NA	The highest: 50 cSt silicone oil sample: 2.43 Hydroxyl terminal groups oil 25 cSt: 14.9 5 kV mm^{-1} (0.2 s^{-1})	NA	Analysis of various kinds of liquid carrier in terms of ER performance, current leakage, and sedimentation ratio. In particular, dimethyl silicone oil of viscosities ranging from 20 to 1000 cSt were tested, as well as silicone oils with differing terminal groups (hydroxyl 25 cSt, hydrogen 50 cSt, and methyl 50cSt).Off-field viscosity of ERF were rather high, indicating their nature as Bingham fluids rather than Newtonian.	Ma and Dong [64]
Nb-doped TiO_2Silicone oil	500 nm	Spheres	10 wt%	NA	52.8 (1 s^{-1})	21.8 4 kV mm^{-1}	Focus on low frequency range in dielectric spectroscopy.	Guo et al. [33]
Ce-doped TiO_2Silicone oil	NA	Crystal-like structure	18 vol%	The highest: 8.5 mol % Ce–doping at 75 °C temperature 1.8×10^{-8}	The most optimal: 8.5 mol % Ce-doping: 173.4 (1.5 s^{-1})	10.6 (65 s^{-1}) 3 kV mm^{-1}	Water-free. Doping at various mol. ratio analysed. Temperature effect on shear stress analysed: Ce-doping increased the working temperature.	Zhao et al. [128]
Rare earth-doped TiO_2Dimethyl-silicone oil	100 − 1000 nm ø	Spheres	27 vol%	10^{-11}	88.7 (2 s^{-1})	6.5 3 kV mm^{-1}	Porous, pore size about 2 − 3 nm. The properties and ER performance was compared with single Ce doped particles, proving the enhancement through the adjusted doping and porous structure, reaching up to 8.1 kPa yield stress in 3 kV mm^{-1}. The temperature-dependence of ER performance was also evaluated.	Yin et al. [129]
Cr-doped TiO_2Silicone oil	7.2 nm	Crystal	18 vol%	NA	356.8 (1 s^{-1})	31.1 5 kV mm^{-1}	Porous, pore size abour 5–7 nM. Size and properties compared with non-porous Cr-doped titania and poroun undoped particles.	Yin and Zhao [110]
Cr-doped TiO_2Silicone oil	1–3 μm average length	Rod-like	5 wt%	NA	The most efficient: 0.7 mol% doping concentration:5436.5	9.7 3 kV mm^{-1}	Nanocavities (their size is expected around 10–20 diameter according to literature) on the surface. Doping concentration tested in range 0–5 mol %. The highest ER effect was shown by 0.7 mol% Cr doped titania.	Almajdalawi et al. [131]

(*continued on next page*)

Table 1 (*continued*)

Material and liquid carrier	Approximate size	Geometry	Concentration	DC Conductivity ($S\ cm^{-1}$)	ER efficiency — 0.1 (s^{-1})	100 (s^{-1})	Additional notes	Publication
SDS–modified TiO_2Silicone oil	120 nm at 1.2 SDS wt%, 500 nm at 2 SDS wt %	Spherical-like	30 vol%	NA	The highest: 1.2 wt% SDS mod.: 30.8 (3 s^{-1})	14.5 3 kV mm^{-1}	SDS modification concentration affects the particle size. Modification significantly improved wettability and sedimentation. The smaller particles resulting from the 1.2 wt%SDS concentration exhibited higher ER effect, but also increased current density.	Qiao et al. [132]
Diammonium phosphate-modified TiO_2Dimethyl silicone oil	1–2 μm average ø	Spheres	30 wt%	NA	The highest:S1 (0.03 mol modification): 1217 5 kV mm^{-1}	NA	Multiple samples with diverse amount of DAP modification (0.03 mol, 0.05 mol, and 0.07 mol). While the 0.03 mol modified sample reached the highest ER efficiency, the 0.07 mol sample reached overall the highest shear stress values.	Ma and Dong [133]
IL-modified TiO_2Silicone oil	430 nm average ø	Spheres, rough surface	20 vol%	NA	5015	29 4 kV mm^{-1}	Modification decreased the particles' size improved sedimentation stability.	Zhang et al. [134]
Succinic acid modified TiO_2Silicone oil	2–3 μm	Wallnut-like	Varied, 30, 40, and 50 wt%	NA	The highest: 30 wt%: 13028.2 (0.14 s^{-1})	30 wt%: 47 3 kV mm^{-1}	Multiple concentrations were compared in terms of ER performance. Sedimentation ratio was evaluated for 30 wt% and 40 wt% samples, being stable at 88.6 % and 91.8 %, respectively, after 30 days. The highest yield stress	Hu et al. [137]
Dual-IL and acetic acid modified TiO_2Silicone oil	Around 50 nm	Grain	Varied, 15, 22, and 25 vol%	1.28×10^{-7}	The most optimal: 15 vol%: 48.66 4 kV mm^{-1}	For 15 % at room temperature: 11.2 2 kV mm^{-1}	Comparison of dual-modified particles with single modifications included. IL-single modification has higher ER effect and yield stress, but also very high current density. Dual-modified particles exhibit the lowest zero field viscosity. Wide working temperature, ER effect evaluated in a temperature range 5–85 °C.	Zhao et al. [138]
TiO_2Silicone oil	3.8 μm	Hollow sea-urchin like	5 vol%	NA	1253 (1 s^{-1})	9.1 3 kV mm^{-1}	Improved sedimentation ratio in comparison to pure TiO_2	Cheng et al. [108]
TiO_2Silicone oil (polydimethyl siloxane)	Approximately 300–400 nm	Hollow cube-like	10 wt%	NA	48.9 (0.4 s^{-1})	5.2 (27 s^{-1}) 3 kV mm^{-1}	Porous. First, $TiOF_2$ nanocubes were synthesised and used as a precursor to the hollowed 'nanobox' titania particles. When compared to the precursor particles, the hollowed nanobox particles proved increased ER performance.	Li et al. [349]
Cr-doped TiO_2Silicone oil	3.2 μm	Sea urchin-like	10 vol%	NA	487.2 (1 s^{-1})	39.1 4 kV mm^{-1}	Rods creating the sea urchin structure are about 20–30 nm. The morphology improved ER behaviour, yield stress, polarization, in comparison to smooth spheres and less–developed sea urchin-shaped particles.	Yin et al. [368]

(*continued on next page*)

Table 1 (*continued*)

Material and liquid carrier	Approximate size	Geometry	Concentration	DC Conductivity ($S\ cm^{-1}$)	ER efficiency — 0.1 (s^{-1})	100 (s^{-1})	Additional notes	Publication
Ce-doped TiO_2Silicone oil	Nano range	Crystal-like structure	Varied, 18, 23, 26, and 33 vol%	NA	The most optimal: 33 vol%: 3381 3 kV mm^{-1} (0.2 s^{-1})	NA	Mesoporous. Pore size 5–7 nm. Very high shear stress reached – nearly 55 kPa at 3 kV mm^{-1} and exceeds 70 kPa at 4 kV mm^{-1}, but at this field fracture-like phenomenon collapses the ER-induced chain-like structures.	Yin and Zhao [373]
Y-doped BaTiO3dimethyl-silicone oil	NA	NA	18 vol%	Varied, depending on the doping. 13.8 mol% doping: In a range 10^{-10}	13.8 mol% sample: 105 (1 s^{-1})	13.8 mol% sample: 8.2 3 kV mm^{-1}	Y-doping applied with varying mol% ratio (0–18 mol%), with 13.8 mol% achieving the most optimal ER results. The doping degree highly influenced the crystal structure of the particles, their dielectric properties, and consequently the ER properties. The ER properties were well-improved in comparison to pure $BaTiO_3$ particles.	Yin and Zhao [141]
$SrTiO_3$Silicone oil	Depending on the pH during synthesis; up to 200 nm	Depending on the pH during synthesis; amorphous or spheres	NA	NA	NA	NA	Porous. Synthesised through ultrasonic irradiation method under various degrees of pH (3–12). The pH affected morphology, particle size, and crystallinity, consequently also the pore size. The 10 pH particles seem to reach the highest ER effect..	Jiang et al. [106]
SiO_2Silicone oil	50, 100, 150, 350 nm	Spheres	3 wt% Further, ratio of spheres to rods was tested from 3-15 wt% spheres to 97–85 wt% rods	NA	The highest ER performance:Mix 1 (3 wt% of 50 nm spheres, 97 wt% 5 L/D rods)53.1	NA	Evaluation of bimodal systems. The spherical and rod-shaped particles of various sizes were evaluated in total of 60 different combinations, with also changing the ratio of spheres to rods. Sedimentation stability evaluated.	Yoon et al. [147]
Pure SiO_2, and modified SiO_2 (Co), SiO_2 (Zr)Silicone oil and vaseline oil compared	SiO_2 1.2 μm, SiO_2 (Co) 1.15 μm, SiO_2 (ZR) 1.35 μm	Grain Amorphous Amorphous	20 wt%	NA	The highest: SiO_2 (ZR) 15.1 at 4 kV mm^{-1} (25 s^{-1})	NA	Each type of silica particles has different porosity and specific surface area (Co-modification the lowest and Zr the highest), Zr-modification also had more favourable dielectric properties. Vaseline oil proved better performance. Confirmed enhanced performance in an ER damper with Zr-silica and Vaseline oil ERF.	Cherif et al. [111]

(*continued on next page*)

Table 1 (*continued*)

Material and liquid carrier	Approximate size	Geometry	Concentration	DC Conductivity ($S\ cm^{-1}$)	ER efficiency — 0.1 (s^{-1})	100 (s^{-1})	Additional notes	Publication
SilicaSilicone oil	80–100 nm	Irregular	10 vol%	8.1×10^{-8}	515.6 (1 s^{-1})	14.1 2 kV mm^{-1}	Post-treatment of agricultural waste. Silica was extracted from rice husk by thermal method.	Kwon et al. [282]
TS-1Silicone oil	Nano-sized: 50–100 nm	Granular-like	10 wt%	10^{-10}	The highest:Nano-sized:199.5	Nano-sized: 3.8 3 kV mm^{-1}	Comparison of nano- and sub-micron particle size. Multiple samples were synthesised in total of 3 series. Resulting particle size was dependent on crystallization conditions (temperature and time). Sedimentation stability evaluated. Zeolite formation model is proposed.	Liu et al. [178]
Goethite,Silicone oil	Sub-micron sized: 100–200 nm	Varied	Varied 2–15 vol%	10^{-11}	NA	NA	Comparison of various types, concentration, elongated particles showed improved ER effect in comparison to hematite.At least 4 vol% concentration is necessary for a reasonable ER response	Ramos Tejada et al. [173]
Goethite,Silicone oil	Varied	Varied		NA			Comparison of various types, concentration, elongated particles showed improved ER effect in comparison to hematite.At least 4 vol% concentration is necessary for a reasonable ER response	
Hematite,Silicone oil	105 nm mean ø Pure SEP Length 1100 ± 600 nm, ø 27 ± 7 nm Pure LAP 21 ± 4 nm	Irregular, polyhedral structure Fiber Plate-like	The most optimal for pure and coated: 10 vol%	NA	(calculated from: 0.4 kV mm^{-1} and 1.4 kV mm^{-1}) The highest: ORG-SEP: 18.5 (0.006 s^{-1}) Pure SEP: 4.6 (0.007 s^{-1})	(calculated from: 0.4 kV mm^{-1} and 1.4 kV mm^{-1}) ORG-SEP 16.5 (0.19 s^{-1}) Pure SEP: 2.1 (1.6 s^{-1})	Extensive analysis of ER performance of pure and ORG-modified MMT, SEP, LAP, as well as mixed systems. The highest yield stress: the treated SEP. The treatment also improved ERF stability in higher el. fields. MMT and ORG MMT generally creates less stable chains on-state, but is improved in a mixed system.	Ramos Tejada et al. [174]
GO Silicone oil [poly (methylphenylsiloxane)]	NA	Sheets	<1 wt%	1×10^{-7}	Solvent exchange method:7.2 Mechanically ground GO:	NA NA	Comparison of suspensions of mechanically ground GO and solvent exchanged GO method. The latter method resulted in considerably	Hong and Jang [189]

(*continued on next page*)

Table 1 (*continued*)

Material and liquid carrier	Approximate size	Geometry	Concentration	DC Conductivity (S cm^{-1})	ER efficiency — 0.1 (s^{-1})	100 (s^{-1})	Additional notes	Publication
					3.4 5 kV mm^{-1}		improved sedimentation stability (in particular, the solvent exchanged particles remained at almost 90 % after 90 days, whereas the alternative dropped to 10 %).	
GO-ModifiedSilicone oil	NA	Sheets	5 wt%	Varied in a range: 2.92—6.62 × 10^{-8} The highest: GO–CBE	The highest:GO-SB:1476.8	GO–SB: 0.733 kV mm^{-1}	Comparison of various modifications (3–(trimethoxysilyl)propane-1- thiol; sulfobetaine moiety; carboxybetaine ester moiety; carboxybetaine moiety were used in separate modifications) GO-SB had highest ER efficiency, GO-CBE reached the highest yield stress. 1 wt% concentration was also ER effective.	Illcikova et al. [193]
rGO-modified by poly(butyl methacrylate)Silicone oil	5 nm thickness	Sheets	5 wt%	6 × 10^{-7}	1065	9.1 (52 s^{-1} γ) 2.5 kV mm^{-1}	Improved ER performance and sedimentation stability in comparison to pure rGO. Enhanced wettability and interaction with silicone oil.	Mrlik et al. [194]
Expanded perliteSilicone oil	7.1 μm average	Amorphous structure	Varied, 2.5–15 vol%	NA	The highest: 10 vol% sample: 16.6 (1 s^{-1})	10 vol% sample: 1.3 3.5 kV mm^{-1}	Different volume concentrations compared. Sedimentation evaluated in the length of 30 days and under different temperatures. High sedimentation and colloidal stability, best sedimentation stability (96 %) at –25 °C.	Cabuk et al. [374]
TEA-modified MCM–41Silicone oil	Primary size 1 μm, agglomerates approx. 11 μm	Nearly spherical	5 vol%	NA	1331.5 (0.5 s^{-1})	6.4 3 kV mm^{-1}	Porous. The pore volume of the modified particles was reduced in comparison to pure MCM-41. The modification enhanced polarization and ER effect, as well as proved higher elasticity.	Cheng at al. [376]
Particulate matterSilicone oil	1–22 μm	Irregular	5 vol%	2.19 × 10^{-8}	122 (1 s^{-1})	21.3 (10 s^{-1}) 4.5 kV mm^{-1}	Post-treatment of dust waste.	Jeong et al. [281]

Table 2
Summary of organic-based particles.

Material and liquid carrier	Approximate size	Geometry	Concentration	DC Conductivity (S cm^{-1})	ER efficiency — 0.1 (s^{-1})	100 (s^{-1})	Additional notes	Publication
PANISilicone oil	200 nm ø, shell thickness 50 nm	Hollow spheres	10 vol%	In a range from 9 × 10^{-9} to 11 × 10^{-9}	36.1 (20 s^{-1})	38.63 kV mm^{-1}	Hollowed particles. Improved sedimentation stability.	Sung et al. [36]
PANICarrier NA	Range in nm	Granular	NA	3.7	NA	NA	Synthesis is focused, no direct ER measurement.Oxidation in highly acidic medium	Stejskal et al. [210]
	Range in nm	Tubes		0.036			Oxidation in weak acidic medium	
	Range in µm	Spheres		<10^{-10}			Oxidation in alkaline medium	
PANISilicone oil	200 nm ø, 1–5 µm lenght	Fibrous	10 wt%	3.9 × 10^{-9}	160.3 (45 s^{-1})	656 kV mm^{-1}	Static yield stress and sedimentation stability were evaluated for varying concentrations (5, 10, and 15 wt %), with the fibrous particles achieving superior results. The flow curve graphs show the dispersions performance until 1000 s^{-1}.	Yin et al. [99]
		Granular		2.1 × 10^{-9}	144 (45 s^{-1})	117.46 kV mm^{-1}		
PANI carbonizedSilicone oil	Micron range, size is varied depending on preparation and carbonization conditions	Spherical, or rather irregular	10 wt%	Varied, the most ER effective: 9.90 × 10^{-8}	The highest: Carb. PANI with 0.2 M NH_4OH:674	Carb. PANI with 0.2 M NH_4OH: 4.2 3 kV mm^{-1}	Conductivity and ER efficiency are varied depending on the molarity of NH_4OH during the synthesis. The highest values were achieved by carbonized PANI with 0.2 M NH_4OH during synthesis.	Plachý et al. [212]
PANISilicone oil	500 nm ø, length can reach several µm	Rectangular tube–like	10 vol%	10^{-11}	219	12.4 2.5 kV mm^{-1}	In comparison to a regular particulate PANI, this morphology resulted in improved dispersion stability, ER performance, and dielectric propertied. The rectangular-like PANI tubes showed rough surface covered with nanorods (average length of these nanorods was about 50 nm).	Lee et al. [369]
Silica-grafted CT from carbonized PANISilicone oil	200 nm ø,Length NA	Nanotubes	10 vol%	NA	3642 (0.4 s^{-1})	43.6 2.5 kV mm^{-1}	Carbonized PANI was used to create CT particles. Silica-grafted CT showed lower zero-field shear stress. Enhanced particle wettability, sedimentation stability (94 % after 1000 h) and efficiency in comparison to pure CT.	Yin et al. [213]
PIL-basedSilicone oil	~1.8 µm	Spheres	Varied: 3–36 vol%	2.2 × 10^{-9}	The highest: 28 vol% sample: 221.2 (0.2 s^{-1})	28 vol% sample: 34.5 3 kV mm^{-1}	Synthesized by microwave-assisted dispersion polymerization method. Hydrophobic and low density (~1.62 g cm^3) is estimated to	Dong et al. [228]

(*continued on next page*)

Table 2 (*continued*)

Material and liquid carrier	Approximate size	Geometry	Concentration	DC Conductivity (S cm^{-1})	ER efficiency — 0.1 (s^{-1})	100 (s^{-1})	Additional notes	Publication
							contribute to a good sedimentation stability (approximately 80 % after one month). The 36 vol% concentration sample reached the highest shear stress, but also had the highest off-field viscosity.	
PPySilicone oil	100–200 nm ø 100–200 nm ø and length 1–2 μm	Granular Fiber	10 vol%	5.8×10^{-9}	45.0 (25 s^{-1})	11.3 4 kV mm^{-1}	The fiber morphology proved to be superior of the two. Temperature effect on conductivity during thermo-oxidative time is evaluated; conductivity declines over the extended time.	Xia et al. [242]
PPySilicone oil	Individual fibers in a range of 25–85 nm	Ribbon-like structure formed by a network of fibers	3 wt%	6.5×10^{-9}	The highest, sample 2: 26.7 (12 s^{-1})	Sample 2: 2.5 3 kV mm^{-1}	The polymer was treated by NH_4OH, sample 1 once and sample 2 double-treated.	Almajdalawi et al. [243]
PNEAP2EAPNMAPOTSilicone oil	PNEA average ø 9.08 μm P2EA average ø 8.51 μm PNMA average ø 11.22 μm POT average ø 13.46 μm	Shared alike closed-packed structure	15 wt%	5.9×10^{-7} 1.2×10^{-7} 2.4×10^{-7} 6.8×10^{-7}	All around similar values in a range of:11 – 35	All around similar values in a range of: 0.2–1.1 (20 s^{-1}) 3 kV mm^{-1}	The sedimentation stability of all derivates is of similar level. The highest ER effect was observed for POT particles.	Gercek et al. [252]
POASilicone oil	1 μm average ø with 190 nm shell	Hollow spheres	5 vol%	NA	32.1 (0.3 s^{-1})	2.6 (10 s^{-1}) 3 kV mm^{-1}	Hollowed structure achieved through template-free synthesis. Enhanced sedimentation stability, but lower ER effect in comparison to regular granular POA particles.	Cheng et al. [372]
PPD oxidized with p-benzoquinoneSilicone oil	Varied, size increases with higher MSA concentration	Irregular	10 wt%	Varied, the most suitable for ERF: 0.2 mol L^{-1} MSA, 8.5×10^{-11}	The highest: 0.2 mol L^{-1} MSA:2259.8	0.2 mol L^{-1} MSA: 8.5 3 kV mm^{-1}	Oxidation in presence of methanesulfonic acid (MSA), its amount affects resulting properties. Most promising when 0.2 and 0.5 mol L^{-1} MSA was used.	Plachý et al. [261]
PPD isomers: P-1,4-PDA,P-1,3-PDA,P-1,2-PDASilicone oil	Varied, maximum 0.1 mm	Varied	10 wt%	P-1,4-PDA 2.4×10^{-10} P-1,3-PDA 2.1×10^{-11} P-1,2-PDA 9.7×10^{-12}	The highest: P-1,4-PDA: 3.5 (0.9 s^{-1})	P-1,4-PDA: 0.5 (2.25 s^{-1}) 2.5 kV mm^{-1}	Comparison of PDP isomers, base and protonated ones. The highest ER effect was observed for P-1,4-PDA.	Trlica et al. [262]
*Pp*PDA carbonizedSilicone oil	Micron range, varied	Irregular	6 vol%	Estimated 2.4×10^{-10}	The highest:Non-carbonized:1307	Non-carbonized: 2.3 2 kV mm^{-1}	Higher temperature of carbonization lead to higher specific surface area. The highest values were achieved by non-carbonized *Pp*PDA and closely after by carbonized at 200 °C.	Plachý et al. [263]

(*continued on next page*)

Table 2 (*continued*)

Material and liquid carrier	Approximate size	Geometry	Concentration	DC Conductivity ($S\ cm^{-1}$)	ER efficiency — 0.1 (s^{-1})	100 (s^{-1})	Additional notes	Publication
PlnSilicone oil	300–400 nm	Spherical, mostly irregular form	5 vol%	1.3×10^{-12}	1498.1	9.46 2.5 kV mm^{-1}	Particles synthesized through emulsion polymerization. Sedimentation stability evaluated and estimated to be appropriate.	Park et al. [269]
PPPSilicone oil	1–22 μm	Grain	15 wt%	Varied, samples range between: 4.8×10^{-9} up to 4.9×10^{-4}	The highest: Sample based on Hirai method: 17.7 (12 s^{-1})	HIR1: 3 at 2.2 kV mm^{-1} (200 s^{-1})	A wide range of samples tested and compared based on: 3 ways of synthesis, different degree of crystallinity, and degree of doping. The correlations between doping and modification were evaluated. The effect of polymer crystallinity was demonstrated.	Krzton-Maziopa et al. [274]
Aminated polyacrylonitrileSilicone oil	45.82 μm, and 220.91 nm	Spheres	20 vol%	NA	The highest: animated micron PAN: 152.7 (20 s^{-1})	12 3 kV mm^{-1}	Particle size focused, micro PAN, nano PAN, aminated micro PAN and aminated nano PAN were compared. The aminate-modification enhanced the particled ER properties, and the micron size animated PAN demonstrated higher ER effect.	Saabone [354]
Ground coffee-basedSilicone oil	20–75 μm	Irregular, but close to crinkled-globular	Varied: 10–50 vol%	The highest: 50 vol%: 16×10^{-9}	The highest: 40 vol %: 69.8 (20 s^{-1})	36.9 3 kV mm^{-1} (200 s^{-1})	Ground coffee waste post-treatment. Conductivity increases with concentration. The 40 vol% sample showed promising ER. The data of shear stress over shear rate are available until 1000 s^{-1}.	Chun et al. [280]
Algae-basedSilicone oil	17–21 μm	Crinkled-globular shape	30 vol%	$<1.4 \times 10^{-11}$	The highest: *C. pyrenoidosa:* 102.7 (20 s^{-1})	*C. pyrenoidosa: 9.5* 3 kV mm^{-1} (200 s^{-1})	Algea post-treatment. Various types of algae were compared with cellulose. *C. pyrenoidosa* shows promising yield stress. The data of shear stress over shear rate values are available until 1000 s^{-1}.	Chun et al. [75]
Cellulose carbamateSilicone oil	In a range between 21.65–205.50 μm	Fiber-like	0.5 wt%	NA	98.9 (22.5 s^{-1})	60 (52 s^{-1}) 2.5 kV mm^{-1}	Cellulose carbamate synthesised from kenaf core pulp through microwave reactor-assisted method.	Gan et al. [81]
Phosphate celluloseSilicone oil	Micron range	Irregular, rod-like	10–25 vol%	NA	87.8 (1.3 s^{-1})	23.6 5 kV mm^{-1}	Various concentrations tested. Yield stress and storage and loss moduli increased with rising concentration.	Kim et al. [124]
Microcrystalline cellulose; nanocelluloseOlive oil	MCC ~34 length, ~11 ø; Nanocellulose 60–100 nm in length and 5–9 nm ø	Fibrous and crystalline, needle-like in a suspension	1 wt%	1.8×10^{-13} 2.0×10^{-13}	MCC: 2025.6 (1 s^{-1}) Nano: 2481.3 (1 s^{-1})	13.2 5 kV mm^{-1} 7.53 5 kV mm^{-1}	Biodegradable. Comparison particle size influence on ER effect evaluated (increased aspect ratio for the nano-sized led to enhanced ER effect). Nano-cellulose also reached higher yield stress.	Kuznetsov et al. [85]

(*continued on next page*)

Table 2 (*continued*)

Material and liquid carrier	Approximate size	Geometry	Concentration	DC Conductivity (S cm^{-1})	ER efficiency — 0.1 (s^{-1})	100 (s^{-1})	Additional notes	Publication
Microcrystalline celluloseSilicone oil	Average ø 10–90 μm	Irregular, crystalline structure	10 vol%	10^{-7}	2934 (0.14 s^{-1})	22.4 1.3 kV mm^{-1}	Particles obtained from natural raw rice husk through alkali treatment, bleaching, and hydrolysis. The ERF reached a considerable ER efficiency in a comparably rather low electrical field.	Sim et al. [292]
PhosphateMicrocrystalline celluloseSilicone oil	25.3 μm average	Irregular, fiber-like	10 vol%	5.3×10^{-8}	931.1 (1 s^{-1})	32.4 3 kV mm^{-1}	Cellulose extracted from rice husk. The cellulose was modified through phosphoric esterification.	Bae et al. [293]
Microfibrillated celluloseSilicone oil	500–1000 nm width up to < 10 μm in lengh	Rod-like	10 vol%	NA	109.6 (16 s^{-1})	18.6 2 kV mm^{-1}	Cellulose extracted from rice husk, then produced through a low-pressure alkaline delignification procedure.	Choi et al. [294]
Urea-terminated silane modified celluloseSilicone oil	20–100 μm	Irregular, rod-like	15 wt%	NA	37174.82	134.2 4 kV mm^{-1}	The modified particles had similar size, but gained porous surface (pore size around 5–20 μm) and their ER properties were improved in comparison to the unmodified particles. The treatment is also assumed to make the particles less sensible to water.	Liu et al. [122]
Hydrolysed cellulose	Varied, depending on the degree of hydrolysation. Pure cellulose: 60–100 μm, HC16: 10–50 μm	Varied,The original pure particles: rod-like shape, HC16: sheets	10 wt%	NA	Raw cellulose: 12,904The most optimal:HC16 sample:6582	Raw cellulose: 43.7 HC16: 102 4 kV mm^{-1}	Various morphology and ER performance are compared depending on a degree of hydrolysation (4, 8, 12 and 16 h). Hydrolysed samples gained higher off-field viscosity.Samples HC12 and HC16 (hydrolysed for 12 and 16 h, respectively) showed similarly high values in terms of shear stress and complex modulus.	Liu et al. [364]
Carbonization-modified celluloseSilicone oil	Up to 100 μm	Irregular	5 wt%	3.48×10^{-6}	1950.1	1.9 1.5 kV mm^{-1}	Performed in two steps, hydrothermal and thermal carbonization. The process enlarged the particles' active surface area, improved conductivity and ER performance.	Plachy et al. [295]
Phosphate starchSilicone oil	5–60 μm	Ovoid	10 vol%	NA	The highest: sample 3: 45.6 (100 s^{-1})	Sample 3: 2.9 (1000 s^{-1}) 3 kV mm^{-1}	Three samples are presented with variety of phosphate substitution (0.027, 0.044, and 0.056). Sample 3 (the highest degree of substitution) showed the best ER performance.	Park et al. [301]

(*continued on next page*)

Table 2 (*continued*)

Material and liquid carrier	Approximate size	Geometry	Concentration	DC Conductivity (S cm^{-1})	ER efficiency — 0.1 (s^{-1})	100 (s^{-1})	Additional notes	Publication
Modified corn starchCorn oil	NA	NA	Varied, optimal 30 wt%	4×10^{-9}	4 (1 s^{-1})	0.3 (20 s^{-1}) 2 kV mm^{-1}	Biodegradable. Modification enables the starch as a dry-base system in contrast to wet-base as pure. Optimal sedimentation stability. Optimal concentration was determined at 30 wt%.	Yavuz et al. [304]
ChitosanCorn oil	Adjusted by 100 μm sieve	Irregular	The most optimal: 25 wt%	5.26×10^{-10}	318.2 (15 s^{-1})	37 3 kV mm^{-1}	Anhydrous and biocompatible. Concentration tested at 10, 15, and 25 wt%, the last proved as the most efficient.	Sung et al. [306]
Chitin, chitosanSilicone oil	17 μm average ø	Irregular, granular-like	30 vol%	$< 6 \times 10^{-8}$	The highest: 87.3 % of DD: 33.5 (2 s^{-1})	10.1 3 kV mm^{-1}	Chitin and chitosan compared. Gelation and different degree of deacetylation (DD) effects analysed (73.2 %, 83.8 %, 87.3 %, 93.4 %, and 99.3 %). Chitosan 87.3 % DD showed the highest ER effect. Shear stress dependence on temperature is evaluated (25 °C used for ER efficiency calculation).	Ko et al. [307]
ChitosanSilicon oil (Polydimethylsiloxane)	50–60 μm, agglomerating up to 300	Spherical, open pore structure	0.1, 0.5, and 1.0 wt%	Varied, from 1.7×10^{-13} to 1.3×10^{-12}	0.1 wt%: 49.2 0.5 wt%: 34.7 5 kV mm^{-1} (1 s^{-1})	NA	An increase of porosity enhanced sedimentation stability (0.5 wt% showed the best sedimentation stability with the 1 wt% almost as high). Low particle concentration evaluated. The concentration threshold of percolation is expected approximately at 0.5 wt%.	Kuznetsov et al. [305]
ChitosanExtra virgin olive oil	Average size 50 – 60 μm, high polydispersity	Spherical	Varied, 0.1, 0.5, and 1.0 wt%	NA	The highest: 0.1 wt%: 138.4 4 kV mm^{-1} (1 s^{-1})	NA	Biodegradable. Low particle concentration is focused. Higher porosity than for pristine chitosan, high sedimentation stability (1.0 wt% sample exhibited the best stability).	Kuznetsov et al. [83]
α-chitinSilicone oil	5.7 nm height and 380 nm length	Rod-like	0.5 wt% and 1.0 wt%	NA	The most promising: 1.0 wt %:2947.48213	For 1.0 wt%: 9 3 kV mm^{-1}	Low particle concentration is focused. Sedimentation stability was evaluated, improvement modification is suggested.	Kovaleva et al. [84]
Derived TiO_2 from Ti-incorporated MOFSilicone oil	400 nm	Square-like	10 wt%	NA	72.2 (0.5 s^{-1})	1.7 3 kV mm^{-1}	MOF prepared through CTAB assisted solvothermal method and then calcined. The effect of amount of CTAB was evaluated, and it influenced the morphology control of MOF. TiO_2 with porous structure was inherited from MOF and the porous titania particles exhibited improved ER properties	He et al. [318]

(*continued on next page*)

Table 2 (*continued*)

Material and liquid carrier	Approximate size	Geometry	Concentration	DC Conductivity ($S\ cm^{-1}$)	ER efficiency — 0.1 (s^{-1})	100 (s^{-1})	Additional notes	Publication
							and current leakage in comparison to the original Ti-incorporated MOF-based ERF.	
Ce-doped MOF-based TiO_2Dimethyl silicone oil	Varied with doping	Decahedron, varied	10 wt%	Varied, changes by doping percentage in range 10^{-8}–10^{-6}	The most optimal: 1.5 % Ce-doped TiO_2: 104.6 (1 s^{-1})	1.5 % Ce-doped TiO_2: 3.9 3 kV mm^{-1}	Cerium doping applied in various molar ratio (resulted in 1, 1.5, 2, 3, and 5 % Ce) during MOF synthesis applied. The doping affected multiple properties, including particle morphology. Obtained porous Ce-doped TiO_2 derived from MOF showcased enhanced ER performance in comparison to regular TiO_2. 2 % Ce-doped TiO_2 exhibited the largest active surface area, but als the highest current leakage density.	Zheng et al. [109]
$Cu_3(BTC)_2$ −based MOFSilicone oil	Expected 3.5 μm	Crystals	15 vol%	NA	7.6 (20 s^{-1})	3.2 (65 s^{-1}) 2.5 kV mm^{-1}	Porous, large active surface area. Enhanced ER properties in comparison to zeolite particles.	Liu et al. [319]

Table 3
Summary of composite particles.

Composite type	Material and liquid carrier	Approximate size	Geometry	Concentration	DC Conductivity (S cm^{-1})	ER efficiency — 0.1 (s^{-1})	100 (s^{-1})	Additional notes	Publication
Inorganic	SiO_2/TiO_2Silicone oil	200, 210, and 230 nm length	Hollow rods	3.0 wt%	NA	65.7 3 kV mm^{-1}	NA	Porous, hollow. Silica template was synthesized according to the modified Stöber method, then the composite was syntetised through sonication-mediated etching and re-deposition method. The resulting shell thickness was around 8 to 10 nm. The most optimal aspect ratio was 3 (rods of L/D 6 were more prone to aggregation).	Yoon et al. [39]
Inorganic	Dye-coated Mica/ TiO_2Silicone oil	Varied	Platelet	3.0 wt%	NA	The highest: Vivid yellow mica/TiO_2: 48.3 3 kV mm^{-1}	NA	Porous. The series of samples varies with dye colour and corresponding additive. The resulting colour also depends on the titania shell thickness (in a range between 41 to 163 nm), with the titania addtion overall improving the colour clarity. The highest colour clarity improvement and ER performance was achieved by vivid yellow sample. Colour tones are further changed during ER performance, suggesting application benefits in devices like tactile displays, ER inks, etc.	Noh et al. [139]
Hybrid	C_3N_4/TiO_2Silicone oil	3–4 μm ø, varied length	Prism-like	10 wt%	1.358×10^{-11}	680	6 3 kV mm^{-1}	Anisotropic structure, composite shows rough surface with about 50–70 nm layer of TiO_2 coating. The composite exhibited enhanced ER performance in comparison to pure C_3N_4.	Sun et al. [118]
Inorganic	SiO_2/TiO_2 doped with Ca-; Sr-; and Ba-dopingSilicone oil (poly (methylphenylsiloxane)	130 nm	Hollow spheres	30.0 vol%	NA	The highest: Ca-doped SiO_2/TiO_2: 100 (low shear rate region) 3 kV mm^{-1}	NA	Porous, hollow. Doping with various alkaline metals evaluated and proved improved ER properties in comparison to non-doped hollowed SiO_2/TiO_2 particles. Especially Ca-doped composite-based sample exhibited high sedimentation stability and the highest ER effect.	Yoon et al. [34]

(*continued on next page*)

Table 3 (*continued*)

Composite type	Material and liquid carrier	Approximate size	Geometry	Concentration	DC Conductivity (S cm^{-1})	ER efficiency — 0.1 (s^{-1})	100 (s^{-1})	Additional notes	Publication
Inorganic	MoS_2/SiO_2Dimethyl silicone oil	Mostly around 170–300 nm	Flower-like	10 wt%	Varied, the most optimal: 12 h-synthesis: 4.96×10^{-9}	The most optimal: 12 h-synthesis sample: 22.5 (0.23 s^{-1})	12 h-synthesis sample: 6.5 (11 s^{-1}) 3 kV mm^{-1}	Porous. Synthesis reaction time affected the resulting conductivity (the 12 h-synthesis sample, although having lower conductivity and slightly lower ER efficiency in low shear rate region than the 3 h-synthesis one, showed extended plateau in higher fields and more optimal ER performance. ER performance of the composite in comparison to pure silica was improved. Also, silica addition helps to control the composite conductivity and significantly improved MoS_2 current leakage issue	Sun et al. [151]
Hybrid	SiO_2/PPySilicone oil	680 nm	Spheres	10 vol%	2.3×10^{-8}	1430	6 1.3 kV mm^{-1}	Rough surface. Silica core was modified with 3–(trimethoxysilyl)propyl methacrylate as an agent, then PPy shell was synthesised by oxidative polymerization. Rough surface. Shell thickness is about 90 nm.	Kim et al. [152]
Inorganic	GO/SiO_2Silicone oil	Around 270 nm	Spheres	3 wt%	NA	The highest: GO/p2SiO_2 sample: 22 3 kV mm^{-1}	NA	Three samples of the same material and similar particle size, but various pore size compared (pores: 1 nm, 2 nm, and 10 nm). The porosity difference resulted in varied density, the relationship between density, the ER behaviour, and sedimentation stability was evaluated: GO/p2SiO_2 sample with the lowest density exhibited the best ER performance and the slowest sedimentation rate.	Yoon et al. [35]
Inorganic	$H_2Ti_2O_5/MoS_2$/ SiO_2Silicone oil(poly-dimethylsiloxane)	In nm range	Honeycomb-like flakes	10 %, 15 % and 20 vol%	Varied, in a range between 10^{-7} to 10^{-9}	The most highlighted: 1.28 mL TEOS and 15 vol%: 53.8 (1 s^{-1})	1.28 mL TEOS and 15 vol%: 6.8 (18 s^{-1}) 2 kV mm^{-1}	Porous. Effect of various dosage of ethyl silicate (TEOS) during synthesis evaluated (0.96 mL, 1.28 mL, 1.60 mL) and multiple concentrations compared, the 15 and 20 vol% concentration exhibited better	Chen et al. [153]

(*continued on next page*)

Table 3 (*continued*)

Composition type	Material and liquid carrier	Approximate size	Geometry	Concentration	DC Conductivity ($S\ cm^{-1}$)	ER efficiency — 0.1 (s^{-1})	100 (s^{-1})	Additional notes	Publication
								ER effect, but also higher current leakage.	
Hybrid	Carbonized glucose/ SiO_2Silicone oil	400 nm	Spherical	5 wt%	1.90×10^{-7}	38.9	8.6 3 kV mm^{-1} (9 s^{-1})	Mesoporous (19.26 nm mean pore diameter). Performance comparison of non-porous and mesoporous silica as a part of the composite. Dielectric properties and sedimentation stability evaluated.	Pavlikova et al. [154]
Inorganic	TS-1/TiO_2Dimethyl silicone oil	100 nm	Mostly amorphous	10 wt%	2.78×10^{-9}	The highest: 1.5 mL TBT:359	1.5 mL TBT: 2.8 3 kV mm^{-1}	Multiple samples were evaluated based on the amount (1, 1.5, 2, and 3 mL) of tetrabutyl titanate (TBT) used during coating. The amount of TBT also influenced the thickness of titania shell (from 5 up to 50 nm), but also affected aggregation of the particles.	Sun et al. [180]
Hybrid	$SrTiO_3$/poly-MMEMSilicone oil	NA	NA	10 wt%	NA	67 (1 s^{-1})	2.6 5 kV mm^{-1}	Composite based on 2-(methacryloyloxy)ethyl maleate polymer (poly-MMEM), synthesised through controlled hydrolysis of Sr–Ti double alkoxide and then reaction with MMEM. Crystalline was controlled by the water amount for hydrolysis. The enhancement of ER properties was confirmed in a comparison to pure titanate particles	Umeda et al. [144]
Hybrid	PS/LAPSilicone oil	50–300 nm ø	Spheres	10 vol%	NA	0.7 (15 s^{-1})	0.6 (28 s^{-1}) 4 kV mm^{-1}	Needle-like covered surface from LAP coating. Composite fabricated through surfactant-free Pickering emulsion polymerization method. The ER effect is rather low in comparison to other alternatives due to low vol% of LAP in the composite	Kim et al. [176]
Hybrid	PANI/attapulgiteSilicone oil	1–μm	Granular, fibres on surface	2.5 vol%	10^{-8}	608	0.3 2 kV mm^{-1}	Pickering emulsion polymerization method was used to cover PANI with attapulgite rods, the composites were dedoped using a NaOH solution. Mason number was evaluated.	Han et al. [116]

(*continued on next page*)

Table 3 (*continued*)

Composite type	Material and liquid carrier	Approximate size	Geometry	Concentration	DC Conductivity (S cm^{-1})	ER efficiency — 0.1 (s^{-1})	100 (s^{-1})	Additional notes	Publication
Hybrid	PANI/SEPSilicone oil	60–70 nm ø, length ranges from hundreds of nm to μm range	Needle-like	8 vol%	NA	24.3 (10 s^{-1})	4.4 1.6 kV mm^{-1}	Composites synthesised through in situ polymerization with ammonium persulfate used as an initiator, then dedoped by NaOH solution.	Jang and Choi [177]
Hybrid	PANI/grapheneSilicone oil	Nano range	Mixed fiber and amorphous morphology	1 wt%	0.1948	20 cSt carrier:207.5	20 cSt carrier: 6.7 (4 s^{-1}) 0.9 kV mm^{-1}	Low particle concentration. Comparison of ER performance of two samples differing in different viscosities of silicone oil (100 and 20 cSt). Overall, the lower viscosity enabled higher ER efficiency; however, in the PANI/graphene in 20 cSt oil case it was possible to measure until 0.9 kV mm^{-1} (rest of samples were measured up to 2 kV mm^{-1} field). PANI/WO_3 has higher aspect ratio.	Roman et al. [62]
	PANI/WO_3Silicone oil	Nano in diameter, micron range in lenght			2.2×10^{-3}	20 cSt carrier:554	20 cSt carrier: 18 (5 s^{-1}) 2 kV mm^{-1}		
Hybrid	GO/PANI PANI/WO_3Silicone oil	NA	Multi-layer sheets	10 vol%	NA	125	4.8 2 kV mm^{-1}	Rough surface. Composites were synthesized with PANI fabricated by in situ polymerization in GO dispersion. High plateau achieved in low shear rate region.	Zhang et al. [182]
Hybrid	GO/PANI	240 nm thickness, Lateral size several μm	Plates	10 vol%	2.5×10^{-9}	The highest: rGO/PANI: 176.3 (1 s^{-1})	rGO/PANI: 182 kV mm^{-1}	Comparison of GO and rGO as parts of composite particles. The rGO/PANI was confirmed to exhibit superior ER effect, higher yield stress and good response in in both AC and DC fields.	Yuan et al. [117]
Hybrid	rGO/PANIDimethyl silicone oil	3.5 nm thickness	Sheets	NA	3.6×10^{-9}	51.2 (1 s^{-1} $\dot{\gamma}$)	11.4 (10 s^{-1} $\dot{\gamma}$) 3 kV mm^{-1}	Improved dispersion stability, ER performance and ER efficiency in comparison to pure GO ERF. The POSS-GO also exhibited more stable chain-like structures in field (as GO sheets were evaluated to show dielectrophoretic effect, weaking its ER performance).	Li et al. [187]
Hybrid	Colloidal-GO/ PANISilicone oil	NA	Coralline-like sheets	NA	2×10^{-9}	NA	NA	Improved thermal stability in comparison to pure colloidal GO. The composite is possible to be dispersed in water owning to the colloidal-GO.	Zhang et al. [195]

(*continued on next page*)

Table 3 (*continued*)

Composite type	Material and liquid carrier	Approximate size	Geometry	Concentration	DC Conductivity (S cm^{-1})	ER efficiency — 0.1 (s^{-1})	100 (s^{-1})	Additional notes	Publication
Hybrid	PANI/SEPCastor oil	20 nm × 40 nm rectangular cross-section, 1 μm length	Bulk: Fiber-likeAgglomerates Slurry: Fiber-like, PANI well-adhered	10 vol%	NA	Slurry: 43.1 (1.25 s^{-1})	1.3 (40 s^{-1}) 1.5 kV mm^{-1}	Comparison of bulk and slurry polymerization methods. The former resulted in good sample yield; however, it lead to agglomerating. The later enabled good coating adhesion. Only the slurry sample was further tested in detail for ER properties. Proportion of SEP and PANI was tested at 70:30 and 50:50, and the latter exhibited superior ER performance results.	Marins et al. [198]
Organic	PANI/carbonized PANISilicone oil	Under 45 μm	NA	10 wt%	NA	PANI/c.PANI: 272.7 Carb. PANI:62.6 Pure PANI: 47.1 (0.13 s^{-1})	5.2 3.1 3.91 kV mm^{-1} (8.8 s^{-1})	Comparison of pure PANI, carbonized PANI and their combination as core–shell composite particles. PANI/c. PANI exhibited lower off-field viscosity and resulted in a higher ER efficiency.	Sedlacik et al. [113]
Hybrid	PANI/TiSilicone oil	200–250 nm ø, 0.5–3.0 μm length	Cable-like	10 vol%	Conductive PANI/Ti: 4 × 10^{-3} Dedoped PANI/Ti: 6 × 10^{-10}	335 (1 s^{-1}) 148.3 (1 s^{-1})	4.43 kV mm^{-1} 8.83 kV mm^{-1}	Comparison of conductive PANI and dedoped PANI as cores. Polarization difference evaluated. The dedoped variant proved to be more stable for an ERF application.	Yin et al. [214]
Hybrid	PANI/MMTSilicone oil	100 nm ø	Granular	30 wt%	38.4 × 10^{-9}	22.7 (2 s^{-1})	3.4 at 3 kV mm^{-1} (75 s^{-1})	Composite synthesised through emulsion intercalation polymerization method. Acceptable current leakage and excellent sedimentation stability over the examined period (98 % ratio over 60 days).	Lu and Zhao [215]
Hybrid	PANI/MoS_2PANI/ tungsten disulphideSilicone oil	NA	Flake-like	10 wt%	PANI/MoS_2: 2.25 × 10^{-7} PANI/WS_2: 6.27 × 10^{-6}	2 0.2	0.16 at 0.5 kV mm^{-1} 0.16 at 0.5 kV mm^{-1}	Tungsten disulphide exhibited higher zero field and on-state viscosity, but lower ER effect in at 0.1 s^{-1} shear rate.	Stejskal et al. [93]
Hybrid	PANI/MoS_2Silicone oil	Average ø 100–200 nm for 4:1 ratio variant	Lamellar	10 wt%	NA	The most efficient: 4:1 ratio sample: 74.9 (1 s^{-1})	4:1 sample: 8.7 at 3 kV mm^{-1} (35 s^{-1})	Polyaniline to MoS_2 material composition tested at proportions of 3:1, 3.5:1, 4:1, and 5:1. The 4:1 sample proved to be the most effective in terms of ER performance, and could withstand voltage	Li et al. [216]

(*continued on next page*)

Table 3 (*continued*)

Composite type	Material and liquid carrier	Approximate size	Geometry	Concentration	DC Conductivity (S cm^{-1})	ER efficiency — 0.1 (s^{-1})	100 (s^{-1})	Additional notes	Publication
								up to 3 kV mm^{-1}. Particle sizes decreased with the increasing PANI ratio.	
Hybrid	PANI/MoS_2Silicone oil	Nano-range	Sea cucumber-like	15 wt%	NA	The most efficient: MoS_2/PANI-NDs-24:1014.2	MoS_2/PANI-NDs-24: 5.13 kV mm^{-1}	Polyaniline nanoneedles were grown onto exfoliated MoS_2 sheet matrix. The aspect ratio of PANI parts increased with prolonged polymerization time, this further enhanced ER performance of the longer polymerized sample (MoS_2/PANI-NDs-24). Electromagnetic microwave absorption property was confirmed.	Zhang et al. [120]
Hybrid	Fe_3O_4/PANISilicone oil	1 μm ø	Spherical	20 wt%	5.56×10^{-8}	181.5 (1 s^{-1})	6.9 2.5 kV mm^{-1}	Dual ER and MR response with efficiency evaluated in both aspects. Grainy-like surface. The composite showed improved sedimentation in comparison to pure Fe_3O_4, this corresponds to lower density as a result of PANI addition.	Sim et al. [217]
Hybrid	Fe_2O_3/PANISilicone oil	1–2 μm	Flower-like	20 wt%	NA	52.8 (0.13 s^{-1})	4.5 (22.7 s^{-1}) 3 kV mm^{-1}	Nanosheets (around 50 nm thickness) assemble into the flower-like structure. The composite possess weak magnetization, but is estimated to be enhanced if synthesis and material is adjusted.	Tian et al. [218]
Hybrid	$MnFe_2O_4$/PANISilicone oil	450 nm	Spheres	5 vol%	6.82×10^{-8}	873.5 (0.2 s^{-1})	3.8 (44.9 s^{-1}) 2 kV mm^{-1}	Dual ER and MR response. Core was synthesized through solvothermal synthesis, then coated vie oxidative polymerization	Jeong et al. [220]
Hybrid	PANI/ZFSilicone oil	2.5–3.5 μm	Raspberry-like	5 vol%	4.7×10^{-7}	43.5 (3.9 s^{-1})	5.1 (35.5 s^{-1}) 1 kV mm^{-1}	Dual ER and MR response. Composite fabricated by Pickering emulsion polymerization with zinc ferrite as a solid stabilizer.	Kim et al. [221]
Hybrid	PANI/ZFSilicone oil	400 nm	Spheres	5 vol%	3.02×10^{-10}	1675 (0.12 s^{-1})	10 (27 s^{-1}) 4 kV mm^{-1}	Dual ER and MR response. Core fabricated a solvothermal method, followed by oxidative polymerization to create the composite. Shell thickness is around 30 nm, rough surface.	Kim et al. [222]

(*continued on next page*)

Table 3 (*continued*)

Composite type	Material and liquid carrier	Approximate size	Geometry	Concentration	DC Conductivity ($S\ cm^{-1}$)	ER efficiency — 0.1 (s^{-1})	100 (s^{-1})	Additional notes	Publication
Hybrid	PDPA/ZFSilicone oil	330 μm	Spheres	5 vol%	NA	104.4 (0.13 s^{-1})	2.4 2 kV mm^{-1}	Dual ER and MR response. ZF core fabricated though solvothermal method, followed by coating done though radical polymerization (shell thickness around 14 nm).	Kim and Choi [223]
Hybrid	ZF/PANISilicone oil	540 nm in median pure ZF, approximately 23.57 μm ZF/PANI	Nodular shape	5 vol%	Varied, the most optimal: ZF/PANI: 2.16×10^{-9}	The highest:ZF/PANI (hematite and benzoic acid dopant):323.9	ZF/PANI: 2.1 (32 $s^{-1}\cdot\gamma$) 3 kV mm^{-1}	Applicable as an anti-corrosion paint. Composite proved to be superior in comparison to pure ZF. A comparison of 2 PANI dopants is evaluated (phosphate acid and benzoic acid, the benzoic one proved to be the better option an as ERF) as well as ZF type comparison (synthetic and natural). ZF/PANI (synthetic hematite origin) particles were evaluated as the most optimal as an ERF.	Munteanu et al. [88]
Hybrid	PILs/PANISilicone oil	Average ø 1.17 μm	Spheres	20 vol%	Thin shell: $1.5 \times 10 - 8$ Thick shell: $1.25 \times 10 - 8$	47.6 (17 $s^{-1}\cdot\gamma$) 166.5 (30 $s^{-1}\cdot\gamma$)	21.7 4 kV mm^{-1} 40.5 (140 $s^{-1}\cdot\gamma$) 4 kV mm^{-1}	The PIL-based spheres were synthesised though a dispersion polymerization and then PANI was coated via low-temperature interfacial polymerization. Based on the PANI dosage, the thickness of PANI shell can be increased (however, too high dosage results in a granulate morphology instead). Therefore, the study compares thin and thick shell-based composites of the same materials. The flow curves show the shear stress trend over more than 1000 s^{-1} shear rate. The yield stress was higher for the thick shell particles, which also showed lower current leakage.	Zheng et al. [115]
Hybrid	GO/PPy/PILSilicone oil	NA	Multilayer sheets	8 wt%	10^{-14}	6805	27.2 (90 s^{-1}) 2 kV mm^{-1}	Double coating. In comparison to pure GO and GO/PPY, the double coated particles showed improved ER properties (including extended plateau at shear rate over 100,	Chen et al. [247]

(*continued on next page*)

Table 3 (*continued*)

Composite type	Material and liquid carrier	Approximate size	Geometry	Concentration	DC Conductivity (S cm^{-1})	ER efficiency — 0.1 (s^{-1})	100 (s^{-1})	Additional notes	Publication
								as well as an appropriate conductivity to enable the ERF in higher el. fields.	
Hybrid	PPy/silicaSilicone oil	200–300 nm	Spherical	2 vol%	Varied, In between 2.62×10^{-8} -2.23×10^{-7}	The most efficient: 7.0 wt ratio of silica-PPy: 118.7 (0.16 s^{-1})	7 wt ratio: 1 (4 s^{-1}) 2 kV mm^{-1}	Suspension polymerization in the presence of silica enabled controlling the ratio of silica/pyrrole during the polymerization. Changes in weight ratio of silica to PPy during the synthesis were focused (ranging between 2.9 to 11.0 %, the 7.0 % wt ratio sample was evaluated further in terms of ER properties) and led to changes in dielectric properties, and ER properties. Yield stress dependence on concentration (tested in a range between 0.5 to 4 vol%), field, and dielectric properties were evaluated. Smaller spherical particles tended to agglomerate into raspberry-like structures	Kim and Hong [245]
Hybrid	PPy/SnOSilicone oil	100–300 nm	Raspberry-like agglomerates	Ranges from 0.1 – 2.5 vol%	Varied, in between: 3.42×10^{-7} – 6.86×10^{-7}	The most efficient: 7.0 wt ratio of PPy to SnO, 1.0 vol%:515.9	7 w ratio, 1.0 vol%: 1.3 2 kV mm^{-1}	Concentration was focused, 1 vol% sample seems to be the most optimal in terms of yield stress. Composite synthesised through suspension polymerization in the presence of tin oxide nanoparticles, while controlling the weight ratio of tin oxide to pyrrole (ranging between 3 to 11 %, with conductivity increasing with the higher amount of tin oxide). The 7 wt ration sample was further investigated in terms of ER performance.	Kim and Yoon [82]
Hybrid	TiO_2/PPySilicone oil (M15 and M200 compared)	Ø in nano-range, length of several μm	Rod-like	Varied, 5–15 wt%	NA	The highest: 5 % wt Py 4 ml: 18.5 (1 s^{-1})	5 % wt Py 4 ml: 0.4 3 kV mm^{-1}	Different proportion of Ti and PPy during synthesis tested (2 g of Ti to 0 up to 4 ml of Py). Different concentration tested (5, 10, and 15 wt%), the higher particle weight concentration decreased the ER efficiency. With increasing amount of PPy coating, the	Mrlík et al. [246]

(*continued on next page*)

Table 3 (*continued*)

Composite type	Material and liquid carrier	Approximate size	Geometry	Concentration	DC Conductivity (S cm^{-1})	ER efficiency — 0.1 (s^{-1})	100 (s^{-1})	Additional notes	Publication
								yield stress and the ER effect increased. Two silicone oils compared, M15 as a carrier showed increased viscosity across all el. fields.	
Hybrid	PPy/MCM-41-ESilicone oil	Nano range	Irregular	5 vol%	NA	1.6 (3 s^{-1})	0.4 (31 s^{-1}) 1.5 kV mm^{-1}	Intercalated PPy in pore-expanded MCM-41 silica (pore Ø 41.42 Å, hexagonal channels). Enhancement of ER performance in comparison to pure MCM-41-E silica and non-expanded PPy/MCM-41 composite.	Fang et al. [248]
Hybrid	PPY/MCM-48	400–800 nm ø	Spheres	NA	NA	NA	NA	No direct ER measurements. Intercalated PPy in silica (pore ø 3 nm). The polymer was then extracted by in 2 M aqueous solution of NaOH for 10 min at 60 °C and the PPy was later dried in nitrogen atmosphere. The extracted PPy slowed improvement in electro-chemical properties compared to chemically-bulk produced PPy as well as the PPy in the original silica matrix.	Wysocka-Zolopa et al. [251]
Hybrid	POT/Zn, Zn content is variedSilicone oil	0.8 Zn wt% 26 μm 2.1 Zn wt% 18 μm 4.1 Zn wt% 83 μm 5.3 Zn wt% 13 μm 7.6 Zn wt% 17 μm	Shared alike sponge-like porous structure	15 wt%	1.3×10^{-2} 3.3×10^{-2} 5.0×10^{-2} 1.7×10^{-2} 1.7×10^{-2}	The highest 4.1 Zn wt% sample: 2.1 (1 s^{-1}) 2 kV mm^{-1}	NA	Various content of Zn was analysed (0.8–7.6 wt%), which resulted in different particle size distribution and conductivity. The most optimal suspension concentration was assessed at 15 wt%. Sedimentation stability was evaluated (best 0.8 Zn wt% sample 66.3 % after 12 days, higher zinc content lead to lower sedimentation stability) Magnetic susceptibility was also tested.	Yilmaz et al. [253]
Organic	PMMA/PNMASilicone oil	1.63 μm	Spheres	10 vol%	5.35×10^{-10}	8970.8 (1 s^{-1})	369.1 3.5 kV mm^{-1}	Rough surface. The composite was synthesised through grafting polymerization process. Significant ER efficiency.	Moon and Choi [255]
Hybrid	PNMA/Fe_3O_4Silicone oil	500 nm	Spheres	10 vol%	3.50×10^{-8}	604.4	6.8 4 kV mm^{-1}	Dual ER and MR response. Rough surface with nano-	Dong et al. [256]

(*continued on next page*)

Table 3 (*continued*)

Composite type	Material and liquid carrier	Approximate size	Geometry	Concentration	DC Conductivity (S cm^{-1})	ER efficiency — 0.1 (s^{-1})	100 (s^{-1})	Additional notes	Publication
								protrusions. Core was synthesised through chemical oxidative polymerization, followed by chemical co-precipitation of Fe_3O_4 to finish the composite. Considerable efficiency in both fields.	
Hybrid	Poly(2-methylaniline) /Fe_3O_4Silicone oil	500 nm	Spheres	5 vol%	NA	2252	8.6 2 kV mm^{-1}	Duel ER and MR response, significant ER efficiency. Rough surface. Composite synthesised through Shirasu porous glass membrane method. Sedimentation stability evaluated.	Lu et al. [257]
Hybrid	PEANI/GOSilicone oil	200 nm thickness, 3–10 μm lateral size	Flakes	4.5 vol%	Varied, in between 1.09 × 10^{-9} up to 2.56 × 10^{-10}	The most optimal: 70 μL hyd.: 9680.3 (1 s^{-1})	70 μL hydrazine: 145.1 1.5 kV mm^{-1}	Dependence of conductivity and ER effect on amount of hydrazine used for reduction was assessed (70 μL, 140 μL, 420 μL, and 1400 μL). The 70 μL hydrazine sample showed the highest ER stability and efficiency.	Wang et al. [125]
Hybrid	Silica/POASilicone oil	1 μm	Spheres	10 vol%	In a range of 10^{-10}	661.8 (1 s^{-1})	16 2.3 kV mm^{-1}	Modified silica core was coated with an assistance of a chemical grafting agent, N-[(3-trimethoxylsilyl)-propyl] aniline. Shell thickness about 50 nm. Sedimentation stability evaluated (no changes for about 10 h and after 20 h, the sedimentation ratio reached plateau approximately at 50 %).	Lee and Choi [259]
Hybrid	Magnetite/POASilicone oil	300 nm average Ø	Spheres	10 vol%	NA	3906.8	9.8 2 kV mm^{-1}	Composite synthesized through a solvothermal process. Conductive shell and magnetic core. Rough surface, 60 nm shell thickness. Significant ER efficiency. The polymer shell is estimated to improve dispersion stability and provide protection from external corrosion.	Lu et al. [121]
Hybrid	PPDA/GOSilicone oil	Approximately 3 μm	Irregular, crumpled structure	8 wt%	NA	17.7 (1 s^{-1})	1.8 (29.4 s^{-1}) 2.5 kV mm^{-1}	GO synthesised through ball-milling method, then composite was created via in situ oxidation polymerization. Compared to PPDA-based	Cao [264]

(*continued on next page*)

Table 3 (*continued*)

Composite type	Material and liquid carrier	Approximate size	Geometry	Concentration	DC Conductivity (S cm^{-1})	ER efficiency — 0.1 (s^{-1})	100 (s^{-1})	Additional notes	Publication
								ERF, the composite-based ERF showed enhanced ER properties and thermal stability.	
Organic	Pln/PESilicone oil	Micron range	Layered structure of PE, granular porous structure of PI, both are apparent	In a range: 5–25 vol%	Highest for sample K5: 6.16×10^{-6}	The highest: sample K5, 15–20 vol%: 28.5 (1.5 s^{-1})	K5, 15–20 vol%: 1.1 3.5 kV mm^{-1}	Five samples are compared, differing in the amount of used reactants and amount of Pln. Sedimentation stability and temperature effect on shear stress in field was analysed, K5 (sample with the highest amount of Pln) showed the highest ER effect as well as sedimentation stability. The most optimal volume fraction in terms of ER efficiency was evaluated between 15–20 vol %. Creep and recovery for K5 sample was evaluated.	Sari et al. [270]
Hybrid	Organo-MMT/PlnSilicone oil	Average Ø 11.88 μm	Granular, sponge-like structure	In a range: 5–25 wt%	3.7×10^{-4}	The highest: 25 wt% concentration;: 4.54 at 0.5 kV mm^{-1} (0.2 s^{-1})	NA	Different concentration effect on ER performance analysed. Organo-MMT/Pln showcased enhanced sedimentation stability for 25 wt% concentration − 82 % sedimentation ratio after 25 days). Magnetic susceptibility and creep response were evaluated, as well as ER performance in temperature range between 0 and 100 °C (at 60 °C and higher the shear stress decreases and current leakage increases).	Erol et al. [271]
Hybrid	Pln/ZFSilicone oil	200 nm	Spheres	5 vol%	5.13×10^{-8}	(Calculated from 0.5 and 3 kV mm^{-1})18.3	(Calculated from 0.5 and 3 kV mm^{-1}) 4.3	Focus on ER response, but MR response is also expected. Rough surface with about 15 nm shell thickness. Particles were synthesised using a simple solvothermal method	Kang and Choi [272]
Hybrid	Fe_3O_4/PlnSilicone oil	Aproximately 400 nm average Ø	Spheres	10 vol%	1.3×10^{-7}	40.6 (0.2 s^{-1})	0.9 1.5 kV mm^{-1} (0.9 s^{-1})	Dual ER and MR response. Composites were synthesised through solvothermal synthesis method and chemical oxidative polymerization. Rough surface, shell thickness around 45 nm. Improved both thermal	Hong et al. [273]

(*continued on next page*)

Table 3 (*continued*)

Composite type	Material and liquid carrier	Approximate size	Geometry	Concentration	DC Conductivity (S cm^{-1})	ER efficiency — 0.1 (s^{-1})	100 (s^{-1})	Additional notes	Publication
								and sedimentation stability as a result of the polymer coating.	
Hybrid	PT/BoraxSilicone oil	2.09 μm	NA	5–25 vol%	4.9×10^{-4}	20 vol%: 14.2 at 2 kV mm^{-1} (1.5 s^{-1})	NA	Effect of concentration on ER performance and sedimentation evaluated. Temperature effect assesed in a range between 20 and 80 °C (the composite ER performace showed a gradual increase with the rising temperature). Creep recovery is considered as suitable for damping applications.	Gumus et at. [276]
Hybrid	Silica/PTSilicone oil(poly (methylphenylsiloxane))	11–26 Ø	Spheres	5–30 vol%	1.0×10^{-7}	The highest: 30 vol%: 20.9 (1 s^{-1})	5.3 3 kV mm^{-1}	The core–shell particles were prepared by seeded polymerization method, with silica as the nanoseed. Enhanced sedimentation stability. The effect of volume fraction was assessed (30 % exhibited the highest ER effect). Composite size effect on ER performance was evaluated (11 nm exhibited the higest).	Hong et al. [277]
Hybrid	Silica/POTSilicone oil	40–60 nm Ø	Spheres	Approx. 20 vol %	5.68×10^{-12}	99. (1 s^{-1})	0.8 2 kV mm^{-1}	Silica was extracted from rice husk (the procedure combined acid and thermal treatments) and modified to activate the methacryloxy group, then the composites were synthesised through chemical oxidative polymerization.	Bach et al. [283]
Hybrid	Cellulose/LAPSilicone oil	80 μm lenght	Irregular flake-like	20 wt%	NA	4051.6	42.4 3 kV mm^{-1}	Particles were synthesised by dissolution–regeneration method. Rough porous surface. Improved ER properties and sedimentation stability in comparison to pure cellulose	Liu et al. [291]
Hybrid	Feldspar/DMSO/ carboxymethyl starchCarrier NA	In nm range	Irregular	30 vol%	18.24×10^{-10}(at 1 kHz)	(Calculated from 1 and 5 kV mm^{-1}) 4.7 (γ NA)	NA	Two-step synthesis: the polar compound was intercalated into the interlayer of nano-ferric oxide, then the complex interacted with carboxymethyl starch by the	Saboktakin et al. [303]

(*continued on next page*)

Table 3 (*continued*)

Composite type	Material and liquid carrier	Approximate size	Geometry	Concentration	DC Conductivity ($S\ cm^{-1}$)	ER efficiency — 0.1 (s^{-1})	100 (s^{-1})	Additional notes	Publication
								solution method, creating the composite.	
Hybrid	chitosan /bentoniteSilicone oil	14–51 μm	Amorphous	Varied 5–25 wt %	Varied, $1.52–3.45 \times 10^{-5}$	The highest: chitosan (5 %)/ bentonite (95 %): 14.48 (0.17 s^{-1})	Chitosan (5 %)/ bentonite (95 %): 19.7 (10 s^{-1}) 1 kV mm^{-1}	Biodegradable. Composites were synthesised by intercalation method using cetyltrimethylammonium bromide as the cationic surfactant. Samples varied by synthesis fraction of both components (1, 5, and 25 % of chitosan to 99, 95 and 75 % of bentonine) and prepared at various particle concentration (25 wt% was the most suitable). Sedimentation stability is said to complie to the industry requirement. Creep recovery was assessed.	Cabuk et al. [308]
Hybrid	chitosan/organo-bentonite	1 wt% CS: 14 μm 5 wt% CS: 23 μm 25 wt% CS: 51 μm	Crystal-like	NA	1.0×10^{-5} 1.7×10^{-5} 3.4×10^{-5}	NA	NA	No direct ER tests.Three types of composites were prepared with different amount of chitosan (CS) content: 1 wt%, 5 wt% and 25 wt%. Anti-bacterial property evaluated. Pure CS and 1 wt% CS samples did not show antibacterial activity, however the bacteria inhibition was highly enhanced with increased CS content, similarly, anti-fungi activity was observed.	Cabuk et al. [309]
Organic	Chitosan/ celluloseSilicone oil (polydimethylsiloxane)	50–60 μm (main fraction of particles)	Spherical, forms agglomerates	1 wt%	In a range: $1.62–11.4 \times 10^{-13}$	The highest: 5/ 1 cel./chit. 1054 7 kV mm^{-1} (1 s^{-1})	NA	High porosity. Low dispersed phase concentrations tested. Cellulose content was tested in different concentrations and affected the ER behaviour, conductivity, sedimentation (the best 0.01 cel./1chit.) and ER performance (the bes 5 cel./1 chit.), possible to apply to higher el. field than 4 kV mm^{-1}.	Kuznetsov et al. [310]
MOF-based	MIL-125/PANISilicone oil	270–390 nm	Approx. spherical	10 wt%	2.64×10^{-10}	69.3	2.8 3 kV mm^{-1}	Solvothermal method. Porous. Polymer coating thickness is approximately 70–90 nm. The ER properties were enhanced	Wen et al. [313]

(*continued on next page*)

Table 3 (*continued*)

Composite type	Material and liquid carrier	Approximate size	Geometry	Concentration	DC Conductivity (S cm^{-1})	ER efficiency — 0.1 (s^{-1})	100 (s^{-1})	Additional notes	Publication
								in comparison to pure MIL-125.	
Organic framework-based	Carbonized covalent organic framework incorporated with $TFSI^-$	3–5 μm	Irregular	20 vol%	Varied, from 1.09×10^{-9} to 1.61×10^{-8}	The highest: ieCOF-390: 648.1 (1 s^{-1})	36.8 3 kV mm^{-1}	Carbonization done at various temperatures (370 °C – 440 °C), resulting in total of 4 samples. Sample carbonized at 390 °C achieved the highest ER efficiency and together 420 °C-sample the highest dynamic yield stress.	Ma et al. [320]
Organic framework-based	Ionic covalent organic polymer incorporated with $TFSI^-$	Low micron range	Granular	20 vol%	Varied, between 2.7×10^{-7} and 1×10^{-10}	102.2 (1 s^{-1})	17.2 4 kV mm^{-1}	Anhydrous system, wide working temperature. Conductivity increased with temperature. The system is stable at even very high shear rate (1000 1 s^{-1}). Low current leakage.	Ma et al. [76]
MOF-based	MOF-TI/PANIDimethyl silicone oil	100–200 nm	Square-like,0.3 PANI variation cube-like	10 wt%	Varied	The most efficient: 0.2 PANI sample: 163.18 (1 s^{-1})	0.2 PANI: 2.6 3 kV mm^{-1}	The polyaniline addition to the composite was tested in various amounts (0.15–0.4 g), the samples with PANI 0.2 g-0.35 g additions proved good ER performance. The polymer proved beneficial in terms of lowering the current leakage, enhancing the particles ER properties and dielectric properties.	Wang et al. [314]
MOF-based	MOF-Ti/TiO_2Dimethyl silicone oil	100 nm	Spherical	10 wt%	2.04×10^{-10}	250.7	2.9 3 kV mm^{-1}	Porous. Prepared by two-step, solvothermal method. In comparison to uncoated MOF and pure TiO_2, the core–shell exhibits enhanced ER properties, higher shear resistance and stability.	Sun et al. [315]
MOF-based	MOT-Ti/ SiO_2Dimethyl silicone oil	200–400 nm	Square-like	10 wt%	Varied, between 1.33×10^{-9} and $> 3.47 \times 10^{-8}$	The most efficient: MOF-Ti/SiO2-1.mL TEOS:545.7	MOF-Ti/ SiO2-1.mL TEOS: 3.4 3 kV mm^{-1}	Porous with inner holes. Prepared by solvothermal method, then coated with SiO_2 by Stöber hydrolysis. Multiple samples were compared, differing in an amount of TEOS introduced during the synthesis (0.75 mL, 1 mL, 1.25 mL, 1.5 mL), the 1 mL TEOS sample achieved the highest yield stress and ER efficiency. Sedimentation stability 96 % after 256 h.	Wang et al. [316]

(*continued on next page*)

Table 3 (*continued*)

Composite type	Material and liquid carrier	Approximate size	Geometry	Concentration	DC Conductivity ($S\ cm^{-1}$)	ER efficiency — 0.1 (s^{-1})	100 (s^{-1})	Additional notes	Publication
								Silica shell also improved current leakage.	
Inorganic	TiO_2/SiO_2Silicone oil (poly (methylphenylsiloxane)	20–25 nm ø 20–25 nm ø, 150–200 nm length 150–200 nm ø, >5 μm length	Spheres Rod-like Tube-like	15 vol%	NA	The highest: tubes: 52.8 (50 s^{-1})	Tubes: 52.8 (50 s^{-1}) 5 kV mm^{-1}	Morphology focused, and is dependent on the shape of core silica particles. Silica prepared by Stöber method, then composites were synthesised by using seed-mediated methods. Aspect ratio compared, ER performance improved with increased aspect ratio	Hong et al. [92]
Inorganic	GO/SiO_2Silicone oil	200 nm ø 100 nm ø, length 4 μm	Spheres Rods	5.0 wt%	NA	The highest: 20 aspect ratio rods:19213.6	222.2	Comparison of spheres and rods with aspect ratios 5 and 20, the higher aspect ratio showed superior ER properties	Lee et al. [95]
Hybrid	PANI/SiO_2Silicone oil (poly(methylphenyl siloxane))	100 nm ø 100 nm ø, length 500 nm 100 nm ø, length 1 μm	Spheres Rod-like Rod-like	3.0 wt%	All in range < 10^{-8}	The highest: 10 aspect ratio rods: 339.5 (γ NA) 3 kV mm^{-1}	NA	Morphology focused. Core synthesized by a modified Stöber method and PANI was coated by a vapor deposition polymerization method. The shape of silica particles was modified by the amount of tetraethyl orthosilicate used during the synthesis. Mesoporous particles with varied pore size; aspect ratio was compared, ER performance improved with increased aspect ratio	Noh et al. [96]
Organic	PS/PANISilicone oil	1.3 μm average	Sea urchin-like	10 vol%	2.34×10^{-11}	601.5 (1 s^{-1})	21 2.5 kV mm^{-1}	Composites were prepared by seeded swelling polymerization method. Sedimentation stability was improved in comparison to pure PS spheres.	Kim et al. [114]
Inorganic	$SiO_2/TiO_2/SiO_2/TiO_2$Carrier NA	300 nm average	Cactus-like spheres	12 wt%	NA	304.7 (2 s^{-1})	4.5 4 kV mm^{-1}	Double shell structure done through a multi-step procedure (Core though Stöber method, then the first TiO_2 shell by the hydrolysis of titanium(IV) isopropoxide, then SiO_2 coating was done by hydrolysis of TEOS, and last layer via a solvothermal process). Suitable for microwave absorption applications.	Ji et al. [119]

(*continued on next page*)

Table 3 (*continued*)

Composite type	Material and liquid carrier	Approximate size	Geometry	Concentration	DC Conductivity (S cm^{-1})	ER efficiency — 0.1 (s^{-1})	100 (s^{-1})	Additional notes	Publication
Hybrid	PPDG/GO/PANISilicone oil	Approximately 2–3 μm	Jellyfish-like shape	8 vol%	NA	12.5 (3 s^{-1})	3 (21.8 s^{-1}) 3 kV mm^{-1}	Composite particles were completed by an interfacial polymerization, showed improved dispersion stability in comparison to pristine PANI. Potential in biomedical and microfluid fields	Zhang et al. [265]
Inorganic	SiO_2/TiO_2 Dimethyl silicone oil	1 μm	Hollow peanut-like	10 wt%	NA	205.7	1.6 3 kV mm^{-1}	Porous. The hollow template was synthesised though hydrothermal method, then Stöber method to finalize the core–shell. Excellent sedimentation stability (over 95 % ratio in comparison to pure silica displaying less than 40 %).	Sun et al. [371]
Inorganic	$TiOF_2/SiO_2$ Silicone oil	300 nm	Cube-like	10 wt%	NA	30.3	1.6 (9.1 s^{-1}) 3 kV mm^{-1}	Simple two-step synthesis: template-free solvothermal method followed by hydrolysis to coat the core. Rough porous surface with about 5–10 nm coating layer, low current leakage.	Li et al. [370]
Hybrid	PANI/SBA-15Silicone oil	NA	NA	5 wt%	10^{-5}	0.05 (1000 s^{-1}) 1 kV mm^{-1}	NA	Polymer intercalated in pores (pore ø around 63 Å). High conductivity.	Cho et al. [377]
Hybrid	PANI/MCM–41 and MEPA/ MCM–41Silicone oil	<10 μm	Twisted rectangular bar-like	1 wt%	10^{-9}	NA	NA	Uniform hexagonal pore structure, polymer intercalated inside the pores.	Lee et al. [80]
Hybrid	PANI/MCM-41Silicone oil	<10 μm	Irregular	5 vol%	10^{-9}	6.7 (125 s^{-1}) 3 kV mm^{-1}	NA	Polymer intercalated in pores (uniform channels of 3.1-nm pore ø). High conductivity and enhanced ER performance in comparison to pure PANI or MCM-41.	Cho et al. [378]
Hybrid	$SiO_2/Ni/TiO_2$Silicone oil	1.92 μm mean ø	Spheres	NA	NA	NA	NA	Porous (3–4 pore ø). Double coating, responsive to magnetic and electrical field, chain-like structure formation confirmed.	Guo et al. [375]

Table 4
Summary of giant electrorheological fluids.

Material and liquid carrier	Approximate size	Geometry	Concentration	ER efficiency	Additional notes	Publication
TiO_2 based PM(L)–ERSilicone oil and hydraulic oil compared	Uneven size distribution	NA	17 vol%	154.5 5 kV mm^{-1} (300 s^{-1})	PM not adsorbed, but dissolved resulting in so-called PM(L)-ER. Sample is based on TiO2, but suggest that other pure oxides should be also suitable for the method. Improved lifetime.	Lu and Shen [324]
Carbon-inlayed TiO_2Silicone oil	500 nm	Jujube cake–like structure	33 vol% / 38 vol%	The highest: 38 vol%: 861.8 5 kV mm^{-1} (0.2 s^{-1})	Good mechanical and thermal stability, low current leakage leading to improved lifetime	Qui et al. [329]
TiO_2	NA	NA	NA	NA	Study of effect of adsorbed water	Qui et al. [331]
$CaTiO_3$Silicone oil	NA	Structure change depending on drying process	NA	NA	Analyses of drying process and its effect on material properties and ER performance	Yang et al. [332]
Urea-coated BaTiO	Average 50 nm	Spheres	0.5 vol%	NA	Effect of liquid carrier on ER performance studied	Hong and Wen [69]
Modified TiO_2Silicone oil	Average ø 919.4 nm	Irregular	NA	61.7 5 kV mm^{-1} (0.06 s^{-1})	Low current density and good sedimentation stability	Xu et al. [336]
Calcium titanyl oxalateMethyl-terminated silicone oil	Average length 4 μm with aspect ratio 3.3	Anisotropic spindly	29 vol% 38 vol%	12 000 5 kV mm^{-1} 6000 5 kV mm^{-1}	Bimodal ERF composed of micron particles and nano-sized fibrous particles. Wettability tested. Further increased volume concentration (up to 49 %) is estimated to increase the ER efficiency higher. The 38 vol% sample exhibited better sedimentation stability, but also higher current density.	Wu et al. [366]
Urea-coated barium titanyl oxalateSilicone oil and alkanes	Varied, 1–3.5 μm	NA	38 vol% 44 vol%	The highest: Dodecane 50 %: 62,000 5 kV mm^{-1} The highest: Hexadecane 50 %: 7700 5 kV mm^{-1}	Effects of different alkanes was evaluated (dodecane, tetradecane and hexadecane). Their addition (especially dodecane brought promising results) and concentration influenced particle size distribution, strength of the chain-like formations and lead to enhancement of the ER efficiency, particle wettability, and exceptional sedimentation stability.	Liang et al. [367]

6. Other material's factors influencing the ER effect

As mentioned in the dispersed phase section, the ER particles have to fulfil certain criteria to be effective (good sedimentation stability, appropriate conductivity and so on). However, some other factors are equally important. The particle concentration and conductivity were mentioned previously. This section further discusses dielectric properties, temperature, particle size, and finally particle morphology.

It should be noted that besides the particle properties, the power of the electric field itself is a key factor to ER performance and should be always noted when evaluating ERF's properties. Generally, higher values of the electrical field result in an increase of ER properties (up to a certain limit, depending on the polarizability of the particles, as afore-mentioned in the introduction part).

Electrorheological fluids can operate in both AC and DC fields, the frequency of AC field can impact ER effect [337]. Material composition can also change the ER response to AC field (as was mentioned in a study by Yuan et al. [117] while comparing GO/PANI and rGO/PANI particles).

6.1. Dielectric properties

As afore-mentioned, particle polarization plays a key role in ER effect, since the phenomenon is induced by an electric field. Dielectric properties are further affected by changes in conductivity, temperature, and particle concentration [32,338].

The properties that are often mentioned in the studies while evaluating ERFs are namely:

Relaxation time, marked as t_{rel}, complex permittivity ε^*, and relaxation strength $\Delta\varepsilon'$. Furthermore, $\Delta\varepsilon'$ is defined as the difference between permittivity at zero frequency ε'_0 and ε'_∞ as the permittivity at very high (infinite) frequency. In general, the value of $\Delta\varepsilon'$ is closely related to the electrostatic interactive forces between the ER particles and is expected to show a peak in a range of 10^2–10^5 Hz

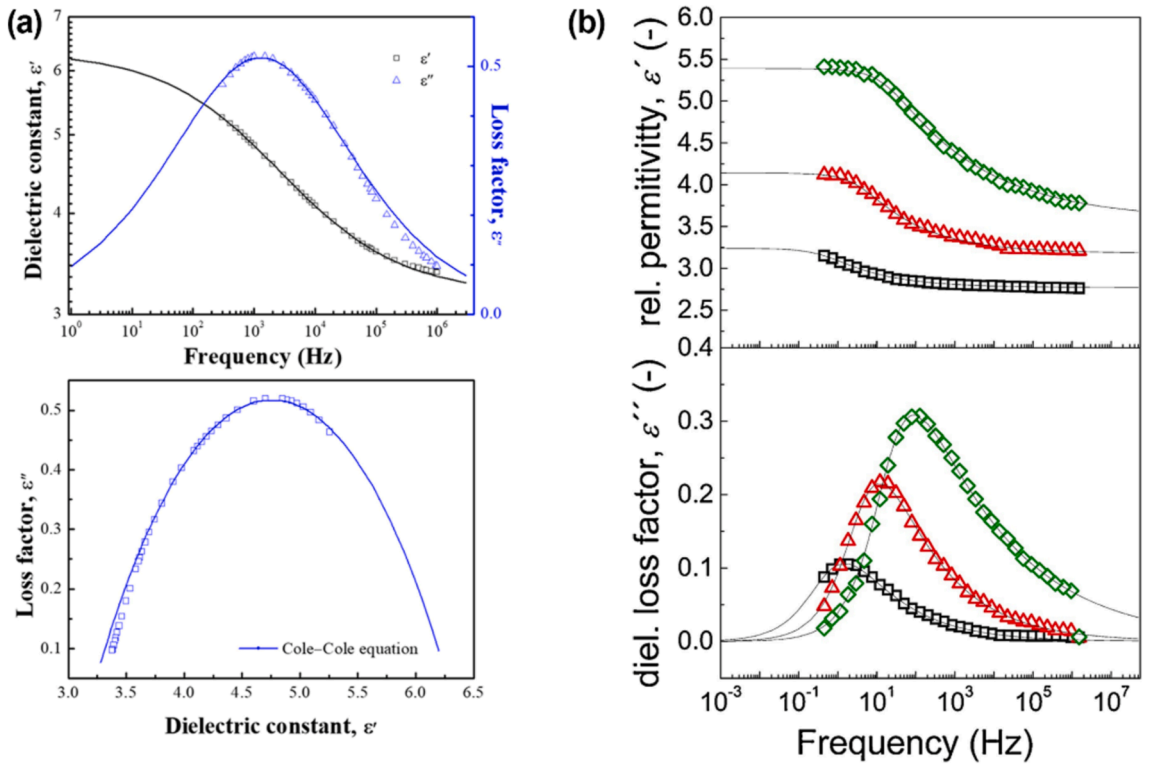

Fig. 15. Example of an applied Cole-Cole model re-printed from Dong et al. [344] showing dielectric properties (top part): dielectric constant (square) and loss factor (triangular) vs. frequency. The bottom part presents loss factor vs. dielectric constant for (a). Example of an applied Havriliak-Negami model re-printed from Mrlik et al. [348], comparing the dielectric spectra of three diverse samples (b).Reproduced with a permission from Refs. [344,348] with a permission from MDPI and Elsevier.

[339,340], while t_{rel} corresponds to the polarization response. Generally, a higher ER effect is expected from increasing $\Delta\varepsilon'$ and lower t_{rel} [95]; however, Wang et al. [341] estimates a threshold of t_{rel} around 10^{-2} s, above which the break shear range changes and is rather influenced by of t_{rel} than by the electrostatic and hydrodynamic forces and thus will lead to a decrease of the ER effect.

To predict these properties of ERF-focused studies, Cole-Cole model [342] or Havriliak-Negami model [343] are often applied. In particular, Cole-Cole is more commonly used [344,345] and can well-predict symmetrical permittivity in both AC and DC fields [346,347]:

$$\varepsilon^{*} = \varepsilon'_{\infty} + \frac{(\varepsilon'_{0} - \varepsilon'_{\infty})}{1 + (i\omega t_{rel})^{1-\alpha}} \tag{2}$$

where ω represents the angular frequency and α is an exponent parameter of a value between 0 and 1, describing polarization relaxation shape in terms of width. However, Havriliak-Negami is suitable in cases of an asymmetrical permittivity dependence on frequency, since the model can manage such asymmetry [206]:

$$\varepsilon^{*} = \varepsilon'_{\infty} + \frac{(\varepsilon'_{0} - \varepsilon'_{\infty})}{(1 + (i\omega t_{rel})^{\alpha})^{\beta}} \tag{3}$$

where in addition to the shape parameter α, it also describes the shape parameter of β (also in the range of 0–1), describing the shape in terms of skewness.

As an illustrative comparison, examples of the models visualization are presented in Fig. 15.

Some materials naturally have high dielectric constant (such as titania [349]) and the dielectric properties can be further influenced by modification [132,194], or in a form of composite particles [245]. In the case of carbonized material, the initial carbonization temperature also affects the dielectric properties [340].

6.2. Temperature

Working temperature of ERFs is mentioned in numerous studies, both in inorganic-based and organic-based systems, as well as in GER fluids and rightfully so. Hao [196] presents two primary reasons, how temperature can influence ER behaviour. Firstly, the

particle conductivity and the dielectric properties vary with temperature, and so the polarizability changes. Secondly, the particle thermal motion is directly impacted and if intensifies enough at high temperatures, it can be strong enough to compete with the chain-like structure formation. Diffusion, which is proportional to the temperate, is generally desired up to a point as it suppresses the sedimentation however, at higher temperatures other mechanisms dominate i.e. a lower viscosity and in the end sedimentation is promoted. Ultimately, depending on which of the forces dominate, the results may include both an intense ER effect or a weakening of performance. Too low temperature can also diminish the ER effect [350]. Therefore, these effective thermal limits of ERFs should be considered for applications. A narrower range is expected for wet-based systems (in particular, Hao mentions between –20 to + 70°C [196]), but can be improved, for instance by doping [128,351]. Yin et al. [352] evaluated the ER effect of PANI derived carbonaceous nanotubes across various temperatures ranging from 25 °C to 115 °C. The latter enables the highest ER effect with great stability even at the high shear rate region, as the critical shear rate kept shifting towards higher rates through the increasing temperatures, also off-field viscosity decreased with the same trend. Changes in the viscosity of carrier medium can be noted, but generally in the case of silicon oil, the difference is rather negligible [138]. However, for other carriers this dependence is very important as the viscosity is proportional to the efficiency of the ERF [353].

It can be estimated that generally wide working temperature will stay as a desirable characteristic for future ERF development.

6.3. *Particle size*

The optimal dimensions of ERF particles are often considered to be in a range between 0.1–100 μm, which is also the supposed range of commercially available ERFs. Bigger particles could achieve a higher yield stress however, at some point the particles are too big thus sediment and agglomerate. On the other hand, smaller particles offer a wider active surface, resulting in a higher amount of polar forces. For instance, Saabome et al. [354] evaluated the performance of aminated polyacrylonitrile particles of nano and micron range and concluded that micron-sized ones exhibited superior ER performance of the two. Yuan et al. [355] came to a similar conclusion while studying PIL particles. Furthermore, particle size has a notable effect onto the stability of chain-like structures in field

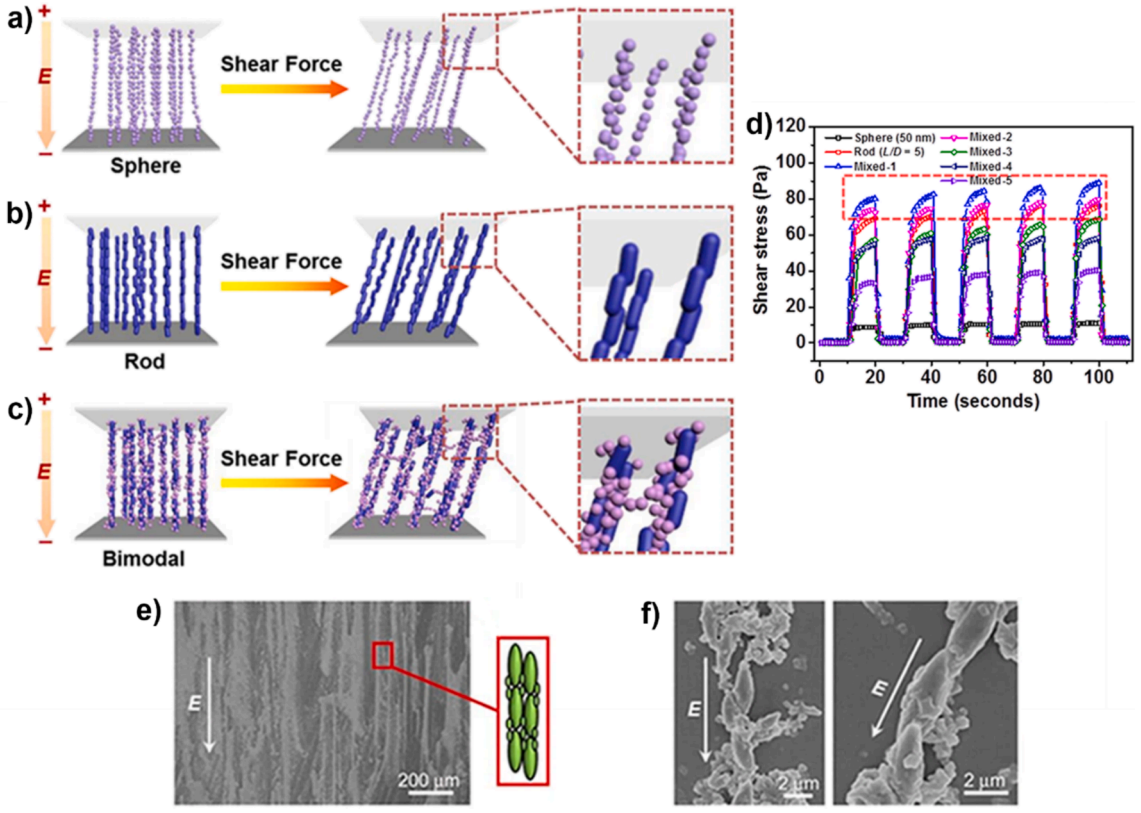

Fig. 16. Yoon et al. [147]: Schematic comparison of ERFs based on spherical particles (a), rod particles (b), and bimodal ERF (c) and their ER effect demonstrated as shear stress over time at a fixed shear rate 0.1 s^{-1} and alternating field of 3 kV mm^{-1}(d). Mixed samples 1–5 represent the composition proportion of spheres to rods, with Mixed 1 with the lowest percentage of rods and Mixed 5 with the highest. Adapted with a permission fom {Yoon C-M, Jang Y, Noh J, Kim J, Lee K, Jang J. Enhanced Electrorheological Performance of Mixed Silica Nanomaterial Geometry. ACS Appl Mater Interfaces; 9: 36358-67} Copyright {2017} American Chemical Society. Wu et al. [366]: Bimodal GER, SEM pictures of the chain-like structures in an active electric field with an illustrative insert (e), and magnified (f). Re-printed from Ref. [366] with a permission of Nature Portfolio.

[71]. If the particles are too small, the created chains may not be stable enough at moderate shear rates, along with the hydrodynamic forces breaking the structured ERF. Last but not least, sedimentation stability is highly influenced by particle size, as overly large particles are more prone to sediment resulting in degrading ER effect [102,196,356,357].

Additionally, certain studies focused on comparing ERFs containing either diverse sized or highly uniform spherical particles. Yuan et al. [358] compared systems of mono-sized PIL particles with systems of varied ratio of smaller and larger particles and concluded, that the best ER performance was indeed achieved with the same particle's dimensions. The sample containing an equal ratio of both particles' sizes showed the lowest ER effect. In contrast, See et al. [359] concluded particularly the 50:50 ratio-based ERF of 15 μm and 50 μm particles of sulfonated poly(styrene-*co*-divinylbenzene) reached the best ER results. Jun et al. [360] focused on hydrolysed styrene-acrylonitrile copolymer-based ERFs and concluded that a particular ratio of 0.2 of 5 μm particles to 15 μm particles resulted in a superior yield stress in comparison to the mono-sized dispersion, with the rest of ERFs based on mixed dimensions showed lower ER performance. Overall, the reported authors estimate that deeper research is needed to fully understand the tendencies of the mixed ERFs and their trends. For the similar magnetorheological suspensions, theory and experiments suggest that particles with high distribution and bidispersed/dimorphic systems provide more robust chain-like structures as the smaller particles fill the gaps of the larger particles [361,362].

As discussed, the dimensions of ERF particles influence the ER behaviour. While most research use more or less alike-sized particles (as can be seen in the summary tables). Besides understanding which size is the most optimal in terms of ER effect, yield stress, sedimentation stability, a number of studies further pay attention to mixed-size systems which may represent an interesting direction of future development.

6.4. *Particle morphology*

There is an immense variety of morphology of particles used as the dispersed phase, as each ER material and their corresponding application usually have their own specifics. Due to this versality, this section is rather extensive.

As aforementioned in the Dispersed phase section, certain base shapes were noted: spheres, flakes, rods, tubes, or fibrous particles, with the latter showing a tendency to gain numerous advantages from their higher aspect ratio [92]. Such geometry can lead to an improved ER effect, a dispersion stability, or other properties. For instance, Yin and Zhao [40] introduced TiO_2 nano-whisker shape-based ERF, confirming the enhanced properties (in addition, this ERF was recently re-evaluated by Zhang et al. [363] Similarly, a decrease in particle size of nanocellulose particles while increasing their aspect ratio led to a more intense ER effect as well as lowering their relaxation time of the polarization process [85].

Furthermore, the synthesis process further affects the morphology of particles and thus can alter some properties. Kutálková et al. [105] experimented with several synthesis conditions of rod-shaped iron oxalate particles and their resulting ER behaviour. The group proved that a variety of synthesis conditions, especially the drip rate and stirring pace, altered the particle's shape and structure which significantly impacted the ER properties of the final material. In particular, the sample with the highest *L/D* ratio, coded as OX3, achieved the best sedimentation stability (90 % after 55 h, compared to other samples which achieved 70 % or lower) and the highest yield stress and ER efficiency. Another similar example includes the ER response of acid-hydrolyzed cellulose-based ERF by Liu et al. [364] which confirmed that the degree of hydrolization affected the shape development of the cellulose particles thus further varying the systems ER performance.

Similarly to above-mentioned studies comparing ERFs spherical particles with mixed diverse sizes, systems based on particles of mixed morphology gained minor attention (in contrary to the traditional dispersions of homogenous particles of a single-type morphology) [365]. Interactions between the particles of, so-called, dimorphic or bimodal morphology may offer promising advantages, such as improving the ER effect and efficiency through more robust chains in field. While the bigger particles form a stable chain-like structure, the smaller ones gather and fill up the spaces between neighbouring large particles (as can be seen in both in schema part and SEM pictures in Fig. 16), thus increasing their stability and improving the yield stress [366].

However, limited amount of research has addressed this type of ERF so far. Yoon et al. [147] introduced bimodal ER systems based

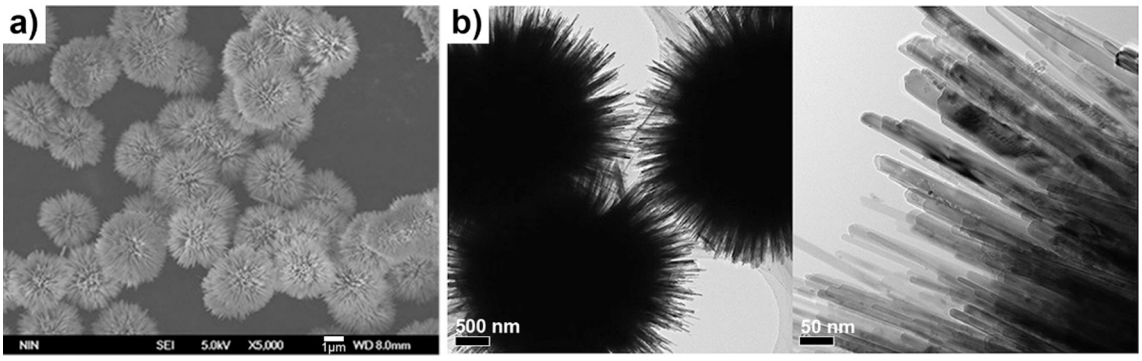

Fig. 17. Example of urchin-like morphology. Yin et al. [368]: Cr-doped titania particles captioned by SEM (a) and TEM (b). Re-printed from Ref. [368] with a permission of the Royal Society of Chemistry.

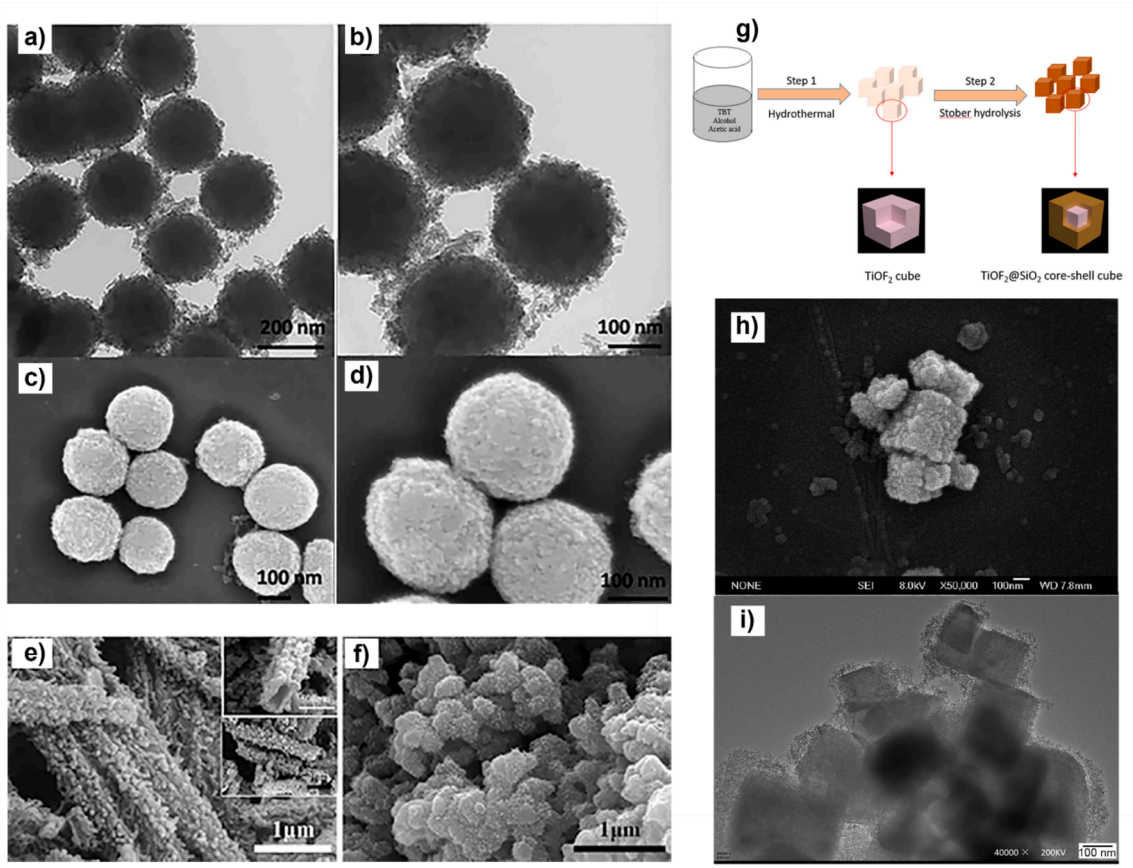

Fig. 18. Ji et al. [119]: Characterization of double-shell structured cactus-like SiO_2&TiO_2 particles, TEM (a, b) and SEM (c, d). Lee et al. [369].: Comparison of SEM pictures of polyaniline tubes with nanorod-covered surface (e) and regular granular PANI (f). Li et al. [370]: Schema of cubic-like $TiOF_2/SiO_2$ composites. Synthesis schema of $TiOF_2/SiO_2$ composites (g) and their characterization through SEM (h) and TEM (i). Re-printed from Refs. [119,369,370] with a permission of Elsevier and Wiley.

on silica particles, combining spherical and rod-like particles, taking advantage of facile particle shape tailoring of this material. The authors investigated the ER behaviour of multiple ERF dispersions of four types of spheres (ranging in size between 50 up to 350 nm) and three kinds of rods with different *L/D* ratio (2, 3, and 5), and of varied concentration-proportion of both shapes of particles. In total, 60 bimodal ER fluid samples were evaluated. Dielectric properties were tested to confirm the enhanced ER effect resulted from the geometry and not from the dielectric properties (permittivity values of bimodal samples were lower than rod-based samples, due to the presence of spheres). In terms of ER effect, composition of 50 nm spheres with 5 aspect ratio rods reached the highest shear stress values at a fixed low shear rate and alternating electric field 3 kV mm^{-1}, as presented in an inserted graph in Fig. 16d. Similar improvement was noticed in GER systems. Wu et al. [366] utilized the bimodal approach, combining spindly anisotropic nano and micron-size particles in a GER fluid (as presented in Fig. 16e, f), whose interactions lead to extraordinary ER efficiency. Liang et al. [367] introduced a binary liquid system, broadening the particle size distribution of the dispersed phase and strengthening the chain-like structures in field as a result, as well as significantly improving the dispersion stability.

The complexity of the morphology further opens the door to more shape variations. One of those, rather popular in terms of research attention, is urchin-like sphere shape, as shown in Fig. 17. Such particles provide a larger active area, if compared their smooth spherical analogue. Besides enhanced ER properties, Cheng et al. [108] demonstrated an increased interfacial polarization, a shorter relaxation time, and as a result, the creation of stiffer and more stable chain-like structures (while comparing the performance of smooth particles of the same material). Kim at al. [114] concluded with similar improvements using polymeric core–shell particles as well as Yin et al. [368] with Cr-doped titania. In particular, Fig. 17a presents SEM picture of the modified titania paricles, complemented with their TEM images (Fig. 17b).

Similarly, cactus-shaped double-shell structured SiO_2&TiO_2 nanocomposites reported by Ji et al. [119] (Fig. 18 a, b, c, d). As can be seen, both SEM and transmission electron microscopy (TEM) were used for characterization to confirm the morphology. In addition, these cactus-like particles exhibited promising microwave absorption properties. Furthermore, other various examples of distinctive morphology shapes were reported. Examples of these are further displayed in the following figures. Lee at al. [369] reported rectangular-shaped PANI tubes with their surface covered by nanorods (Fig. 18e), differing from the rather-usual irregularly-shaped PANI particles. For comparison, general particulate PANI is captioned in Fig. 18f. Utilizing silica as a template, Li et al. [349,370]

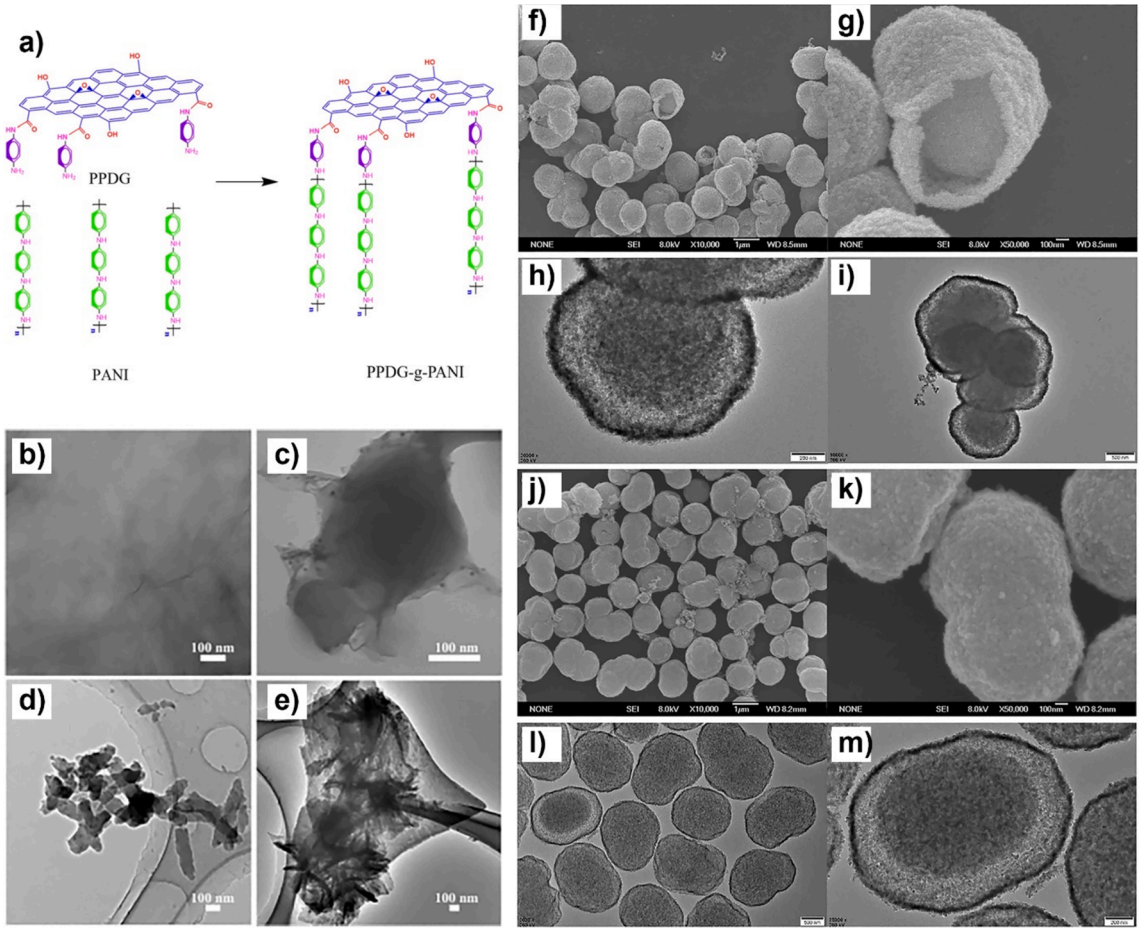

Fig. 19. Zhang et al. [265]: Synthesis schema of PPDG-g-PANI particles (a), followed by TEM images of each component, namely of pure GO (b), PPDG (c), PANI (d) and finally the PPDG-g-PANI composite (e). Reproduced from Ref. [265] with permission of Elsevier. Sun et al. [371]: TiO_2 template of hollow peanut-like particles depicted by SEM (f, g) and TEM (h, i). TiO_2/SiO_2 composite characterized by SEM (j, k) and TEM (l, m). Re-printed from Ref. [371] with the permission of Wiley.

reported unique cubic-like morphology, firstly hollow titania particles [349], and later $TiOF_2/SiO_2$ core–shell nanoparticles with smooth surface [370]. The later was obtained utilizing hydrothermal method to obtain the cubic template. Fig. 18 further presents the schema of the template formation and application during the synthesis (g) alongside SEM (h) and TEM pictures (i) of the resulting composites. In addition, titanium oxydifluoride was presented as a fairly novel material to ERFs (although its ER efficiency is rather low, so far).

As the next example, the peculiar structure of already-mentioned PPDG-g-PANI jellyfish-shaped particles with enhanced sedimentation stability should be highlighted [265] (Fig. 19 a-e). Fig. 19a illustrates the synthetic route of the composite, while 17b-d TEM images of the pure individual starting components and finally Fig. 19e shows the TEM image of the final composite. Although its ER efficiency is not as high in comparison to other particles (as compared in Table 3), the composite exhibits excellent dispersion stability and may find applications in biomedical or microfluidic devices, as the authors note. Sun et al. [371] synthesised peanut-like shaped hollow SiO_2&TiO_2 core–shell particles of anisotropic growth (as can be seen in Fig. 19 f-m), possessing enhanced ER properties and lower current-leakage density. The figure in detail demonstrates the formed titania template (parts f-i) presented by SEM and TEM characterization, which was achieved by hydrothermal method and followed by Stöber hydrolysis step, the core–shell particles were formed. As can be seen in Fig. 19 (j-k), SEM and TEM were used to confirm the anisotropic shape of the hollow composite.

Similarly to the peanut-shaped particles, other studies focused on hollowed particles. This approach offers several benefits, such as higher specific active area, improved sedimentation stability or even enhanced dielectric properties, as mentioned by Yoon et al. [34,39] Enhanced sedimentation stability was demonstrated by Cheng et al. [372] who introduced template-free method to create hollow POA microspheres, however, their ER effect was lower than regular POA granular particles. To briefly remind other already-mentioned hollow examples of this approach: PANI spheres by Sung et al. [36], urchin-like titania spheres by Cheng et al. [108].

Furthermore, sheet-based particles should be worthy of an interest. The sheet-like morphology is typical for GO-based particles, which due to their unique structure may form extremely thin sheets, as was above-mentioned in the graphene dedicated section. To name a few examples that were mentioned: Chen et al. [247] presented multi-layered GO/PPy/PIL nanosheets. Mrlik et al. [194]

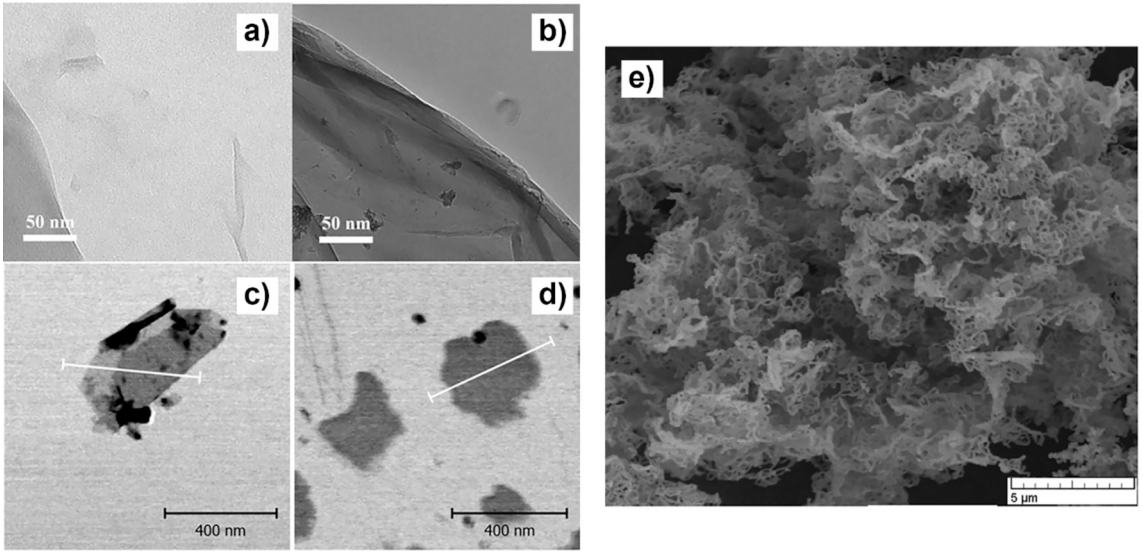

Fig. 20. Mrlik et al.[194] Comparison of pure GO and modified GO sheets. Characterization images of TEM of the pure (a) and the modified (b) GO. Atomic force microscopy images of the neat GO (c) and PBMA modified GO (d). Re-printed from Ref. [194] with a permission from the Royal Society of Chemistry. Almajdalawi et al.[243]: Scanning electron microscopy picture of ribbon-like PPy particles (e). Re-printed with a permission from {Shawqi Almajdalawi; Vladimir Pavlinek; Qilin Cheng; Petr Saha; Miroslav Mrlik; Martin Stenicka. Electrorheological Properties of Suspensions of Polypyrrole Ribbon Particles in Silicone Oil. *AIP Conf. Proc.* 1375, 275–283 (2011)}. Copyright {2011} American Chemical Society.

compared pure GO sheets with modified GO in their publication, as demonstrated in Fig. 20 (a-d). The pure GO thickness was determined about 1 nm, whereas the PBMA modification increased it to about 5 nm. In particular, the neat GO was well exfoliated and resulted in very few layers, as can be seen in Fig. 20a. The modified counterpart is depicted as floss-like with darker colour (Fig. 20b). The authors further demonstrated the layer structure by atomic force microscopy images, as presented in the Fig. 20 parts c and d, with the darker areas representing additional particles.

Layered structure can be also accomplished by other materials, as an above-mentioned example, Almajdalawi et al. [243] synthesised unique ribbon-like-shaped PPy particles as a result of a network formation of nanowires (Fig. 20e).

Finally, significant attention has been focused on particles featuring porous surfaces, as the porosity naturally provides a larger active interface area, similarly to the abovementioned examples of zeolite-based particles, chitosan or porous MOFs. For that reason, alike urchin-like and other alternatively-shaped particles, the usage of porous or mesoporous materials offers additional ways of improving the ER performance or acquiring unique properties. Yin's and Zhao's [373] preparation of mesoporous Ce-doped TiO_2 ER material by a copolymer-templated sol–gel method resulted in considerate enhancement of ER activity (yield stress peaking over 70 kPa at 4 kV mm^{-1} field for 33 vol% suspension), exceeding both pure non-porous and mesoporous titania ER systems. Expanded perlite particles-based ERFs in silicone oil were also reported to gain enhanced yield stress values and improved sedimentation stability due to the pores [374]. Guo et al. [375] demonstrated multicoated porous SiO_2/Ni/TiO_2 composite particles achieving not only good ER response, but MR behaviour as well, while introducing an altered facile method of their preparation. This result might indicate a variety of options to exploit individual functions of each layer of the composite [376] As a final example, a number of studies focused on composites of pore-expanded silica (especially MCM-41-E type) with polymer particles included inside the pore channels [80,376,377]. An MCM-41-E/PPy type dispersed phase particles confirmed enhanced ER properties in comparison with regular MCM-41-E particles, as well as when compared to MCM-41/PANI [248,378]. Additionally, as mentioned above [251], an extraction of the polymer from the porous matrix is also possible and may offer an additional route for the research. Additionally, more information about mesoporous suspensions can be found, for instance, in this review by Kwon et al. [379].

As discussed, the ER performance is affected not only by the types of dispersed material or liquid carriers used, but by numerous other particular particle properties. These aspects should be considered when designing ERF particles/system for a specific purpose, their size, morphology, synthesis protocol should not be overlooked, as well as their temperature range, and dielectric properties. In particular, tube or whisker-like particle geometry can lead to enhanced ER efficiency when compared to dimensions of lower aspect ratio. Similarly, some of the rather complex geometry, such as urchin-like particles or particles with larger surface-active area, were proven to be beneficial to the ER effect.

7. Conclusion

In this material's review, ERFs were covered, including their general aspects and properties giving emphasis on the variety of materials used during different types of ER effects. The effect of different liquid carriers, types of dispersed phase along with its morphology on the ER performance, usage and stability were investigated. Concurrently, a wide range of inorganic, organic, and

hybrid materials are available, alongside with their immense amount of material combinations and further possible adjustments. The resulting properties of the majority of the covered ERF particles were summarized for further comparison in the summary tables.

As can be seen, even after many decades of research, ERFs keep their relevance and attract further attention up to date. The aim of commercializing ERF-based systems yet faces a lot of challenges, as such, a lot of efforts have been focused to enhance the ER properties or to minimalize weaknesses of individual materials through various means (composite material combination, geometry and surface modification, doping, lowering density, and more as was discussed). Namely the sedimentation stability, efficient energy cost of operating ERFs, and impactful ER efficiency needs to be improved. In comparison with MR systems (which can be considered a great ER competitors), ERFs generally have lower efficiency, but are relevant in applications in which magnetic field is counterproductive. Additionally, a rich variety of materials can be prospective as ER systems, as presented. Lastly, there is a lack of theoretical studies which would serve to predict the best ER materials which hurts especially in composites. Instead of studding and thus predicting what materials or concentrations are the most optimal, researchers usually use the trial and failure methods which is time consuming and expensive.

As such, high-performance ERFs with great long-term stability and lifetime are bound to remain a hot research topic. The development of dispersed phase materials with ideal polarization (low relaxation time, high dielectric relaxation strength, high specific active surface area for higher polarization, and alike) is estimated to continue. However, we can expect other directions of future research trends. As the global attention has been turning towards sustainable resources, environmentally-friendly or biodegradable materials are likely to attract attention. A similar estimation can be said about materials with environmentally-nondemanding and facile synthesis. Additionally, efficient materials made through a post-treatment or recirculation could represent an interesting challenge. Further particles with, low-cost materials, or those which are effective with very low concentration can be expected to satisfy needs of economically-oriented customers. Also, materials that are ER-efficient in lower fields (and in that way can be economical in terms of electrical energy consumption) are bound to attract demand. Finally, certain applications may require very specific combination of properties which may give demand to niche materials, for instance, materials with dual ER and MR response.

Considering the potential of these smart systems, electrorheology remains to represent a rich and attention-worthy field that needs to be re-evaluated consistently in terms of the materials used. It may be technology known for a long time, but now it is the crucial time to further develop it.

Additionally, the authors would like to encourage fellow researches to contact us to include their ERF published data into the attached living document, to gradually create a rich resource for the ER community.

CRediT authorship contribution statement

Lenka Munteanu: Writing – original draft, Visualization. **Andrei Munteanu:** Writing – review & editing. **Michal Sedlacik:** Writing – review & editing, Supervision, Project administration.

Declaration of competing interest

The authors declare that they have no known competing financial interests or personal relationships that could have appeared to influence the work reported in this paper.

Acknowledgement

The authors thank the DKRVO grant no. RP/CPS/2024-28/007 for financial support.

Data availability

No data was used for the research described in the article.

References

[1] Winslow WM. Induced fibration of suspensions. J Appl Phys 1949;20:1137–40. https://doi.org/10.1063/1.1698285.
[2] Kuznetsov N, Kovaleva V, Belousov S, Chvalun S. Electrorheological fluids: from historical retrospective to recent trends. Mater Today Chem 2022;26:101066. https://doi.org/10.1016/j.mtchem.2022.101066.
[3] Kamath GM, Hurt MK, Wereley NM. Analysis and testing of Bingham plastic behavior in semi-active electrorheological fluid dampers. Smart Mater Struct 1996;5:576. https://doi.org/10.1088/0964-1726/5/5/007.
[4] Cho M, Choi H, Jhon M. Shear stress analysis of a semiconducting polymer based electrorheological fluid system. Polymer 2005;46:11484–8. https://doi.org/10.1016/j.polymer.2005.10.029.
[5] Seo YP, Seo Y. Modeling and analysis of electrorheological suspensions in shear flow. Langmuir 2012;28:3077–84. https://doi.org/10.1021/la204515q.
[6] Yamaguchi H, Zhang XR, Niu XD. Damping characteristics and flow behaviors of an ER fluid with a piston sine vibration in a viscous damper. Smart Mater Struct 2010;19:105032. https://doi.org/10.1088/0964-1726/19/10/105032.
[7] Liu W, Jin H, Yao J. Vibration performance analysis of a self-energized damper composed of electrorheological fluid and piezoelectric ceramics. Mech Based Des Struct Mach 2022;51:5968–82. https://doi.org/10.1080/15397734.2022.2027781.
[8] Heinken H, Ulrich S, Bruns R, Schneider S. High-response electrorheological servo valve. J Intell Mater Syst Struct 2020;31:297–307. https://doi.org/10.1177/1045389X19873427.

[9] Bauerochs T, Ulrich S, Bruns R. Experimental study on the behaviour of an electrorheological double miniature valve. J Intell Mater Syst Struct 2021;32:1368–76. https://doi.org/10.1177/1045389X20966055.
[10] Sun Y, Thomas M. Control of torsional rotor vibrations using an electrorheological fluid dynamic absorber. J Vib Control 2011;17:1253–64. https://doi.org/10.1177/1077546309359759.
[11] Musiałek I, Migus M, Olszak A, Osowski K, Kęsy Z, Kęsy A, Kim GW, Choi SB. Analysis of a combined clutch with an electrorheological fluid. Smart Mater Struct 2020;29(8):087006. https://doi.org/10.1088/1361-665X/ab9fd7.
[12] Mazursky A, Koo JH, Yang TH. Design, modeling, and evaluation of a slim haptic actuator based on electrorheological fluid. J Intell Mater Syst Struct 2019;30:2521–33. https://doi.org/10.1177/1045389X19836172.
[13] Jing H, Hua L, Long F, Lv B, Wang B, Zhang H, et al. Variable stiffness and fast-response soft structures based on electrorheological fluids. J Mater Chem C 2023;11:11842–50. https://doi.org/10.1039/D3TC01563G.
[14] Liu YD, Lee BM, Park TS, Kim JE, Choi HJ, Booh SW. Optically transparent electrorheological fluid with urea-modified silica nanoparticles and its haptic display application. J Colloid Interface Sci 2013;404:56–61. https://doi.org/10.1016/j.jcis.2013.05.012.
[15] Mazursky A, Koo JH, Mason T, Woo SY, Yang TH. Design and Experimental Evaluation of an Electrorheological Haptic Module with Embedded Sensing. Appl Sci. 2021;11(16):7723. https://doi.org/10.3390/app11167723.
[16] Qu WL, Xu YL, Lv MY. Seismic response control of large-span machinery building on top of ship lift towers using ER/MR moment controllers. Eng Struct 2002;24:517–27. https://doi.org/10.1016/S0141-0296(01)00118-3.
[17] Pnevmatikos NG, Kallivokas LF, Gantes CJ. Feed-forward control of active variable stiffness systems for mitigating seismic hazard in structures. Eng Struct 2004;26:471–83. https://doi.org/10.1016/j.engstruct.2003.11.003.
[18] Behbahani SB, Tan X. Design and dynamic modeling of electrorheological fluid-based variable-stiffness fin for robotic fish. Smart Mater Struct 2017;26:085014. https://doi.org/10.1088/1361-665X/aa7238.
[19] Zatopa A, Walker S, Menguc Y. Fully soft 3D-printed electroactive fluidic valve for soft hydraulic robots. Soft Rob 2018;5:258–71. https://doi.org/10.1089/soro.2017.0019.
[20] Hwang Y-H, Kang S-R, Cha S-W, Choi S-B. An electrorheological spherical joint actuator for a haptic master with application to robot-assisted cutting surgery. Sens Actuators, A 2016;249:163–71. https://doi.org/10.1016/j.sna.2016.08.033.
[21] Sadi F, Holthausen J, Stallkamp J, Siegfarth M. Development of novel hydraulic 3D printed actuator using electrorheological fluid for robotic endoscopy. In: Actuators, Vol. 13, No. 4. MDPI; 2024. p. 119. https://doi.org/10.3390/act13040119.
[22] Li Y, Maeda Y, Hashimoto M. Lightweight, soft variable stiffness gel spats for walking assistance. Int J Adv Rob Syst 2015;12:175. https://doi.org/10.5772/61815.
[23] Davidson JR, Krebs HI. An electrorheological fluid actuator for rehabilitation robotics. IEEE/ASME Trans Mechatron 2018;23:2158–67. https://doi.org/10.1109/TMECH.2018.2869126.
[24] Kim W, Lee S, Kim Y, Lee E. The electromechanical principle of electrorheological fluid-assisted polishing. Int J Mach Tool Manu 2003;43:81–8. https://doi.org/10.1016/S0890-6955(02)00143-8.
[25] Sun H, Hu X, Zhao X, Ngai T, Yin J. Hollow poly(ionic liquid)/α-Al_2O_3 composite particles prepared by microwave-assisted pickering emulsion polymerization and their electrorheological polishing property. ACS Appl Polym Mater 2023;5:6412–20. https://doi.org/10.1021/acsapm.3c01001.
[26] Kuriyagawa T, Saeki M, Syoji K. Electrorheological fluid-assisted ultra-precision polishing for small three-dimensional parts. Precis Eng 2002;26:370–80. https://doi.org/10.1016/S0141-6359(02)00112-5.
[27] Tao R, Tang H. Reducing viscosity of paraffin base crude oil with electric field for oil production and transportation. Fuel 2014;118:69–72. https://doi.org/10.1016/j.fuel.2013.10.056.
[28] Zhang C, Li H, Wang Y, Xie Y, Kang J, Su Y, Li J, Han S, Zhang J. An energy perspective on the mechanism of crude oil electrorheological effect. Phys Fluids 2024;36(4). https://doi.org/10.1063/5.0202010.
[29] Anitas EM, Munteanu A, Sedlacik M, Bica I, Munteanu L, Stejskal J. Magnetic and electric effects in magnetorheological suspensions based on silicone oil and polypyrrole nanotubes decorated with magnetite nanoparticles. Results Phys 2024;61:107768. https://doi.org/10.1016/j.rinp.2024.107768.
[30] Web of Science. 2024.
[31] Block H, Kelly JP, Qin A, Watson T. Materials and mechanisms in electrorheology. Langmuir 1990;6:6–14. https://doi.org/10.1021/la00091a002.
[32] Hao T. The interfacial polarization-induced electrorheological effect. J Colloid Interface Sci 1998;206:240–6. https://doi.org/10.1006/jcis.1998.5658.
[33] Guo X, Chen Y, Su M, Li D, Li G, Li C, et al. Enhanced electrorheological performance of Nb-doped TiO2 microspheres based suspensions and their behavior characteristics in low-frequency dielectric spectroscopy. ACS Appl Mater Interfaces 2015;7:26624–32. https://doi.org/10.1021/cm103489r.
[34] Yoon CM, Lee S, Cheong OJ, Jang J. Enhanced electroresponse of alkaline earth metal-doped silica/titania spheres by synergetic effect of dispersion stability and dielectric property. ACS Appl Mater Interfaces 2015;7:18977–84. https://doi.org/10.1021/acsami.5b02388.
[35] Yoon CM, Lee S, Hong SH, Jang J. Fabrication of density-controlled graphene oxide-coated mesoporous silica spheres and their electrorheological activity. J Colloid Interface Sci 2015;438:14–21. https://doi.org/10.1016/j.jcis.2014.09.074.
[36] Sung BH, Choi US, Jang HG, Park YS. Novel approach to enhance the dispersion stability of ER fluids based on hollow polyaniline sphere particle. Colloids Surf A Physicochem Eng Asp 2006;274:37–42. https://doi.org/10.1016/j.colsurfa.2005.08.030.
[37] Han J, Song G, Guo R. A facile solution route for polymeric hollow spheres with controllable size. Adv Mater 2006;18:3140–4. https://doi.org/10.1002/adma.200600282.
[38] Krzton-Maziopa A, Gorkier M, Plocharski J. ER suspensions of composite core-shell microspheres with improved sedimentation stability. Polym Adv Technol 2012;23:702–9. https://doi.org/10.1002/pat.1951.
[39] Yoon CM, Noh J, Jang Y, Jang J. Fabrication of a silica/titania hollow nanorod and its electroresponsive activity. RSC Adv 2017;7:19754–63. https://doi.org/10.1039/C7RA01786C.
[40] Yin J, Zhao X. Titanate nano-whisker electrorheological fluid with high suspended stability and ER activity. Nanotechnology 2006;17:192–6. https://doi.org/10.1088/0957-4484/17/1/031.
[41] Boissy C, Allen P, Foulc J-N. On a negative electrorheological effect. J Electrostat 1995;35:13–20. https://doi.org/10.1016/0304-3886(95)00015-3.
[42] Komoda Y, Sakai N, Rao TN, Tryk DA, Fujishima A. Photoelectrorheological phenomena involving TiO_2 particle suspensions. Langmuir 1998;14:1081–91. https://doi.org/10.1021/la9706633.
[43] Jin J, Wang X, Hu S, Geng J, Jing D. Unusual photorheological properties of TiO_2 nanoparticle suspensions under UV light irradiation. J Phys D Appl Phys 2019;52:275301. https://doi.org/10.1088/1361-6463/ab1a91.
[44] Kelbysheva ES, Danilin AN, Ezernitskaya MG, Semenov NA. Photoelectrorheological properties of polyimides with sulfo-acid and sodium salt sulfo-acid groups: a comparative study. The European Physical Journal Plus 2023;138:1–10. https://doi.org/10.1140/epjp/s13360-023-04383-6.
[45] Hao T. Electrorheological fluids. Adv Mater 2002;13:1847–57. https://doi.org/10.1002/0471216275.esm035.
[46] Trlica J, Quadrat O, Bradna P, Pavlinek V, Saha P. An anomalous electrorheological behavior of magnesium hydroxide suspensions in silicone oil. J Rheol 1996;40:943–6. https://doi.org/10.1122/1.550769.
[47] Mitsumata T, Sugitani K. Negative electrorheological effect of silicone gels containing barium titanate. Macromol Rapid Commun 2004;25:848–52. https://doi.org/10.1002/marc.200300278.
[48] Mitsumata T, Sugitani K, Koyama K. Electrorheological response of swollen silicone gels containing barium titanate. Polymer 2004;45:3811–7. https://doi.org/10.1016/j.polymer.2004.03.056.
[49] Ko YG, Lee HJ, Chun YJ, Choi US, Yoo KP. Positive and negative electrorheological response of alginate salts dispersed suspensions under electric field. ACS Appl Mater Interfaces 2013;5:1122–30. https://doi.org/10.1021/am302891w.
[50] Plachy T, Masar M, Mrlik M, Machovsky M, Machovska Z, Kutalkova E, et al. Switching between negative and positive electrorheological effect of g-C_3N_4 by copper ions doping. Adv Powder Technol 2019;30:714–23. https://doi.org/10.1016/j.apt.2019.01.001.

[51] Agafonov AV, Kraev AS, Kusova TV, Evdokimova OL, Ivanova OS, Baranchikov AE, Shekunova TO, Kozyukhin SA. Surfactant-switched positive/negative electrorheological effect in tungsten oxide suspensions. Molecules 2019;24(18):3348. https://doi.org/10.3390/molecules24183348.

[52] Cetin B, Unal HI, Erol O. The negative and positive electrorheological behavior and vibration damping characteristics of colemanite and polyindene/colemanite conducting composite. Smart Mater Struct 2012;21:125011. https://doi.org/10.1088/0964-1726/21/12/125011.

[53] Ramos-Tejada MM, Arroyo FJ, Delgado AV. Negative electrorheological behavior in suspensions of inorganic particles. Langmuir 2010;26:16833–40. https://doi.org/10.1021/la1029036.

[54] Do T, Ko YG, Jung Y, Chun Y, Choi US. Design of negative electrorheological materials inspired by electrophoretic separation of biomolecules. J Mater Chem C 2017;5:11683–93. https://doi.org/10.1039/c7tc03566g.

[55] Do T, Ko YG, Chun Y, Jung Y, Choi US, Park YS, et al. Switchable electrorheological activity of polyacrylonitrile microspheres by thermal treatment: from negative to positive. Soft Matter 2018;14:8912–23. https://doi.org/10.1039/c8sm01691g.

[56] Yang M, Liu G, Zeng Z, Zhang S, Liu J, Qin Z, Chen Z, Yang BR. Dual-Mode Switching E-Paper by Negative Electrorheological Fluid with Reversible Silica Networks. Adv Mater Technol 2022;7(12):2200371. https://doi.org/10.1002/admt.202200371.

[57] Bica I, Anitas EM, Sedlacik M, Munteanu A, Munteanu L, Chirigiu LME, et al. Electromagnetic modulation of conductance and susceptance in electrical devices based on silicone oil with polypyrrole–magnetite particle composites. J Mater Chem C 2024. https://doi.org/10.1039/D4TC02073A.

[58] Bica I, Anitas EM, Sedlacik M, Munteanu A, Munteanu L, Chirigiu LME. Electrorheological and magnetorheological properties of liquid composites based on polypyrrole nanotubes/magnetite nanoparticles. Smart Mater Struct 2024;33:065007. https://doi.org/10.1088/1361-665X/ad3ca9.

[59] Niu C, Dong X, Qi M. Enhanced electrorheological properties of elastomers containing TiO_2/urea core-shell particles. ACS Appl Mater Interfaces 2015;7:24855–63. https://doi.org/10.1021/acsami.5b08127.

[60] Borin DY, Stepanov GV. Elastomer with magneto- and electrorheological properties. J Intell Mater Syst Struct 2015;26:1893–8. https://doi.org/10.1177/1045389X15581521.

[61] Yuan X, Zhou X, Liang Y, Wang L, Chen R, Zhang M, et al. A stable high-performance isotropic electrorheological elastomer towards controllable and reversible circular motion. Compos B Eng 2020;193:107988. https://doi.org/10.1016/j.compositesb.2020.107988.

[62] Roman C, García-Morales M, Goswami S, Marques AC, Cidade MT. The electrorheological performance of polyaniline-based hybrid particles suspensions in silicone oil: influence of the dispersing medium viscosity. Smart Mater Struct 2018;27(7):075001. https://doi.org/10.1088/1361-665X/aac245.

[63] Davydova OI, Kraev AS, Redozubov AA, Trusova TA, Agafonov AV. Effect of polydimethylsiloxane viscosity on the electrorheological activity of dispersions based on it. Russ J Phys Chem A 2016;90:1269–73. https://doi.org/10.1134/S0036024416060054.

[64] Ma ND, Xufeng. Effect of carrier liquid on electrorheological performance and stability of oxalate group-modified TiO2 suspensions. J Wuhan Univ Technol-Mater Sci Ed 2017;32:854–61. https://doi.org/10.1007/s11595-017-1679-6.

[65] Roudnick LR. Synthetics, mineral oils, and bio-based lubricants: chemistry and technology. Second edition ed: CRC Press; 2013.

[66] Hong CH, Sung JH, Choi HJ. Effects of medium oil on electroresponsive characteristics of chitosan suspensions. Colloid Polym Sci 2009;287:583–9. https://doi.org/10.1007/s00396-009-2006-3.

[67] Davies JL, Blagbrough IS, Staniforth JN. Electrorheological behaviour at low applied electric fields of microcrystalline cellulose in BP oils. Chem Commun 2157-8; 1998. 10.1039/a806533k.

[68] Park S, Gwon H, Lee S. Electroresponsive performances of ecoresorbable smart fluids consisting of various plant-derived carrier liquids. Chem–A Eur J 2021;27:13739–47. https://doi.org/10.1002/chem.202101597.

[69] Hong Y, Wen W. Influence of carrier liquid on nanoparticle-based giant electrorheological fluid. J Intell Mater Syst Struct 2016;27:866–71. https://doi.org/10.1177/1045389X15596623.

[70] Jun CS, Kwon SH, Choi HJ, Seo Y. Polymeric nanoparticle-coated pickering emulsion-synthesized conducting polyaniline hybrid particles and their electrorheological study. ACS Appl Mater Interfaces 2017;9:44811–9. https://doi.org/10.1021/acsami.7b13808.

[71] Lee S. Highly uniform silica nanoparticles with finely controlled sizes for enhancement of electro-responsive smart fluids. J Ind Eng Chem 2019;77:426–31. https://doi.org/10.1016/j.jiec.2019.05.007.

[72] Seo YP, Choi HJ, Seo Y. A simplified model for analyzing the flow behavior of electrorheological fluids containing silica nanoparticle-decorated polyaniline nanofibers. Soft Matter 2012;8:4659–63. https://doi.org/10.1039/C2SM07275K.

[73] Daubert C, Steffe J. Electrorheological behavior of milk chocolate. J Texture Stud 1996;27:93–108. https://doi.org/10.1111/j.1745-4603.1996.tb00062.x.

[74] Clercx H, Bossis G. Many-body electrostatic interactions in electrorheological fluids. PhysRevE 1993;48:2721. https://doi.org/10.1103/PhysRevE.48.2721.

[75] Chun Y, Ko YG, Do T, Jung Y, Kim SW, Chun YJ, et al. Electrorheological properties of algae dispersed suspension: New application of harmful algae. Colloids Surf A Physicochem Eng Asp 2018;539:354–63. https://doi.org/10.1016/j.colsurfa.2017.12.022.

[76] Ma R, Xue B, Zhao X, Yin J. A water-free ionic covalent organic polymer with high electrorheological activity and temperature stability. ACS Appl Polym Mater 2023;5:5772–82. https://doi.org/10.1021/acsapm.3c01161.

[77] Wu J, Zhang L, Xin X, Zhang Y, Wang H, Sun A, et al. Electrorheological fluids with high shear stress based on wrinkly tin titanyl oxalate. ACS Appl Mater Interfaces 2018;10:6785–92. https://doi.org/10.1021/acsami.8b00869.

[78] Lengalova A, Pavlinek V, Saha P, Quadrat O, Takeshi K, Jaroslav S. Influence of particle concentration on the electrorheological efficiency of polyaniline suspensions. Eur Polym J 2003;39:641–5. https://doi.org/10.1016/S0014-3057(02)00281-1.

[79] Hao T, Kawai A, Ikazaki F. Mechanism of the electrorheological effect: evidence from the conductive, dielectric, and surface characteristics of water-free electrorheological fluids. Langmuir 1998;14:1256–62. https://doi.org/10.1021/la971062e.

[80] Lee IS, Cho MS, Hong CH, Choi HJ, Yoon SS, Ahn W-S. Preparation and electrorheological property of conducting copolyaniline/MCM-41 nanocomposite. Stud Surf Sci Catal 2005;156:517–22. https://doi.org/10.1016/S0167-2991(05)80250-2.

[81] Gan S, Piao SH, Choi HJ, Zakaria S, Chia CH. Synthesis of kenaf cellulose carbamate and its smart electric stimuli-response. Carbohydr Polym 2016;137:693–700. https://doi.org/10.1016/j.carbpol.2015.11.035.

[82] Kim YD, Yoon DJ. Electrorheological fluids of polypyrrole-tin oxide nanocomposite particles. Korea-Aust Rheol J 2016;28:275–9. https://doi.org/10.1007/s13367-016-0029-0.

[83] Kuznetsov NM, Zagoskin YD, Bakirov AV, Vdovichenko AY, Malakhov SN, Istomina AP, et al. Is chitosan the promising candidate for filler in nature-friendly electrorheological fluids? ACS Sustain Chem Eng 2021;9:3802–10. https://doi.org/10.1021/acssuschemeng.0c08793.

[84] Kovaleva VV, Kuznetsov NM, Istomina AP, Bogdanova OI, Vdovichenko AY, Streltsov DR, et al. Low-filled suspensions of α-chitin nanorods for electrorheological applications. Carbohydr Polym 2022;277:118792. https://doi.org/10.1016/j.carbpol.2021.118792.

[85] Kuznetsov NM, Kovaleva VV, Vdovichenko AY, Chvalun SN. Natural electrorheological fluids based on cellulose particles in olive oil: the filler size effect. Colloid J 2023;85:408–17. https://doi.org/10.1134/S1061933X23600276.

[86] Hao T. Chapter 8 - Dielectric properties of ER suspensions. In: Hao T, editor. Electrorheological Fluids: Elsevier; 2005. p. 424-74.

[87] Rejon L, Ponce MA, De La Luz C, Nava R, Castano VM. Effect of dielectric constant of the liquid phase of electrorheological fluids. J Intell Mater Syst Struct 1995;6:840–5. https://doi.org/10.1177/1045389X9500600612.

[88] Munteanu L, Munteanu A, Sedlacik M, Kutalkova E, Kohl M, Kalendova A. Zinc ferrite/polyaniline composite particles: pigment applicable as electro-active paint. J Ind Eng Chem 2022. https://doi.org/10.1016/j.jiec.2022.08.030.

[89] Davis LC. Polarization forces and conductivity effects in electrorheological fluids. J Appl Phys 1992;72:1334–40. https://doi.org/10.1063/1.351743.

[90] Hao T, Xu Z, Xu Y. Correlation of the dielectric properties of dispersed particles with the electrorheological effect. J Colloid Interface Sci 1997;190:334–40. https://doi.org/10.1006/jcis.1997.4871.

[91] Tang X, Li W, Wang X, Zhang P. Structure evolution of electrorheological fluids under flow conditions. Int J Mod Phys B 1999;13:1806–13. https://doi.org/10.1142/S021797929900182X.

[92] Hong J-Y, Choi M, Kim C, Jang J. Geometrical study of electrorheological activity with shape-controlled titania-coated silica nanomaterials. J Colloid Interface Sci 2010;347:177–82. https://doi.org/10.1016/j.jcis.2010.03.054.

[93] Stejskal J, Mrlík M, Plachý T, Trchová M, Kovářová J, Li Y. Molybdenum and tungsten disulfides surface-modified with a conducting polymer, polyaniline, for application in electrorheology. React Funct Polym 2017;120:30–7. https://doi.org/10.1016/j.reactfunctpolym.2017.09.004.

[94] Gonon P, Foulc J-N, Atten P, Boissy C. Particle–particle interactions in electrorheological fluids based on surface conducting particles. J Appl Phys 1999;86:7160–9. https://doi.org/10.1063/1.371807.

[95] Lee S, Yoon C-M, Hong J-Y, Jang J. Enhanced electrorheological performance of a graphene oxide-wrapped silica rod with a high aspect ratio. J Mater Chem C 2014;2:6010. https://doi.org/10.1039/C4TC00635F.

[96] Noh J, Yoon C-M, Jang J. Enhanced electrorheological activity of polyaniline coated mesoporous silica with high aspect ratio. J Colloid Interface Sci 2016;470:237–44. https://doi.org/10.1016/j.jcis.2016.02.061.

[97] Jin T, Cheng Y, He R, Luo Y, Jiang M, Chen C, et al. Electric-field-induced structure and optical properties of electrorheological fluids with attapulgite nanorods. Smart Mater Struct 2014;23:075005. https://doi.org/10.1088/0964-1726/23/7/075005.

[98] Kuznetsov NM, Bakirov AV, Banin EP, Belousov SI, Chvalun SN. In situ X-ray analysis of montmorillonite suspensions in polydimethylsiloxane: Orientation in shear and electric field. Colloids Surf A Physicochem Eng Asp 2021;622:126663. https://doi.org/10.1016/j.colsurfa.2021.126663.

[99] Yin J, Zhao X, Xia X, Xiang L, Qiao Y. Electrorheological fluids based on nano-fibrous polyaniline. Polymer 2008;49:4413–9. https://doi.org/10.1016/j.polymer.2008.08.009.

[100] Tsuda K, Takeda Y, Ogura H, Otsubo Y. Electrorheological behavior of whisker suspensions under oscillatory shear. Colloids Surf A Physicochem Eng Asp 2007;299:262–7. https://doi.org/10.1016/j.colsurfa.2006.11.050.

[101] López-López MT, Vertelov G, Bossis G, Kuzhir P, Durán JD. New magnetorheological fluids based on magnetic fibers. J Mater Chem 2007;17:3839–44. https://doi.org/10.1039/b705871c.

[102] Qi Y, Wen W. Influences of geometry of particles on electrorheological fluids. J Phys D Appl Phys 2002;35:322. https://doi.org/10.1088/0022-3727/35/17/322.

[103] Shang Y, Ma S, Li J, Li M, Wang J, Zhang S. Effect of microstructure on electrorheological property for pure TiO2 particle material. J Mater Sci Technol 2006;22:572.

[104] Jiang W, Jiang C, Gong X, Zhang Z. Structure and electrorheological properties of nanoporous BaTiO 3 crystalline powders prepared by sol–gel method. J Sol-Gel Sci Technol 2009;52:8–14. https://doi.org/10.1007/s10971-009-2011-5.

[105] Kutalkova E, Ronzova A, Osicka J, Skoda D, Sedlacik M. The influence of synthesis conditions on the electrorheological performance of iron(II) oxalate rod-like particles. J Ind Eng Chem 2021;100:280–7. https://doi.org/10.1016/j.jiec.2021.05.011.

[106] Jiang W, Zhu W, Jiang C, Zhang X, Xuan S, Gong X, et al. The controllable synthesis of nanoporous $SrTiO_3$ by an ultrasound irradiation approach. Smart Mater Struct 2011;20:065002. https://doi.org/10.1088/0964-1726/20/6/065002.

[107] Kuznetsov N, Bakirov A, Belousov S, Chvalun S. Orientation of layered aluminosilicates particles with a high aspect ratio in paraffin under an electric field. In: Doklady Physics, Vol. 64. Pleiades Publishing; 2019. p. 249–52. https://doi.org/10.1134/S1028335819060077.

[108] Cheng Q, Pavlinek V, He Y, Yan Y, Li C, Saha P. Synthesis and electrorheological characteristics of sea urchin-like TiO_2 hollow spheres. Colloid Polym Sci 2011;289:799–805. https://doi.org/10.1007/s00396-011-2398-8.

[109] Zheng H, Sun W, Chen Y, Kong X, Wang B, Hao C. Preparation and enhanced electrorheological properties of ce-doped porous titanium oxide nanoparticles. Ind Eng Chem Res 2021;60:1642–55. https://doi.org/10.1021/acs.iecr.0c04674.

[110] Yin JBZ, Xiao P. Enhanced electrorheological activity of mesoporous Cr-doped TiO_2 from activated pore wall and high surface area. J Phys Chem B 2006;110:12916–25. https://doi.org/10.1021/jp0554588.

[111] Cherif K, Moalla S, Sassi S, Zarrouk H. Electrorheological response of modified silica suspensions. J Eur Ceram Soc 2007;27:1199–202. https://doi.org/10.1016/j.jeurceramsoc.2006.05.094.

[112] Cho MS, Choi HJ, Chin I-J, Ahn W-S. Electrorheological characterization of zeolite suspensions. Microporous Mesoporous Mater 1999;32:233–9. https://doi.org/10.1016/S1387-1811(99)00109-2.

[113] Sedlacik M, Pavlinek V, Mrlik M, Morávková Z, Hajná M, Trchová M, et al. Electrorheology of polyaniline, carbonized polyaniline, and their core-shell composites. Mater Lett 2013;101:90–2. https://doi.org/10.1016/j.matlet.2013.03.084.

[114] Kim D, Tian Y, Choi HJ. Seeded swelling polymerized sea urchin-like core–shell typed polystyrene/polyaniline particles and their electric stimuli-response. RSC Adv 2015;5:81546–53. https://doi.org/10.1039/C5RA15835D.

[115] Zheng C, Liu Y, Dong Y, He F, Zhao X, Yin J. Low-temperature interfacial polymerization and enhanced electro-responsive characteristic of poly (ionic liquid) s@ polyaniline core-shell microspheres. Macromol Rapid Commun 2019;40:1800351. https://doi.org/10.1002/marc.201800351.

[116] Han WJC, Jin H, Seo Y. Pickering emulsion fabricated smart polyaniline/clay composite particles and their tunable rheological response under electric field. Smart Mater Struct 2020;29:085022. https://doi.org/10.1088/1361-665X/ab9548.

[117] Yuan J, Wang Y, Xiang L, Zhao X, Yin J. Understanding the enhanced electrorheological effect of reduced graphene oxide-supported polyaniline dielectric nanoplates by a comparative study with graphene oxide as the support core. Nanodielectrics 2021;4:143–54. https://doi.org/10.1049/nde2.12021.

[118] Sun W, Chen Y, Zheng H, Li C, Zhang B, Wang B, et al. Electrorheological properties of titanium oxide loaded C_3N_4 composites. Mater Chem Phys 2022;282:125941. https://doi.org/10.1016/j.matchemphys.2022.125941.

[119] Ji X, Zhang W, Jia W, Wang X, Tian Y, Deng L, et al. Cactus-like double-shell structured SiO_2@TiO_2 microspheres: Fabrication, electrorheological performances and microwave absorption. J Ind Eng Chem 2017;56:203–11. https://doi.org/10.1016/j.jiec.2017.07.013.

[120] Zhang WL, Jiang D, Wang X, Hao BN, Liu YD, Liu J. Growth of polyaniline nanoneedles on MoS_2 nanosheets, tunable electroresponse, and electromagnetic wave attenuation analysis. J Phys Chem C 2017;121:4989–98. https://doi.org/10.1021/acs.jpcc.6b11656.

[121] Lu Q, Lee JH, Lee JH, Choi HJ. Magnetite/poly(Ortho-anisidine) composite particles and their electrorheological response. Materials; 14; 2021. 10.3390/ma14112900.

[122] Liu Z, Chen P, Jin X, Wang L-M, Liu Y, Choi H. Enhanced electrorheological response of cellulose: a double effect of modification by urea-terminated silane. Polymers 2018;10:867. https://doi.org/10.3390/polym10080867.

[123] Ko YG, Lee HJ, Shin SS, Choi US. Dipolar-molecule complexed chitosan carboxylate, phosphate, and sulphate dispersed electrorheological suspensions. Soft Matter 2012;8:6273–9. https://doi.org/10.1039/c2sm25250c.

[124] Kim S, Kim J, Jang W, Choi H, Jhon M. Electrorheological characteristics of phosphate cellulose-based suspensions. Polymer 2001;42:5005–12. https://doi.org/10.1016/S0032-3861(00)00887-9.

[125] Wang Y, Yang M, Chen H, Zhao X, Yin J. Dielectric polarization and electrorheological response of poly(ethylaniline)-coated reduced graphene oxide nanoflakes with different reduction degrees. Polymers 2020;12:2528. https://doi.org/10.3390/polym12112528.

[126] Komoda Y, Rao TN, Fujishima A. Photoelectrorheology of TiO_2 nanoparticle suspensions. Langmuir 1997;13:1371–3. https://doi.org/10.1021/la961059f.

[127] Sun L, Zhao Q, Zhang Y, Gao W, Jing D. Insights into the rheological behavior of ethanol-based metal oxide nanofluids. J Mol Liq 2021;323:115006. https://doi.org/10.1016/j.molliq.2020.115006.

[128] Zhao XP, Yin JB, Xiang LQ, Zhao Q. Electrorheological fluids containing Ce-doped titania. J Mater Sci 2002;37:2569–73. https://doi.org/10.1023/A:1015464228736.

[129] Yin JB, Zhao XP. Preparation and electrorheological activity of mesoporous rare-earth-doped TiO2. Chem Mater 2002;14:4633–40. https://doi.org/10.1021/cm020388s.

[130] Yin JB, Zhao XP. Preparation and enhanced electrorheological activity of TiO2 doped with chromium ion. Chem Mater 2004;16:321–8. https://doi.org/10.1021/cm034787e.

[131] Almajdalawi S, Pavlinek V, Mrlik M, Cheng Q, Sedlacik M. Synthesis and electrorheological effect of Cr doped TiO_2 nanorods with nanocavities in silicone oil suspensions. J Phys: Conf Ser; 412; 2013. 10.1088/1742-6596/412/1/012003.

[132] Qiao Y, Yin J, Zhao X. Oleophilicity and the strong electrorheological effect of surface-modified titanium oxide nano-particles. Smart Mater Struct 2007;16:332–9. https://doi.org/10.1088/0964-1726/16/2/011.

[133] Ma N, Dong X. Diammonium phosphate modified titanium dioxide suspensions with improved ER efficiency. Smart Mater Struct 2015;24:065009. https://doi.org/10.1088/0964-1726/24/6/065009.
[134] Zhang G, Zhao X, Jin X, Zhao Z, Ren Y, Wang LM, et al. Ionic-liquid-modified TiO_2 spheres and their enhanced electrorheological responses. Molecular Liquids 2021;338:116696. https://doi.org/10.1016/j.molliq.2021.116696.
[135] Zhou J, Hu M, Jing D. The synergistic effect between surfactant and nanoparticle on the viscosity of water-based fluids. Chem Phys Lett 2019;727:1–5. https://doi.org/10.1016/j.cplett.2019.04.052.
[136] Hu M, Zhang Y, Gao W, Jing D. Effects of the complex interaction between nanoparticles and surfactants on the rheological properties of suspensions. Colloids Surf A Physicochem Eng Asp 2020;588:124377. https://doi.org/10.1016/j.colsurfa.2019.124377.
[137] Hu X, Wei H, Li C, Liu S, Zhou Y, Huang Y, et al. A highly homogeneous electrorheological fluid with potential applications in optics. Smart Mater Struct 2024;33:025010. https://doi.org/10.1088/1361-665X/ad1c39.
[138] Zhao Z, Jin X, Liang Y, Wang L-M, Liu YD. TiO_2 nanoparticles dual-modified with ionic liquid and acetic acid for use as electrorheological materials to achieve ultrahigh and stable electroresponsive performances. ACS Appl Nano Mater 2022;5:17928–38. https://doi.org/10.1021/acsanm.2c03896.
[139] Noh J, Jekal S, Kim J, Kim H-Y, Chu Y-R, Kim C-G, et al. Vivid-Colored Electrorheological fluids with simultaneous enhancements in color clarity and Electro-Responsivity. J Colloid Interface Sci 2024;657:373–83. https://doi.org/10.1016/j.jcis.2023.11.183.
[140] Miller DV, Randall CA, Bhalla AS, Newham RE, Adair JH. Electrorheological properties of BaTiO3 suspensions. Ferroelectr Lett Sect 1993;15:141–51. https://doi.org/10.1080/07315179308204251.
[141] Yin J-B, Zhao X-P. Preparation and electrorheological characteristic of Y-doped $BaTiO_3$ suspension under dc electric field. J Solid State Chem 2004;177:3650–9. https://doi.org/10.1016/j.jssc.2004.06.013.
[142] Wu M, Zhao M, Lu X, Wang ZL. Suppressing the self-discharge of high-frequency supercapacitors using electrolytes containing $BaTiO_3$ nanoparticles. J Power Sources 2024;594:234005. https://doi.org/10.1016/j.jpowsour.2023.234005.
[143] Chen S-M, Wei C-G. Experimental study of the rheological behavior of electrorheological fluids. Smart Mater Struct 2006;15:371. https://doi.org/10.1088/0964-1726/15/2/018.
[144] Umeda J, Sakamoto W, Yogo T. Synthesis and field-responsive properties of $SrTiO_3$ nanoparticle/polymer hybrid. J Mater Res 2009;24:2221–8. https://doi.org/10.1557/JMR.2009.0276.
[145] Otsubo Y, Sekine M, Katayama S. Effect of adsorbed water on the electrorheology of silica suspensions. J Colloid Interface Sci 1992;150:324–30. https://doi.org/10.1016/0021-9797(92)90201-V.
[146] Nooney RI, Thirunavukkarasu D, Yimei C, Josephs R, Ostafin AE. Synthesis of nanoscale mesoporous silica spheres with controlled particle size. Chem Mater 2002;14:4721–8. https://doi.org/10.1021/cm0204371.
[147] Yoon C-M, Jang Y, Noh J, Kim J, Lee K, Jang J. Enhanced electrorheological performance of mixed silica nanomaterial geometry. ACS Appl Mater Interfaces 2017;9:36358–67. https://doi.org/10.1021/acsami.7b08298.
[148] Jankiewicz BJ, Jamiola D, Choma J, Jaroniec M. Silica-metal core-shell nanostructures. Adv Colloid Interface Sci 2012;170:28–47. https://doi.org/10.1016/j.cis.2011.11.002.
[149] Li X, Pan J, Shi J, Chai Y, Hu S, Han Q, et al. Nanoparticle-induced drag reduction for polyacrylamide in turbulent flow with high Reynolds numbers. Chin J Chem Eng 2023;56:290–8. https://doi.org/10.1016/j.cjche.2022.07.015.
[150] Roosz N, Euvrard M, Lakard B, Viau L. A straightforward procedure for the synthesis of silica@polyaniline core-shell nanoparticles. Physicochem Eng Aspects 2019;573:237–45. https://doi.org/10.1016/j.colsurfa.2019.04.036.
[151] Sun W, Xi Z, Zheng H, Chen Y, Li C, Wang B, et al. Synthesis and electrorheological properties of silica-coated MoS_2 nanocomposites with hierarchical and core-shell structure. J Taiwan Inst Chem Eng 2021;118:271–83. https://doi.org/10.1016/j.jtice.2021.01.009.
[152] Kim MW, Moon IJ, Choi HJ, Seo Y. Facile fabrication of core/shell structured SiO_2/polypyrrole nanoparticles with surface modification and their electrorheology. RSC Adv 2016;6:56495–502. https://doi.org/10.1039/c6ra10349a.
[153] Chen Y, Sun W, Zheng H, Li C, Zhang B, Wang B, et al. Electrorheological response behavior of $H_2Ti_2O_5$@MoS_2@SiO_2 core-shell nanoparticles. Ceram Int 2021;47:24080–91. https://doi.org/10.1016/j.ceramint.2021.05.118.
[154] Pavlikova E, Plachy T, Urbanek M, Cvek M. Engineering conductivity and performance in electrorheological fluids using a nanosilica grafting approach. ACS Appl Nano Mater 2023;6:9768–76. https://doi.org/10.1021/acsanm.3c01475.
[155] Li Y, Zhu H, Shen F, Wan J, Han X, Dai J, et al. Highly conductive microfi ber of graphene oxide templated carbonization of nanofibrillated cellulose. Adv Funct Mater 2014;24:7366–72. https://doi.org/10.1002/adfm.201402129.
[156] Konikkara N, Kennedy LJ, Aruldoss U, Vijaya JJ. Electrical conductivity studies of nanoporous carbon derived from leather waste: Effect of pressure, temperature and porosity. J Nanosci Nanotechnol 2016;16:8829–38. https://doi.org/10.1166/jnn.2016.11652.
[157] Zhang S, Niu G, Yu H, Huang J. Carbonized cellulose fiber. BioResources; 14: 8656-63; 2019. 10.15376/biores.14.4.8656-8663.
[158] Rhim YR, Zhang D, Fairbrother DH, Wepasnick KA, Livi KJ, Bodnar RJ, et al. Changes in electrical and microstructural properties of microcrystalline cellulose as function of carbonization temperature. Carbon 2010;48:1012–24. https://doi.org/10.1016/j.carbon.2009.11.020.
[159] Konikkara N, Punithavelan N, Kennedy LJ, Vijaya JJ. A new approach to solid waste management: fabrication of supercapacitor electrodes from solid leather wastes using aqueous KOH electrolyte. Clean Techn Environ Policy 2017;19:1087–98. https://doi.org/10.1007/s10098-016-1301-1.
[160] Fong H, Vaia RA, Sanders JH, Lincoln D, Vreugdenhil AJ, Liu W, et al. Self-passivation of polymer-layered silicate nanocomposites. Chem Mater 2001;13:4123–9. https://doi.org/10.1021/cm010150o.
[161] Hyun YH, Lim ST, Choi HJ, Jhon MS. Rheology of poly (ethylene oxide)/organoclay nanocomposites. Macromolecules 2001;34:8084–93. https://doi.org/10.1021/ma002191w.
[162] Alexandre M, Beyer G, Henrist C, Cloots R, Rulmont A, Jérôme R, et al. Preparation and properties of layered silicate nanocomposites based on ethylene vinyl acetate copolymers. Macromol Rapid Commun 2001;22:643–6. https://doi.org/10.1002/1521-3927(20010501)22:8<643::AID-MARC643>3.0.CO;2-%23.
[163] Lim ST, Hyun YH, Choi HJ, Jhon MS. Synthetic biodegradable aliphatic polyester/montmorillonite nanocomposites. Chem Mater 2002;14:1839–44. https://doi.org/10.1021/cm010377j.
[164] Chen B, Evans JR, Greenwell HC, Boulet P, Coveney PV, Bowden AA, et al. A critical appraisal of polymer–clay nanocomposites. Chem Soc Rev 2008;37:568–94. https://doi.org/10.1039/B702653F.
[165] Piao SH, Kwon SH, Choi HJ. Stimuli-responsive polymer-clay nanocomposites under electric fields. Materials 2016;9:52. https://doi.org/10.3390/ma9010052.
[166] Xiang L, Zhao X. Preparation of montmorillonite/titania nanocomposite and enhanced electrorheological activity. J Colloid Interface Sci 2006;296:131–40. https://doi.org/10.1016/j.jcis.2005.08.059.
[167] Xiang L, Zhao X, Yin J. Micro/nano-structured montmorillonite/titania particles with high electrorheological activity. Rheol Acta 2011;50:87–95. https://doi.org/10.1007/s00397-010-0516-z.
[168] Kim JW, Kim SG, Choi HJ, Jhon MS. Synthesis and electrorheological properties of polyaniline-Na+-montmorillonite suspensions. Macromol Rapid Commun 1999;20:450–2. https://doi.org/10.1002/(SICI)1521-3927(19990801)20:8<450::AID-MARC450>3.0.CO;2-N.
[169] Liu Y, Zhao X, Yin J. Enhanced electro-responsive electrorheological efficiency of polyethylene oxide-intercalated montmorillonite nanocomposite suspension. Colloids Surf A Physicochem Eng Asp 2023;666:131239. https://doi.org/10.1016/j.colsurfa.2023.131239.
[170] Frost RL, Kristof J, Horvath E, Kloprogge JT. Molecular structure of dimethyl sulfoxide in DMSO-intercalated kaolinites at 298 and 77 K. Chem A Eur J 1999;103:9654–60. https://doi.org/10.1021/jp991763f.
[171] Wang B-x, Zhao X-p. Electrorheological effect coordinated by kaolinite–carboxymethyl starch hybrid materials. J Mater Chem 2002;12:2869–71. https://doi.org/10.1039/B207566K.
[172] Wang B, Zhao X. Electrorheological behavior of kaolinite–polar liquid intercalation composites. J Mater Chem 2002;12:1865–9. https://doi.org/10.1039/b201592g.

[173] Ramos-Tejada MM, Espin MJ, Perea R, Delgado AV. Electrorheology of suspensions of elongated goethite particles. Non-Newtonian Fluid Mechanics 2009;159:34–40. https://doi.org/10.1016/j.jnnfm.2008.12.004.
[174] Ramos-Tejada MM, Rodríguez JM, Delgado ÁV. Electrorheology of clay particle suspensions. Effects of shape and surface treatment. Rheol Acta 2018;57:405–13. https://doi.org/10.1007/s00397-018-1086-8.
[175] Kutalkova E, Plachy T, Sedlacik M. On the enhanced sedimentation stability and electrorheological performance of intelligent fluids based on sepiolite particles. J Mol Liq 2020;309:113120. https://doi.org/10.1016/j.molliq.2020.113120.
[176] Kim YJ, Liu YD, Choi HJ, Park SJ. Facile fabrication of Pickering emulsion polymerized polystyrene/laponite composite nanoparticles and their electrorheology. J Colloid Interface Sci 2013;394:108–14. https://doi.org/10.1016/j.jcis.2012.12.040.
[177] Jang DSC, Jin H. Conducting polyaniline-wrapped sepiolite composite and its stimuli-response under applied electric fields. Colloids Surf A Physicochem Eng Asp 2015;469:20–8. https://doi.org/10.1016/j.colsurfa.2015.01.004.
[178] Liu X, Song H, Sun W, Wang B, Zhang P, Yuan X, et al. Strong nano size effect of titanium silicalite (TS-1) zeolites for electrorheological fluid. Chem Eng J; 384; 2020. 10.1016/j.cej.2019.123267.
[179] Zhou WZ, Kongshuang. Confirmation of water mechanism in zeolite electrorheological fluid by dielectric spectroscopy. J Non Cryst Solids 2010;356:1522–5. https://doi.org/10.1016/j.jnoncrysol.2010.05.004.
[180] Sun W, Song H, Xi Z, Ma J, Wang B, Liu X, et al. Synthesis and enhanced electrorheological properties of TS-1/titanium oxide core/shell nanocomposite. Ind Eng Chem Res 2020;59:1168–82. https://doi.org/10.1021/acs.iecr.9b05936.
[181] Novoselov KS, Geim AK, Morozov SV, Jiang D, Zhang Y, Dubonos SV, et al. Electric field effect in atomically thin carbon films. Science 2004;306:666–9. https://doi.org/10.1126/science.1102896.
[182] Zhang WL, Liu YD, Choi HJ. Fabrication of semiconducting graphene oxide/polyaniline composite particles and their electrorheological response under an applied electric field. Carbon 2012;50:290–6. https://doi.org/10.1016/j.carbon.2011.08.049.
[183] Zhang WL, Liu YD, Choi HJ, Kim SG. Electrorheology of graphene oxide. ACS Appl Mater Interfaces 2012;4:2267–72. https://doi.org/10.1021/am300267f.
[184] Paredes JI, Villar-Rodil S, Martínez-Alonso A, Tascón JMD. Graphene oxide dispersions in organic solvents. Langmuir 2008;24:10560–4. https://doi.org/10.1021/la801744a.
[185] Dong Y, Liu Y, Yin J, Zhao X. Preparation and enhanced electro-responsive characteristic of graphene/layered double-hydroxide composite dielectric nanoplates. J Mater Chem C 2014;2:10386–94. https://doi.org/10.1039/C4TC02085E.
[186] Yin J, Wang X, Chang R, Zhao X. Polyaniline decorated graphene sheet suspension with enhanced electrorheology. Soft Matter 2012;8:294–7. https://doi.org/10.1039/c1sm06728a.
[187] Li Y, Guan Y, Liu Y, Yin J, Zhao X. Highly stable nanofluid based on polyhedral oligomeric silsesquioxane-decorated graphene oxide nanosheets and its enhanced electro-responsive behavior. Nanotechnology 2016;27:195702. https://doi.org/10.1088/0957-4484/27/19/195702.
[188] Yin J, Chang R, Kai Y, Zhao X. Highly stable and AC electric field-activated electrorheological fluid based on mesoporous silica-coated graphene nanosheets. Soft Matter 2013;9:3910–4. https://doi.org/10.1039/C3SM27835B.
[189] Hong J-Y, Jang J. Highly stable, concentrated dispersions of graphene oxide sheets and their electro-responsive characteristics. Soft Matter 2012;8:7348. https://doi.org/10.1039/c2sm25865j.
[190] Si Y, Samulski ET. Exfoliated graphene separated by platinum nanoparticles. Chem Mater 2008;20:6792–7. https://doi.org/10.1021/cm801356a.
[191] Yin J, Chang R, Shui Y, Zhao X. Preparation and enhanced electro-responsive characteristic of reduced graphene oxide/polypyrrole composite sheet suspensions. Soft Matter 2013;9:7468–78. https://doi.org/10.1039/c3sm51128f.
[192] Shin K-Y, Lee S, Hong S, Jang J. Graphene size control via a mechanochemical method and electroresponsive properties. ACS Appl Mater Interfaces 2014;6:5531–7. https://doi.org/10.1021/am405930k.
[193] Ilčíková M, Mrlík M, Babayan V, Kasák P. Graphene oxide modified by betaine moieties for improvement of electrorheological performance. RSC Adv 2015;5:57820–7. https://doi.org/10.1039/C5RA08403B.
[194] Mrlik M, Ilcikova M, Osicka J, Kutalkova E, Minarik A, Vesel A, et al. Electrorheology of SI-ATRP-modified graphene oxide particles with poly(butyl methacrylate): effect of reduction and compatibility with silicone oil. RSC Adv 2019;9:1187–98. https://doi.org/10.1039/C8RA08518H.
[195] Zhang WL, Park BJ, Choi HJ. Colloidal graphene oxide/polyaniline nanocomposite and its electrorheology. Chem Commun 2010;46:5596. https://doi.org/10.1039/c0cc00557f.
[196] Hao T. Chapter 5 - Critical parameters to the electrorheological effect. In: Hao T, editor. Electrorheological Fluids2005. p. 152-234.
[197] Hao T. Chapter 4 - The electrorheological materials. In: Hao T, editor. Electrorheological Fluids: Elsevier; 2005. p. 114-51.
[198] Marins JA, Giulieri F, Soares BG, Bossis G. Hybrid polyaniline-coated sepiolite nanofibers for electrorheological fluid applications. Synth Met 2013;185:9–16. https://doi.org/10.1016/j.synthmet.2013.09.037.
[199] Chandrakanthi N, Careem MA. Thermal stability of polyaniline. Polym Bull 2000;44:101–8. https://doi.org/10.1007/s002890050579.
[200] Blinova NV, Sapurina I, Klimovič J, Stejskal J. The chemical and colloidal stability of polyaniline dispersions. Polym Degrad Stabil 2005;88:428–34. https://doi.org/10.1016/j.polymdegradstab.2004.11.014.
[201] Stejskal J, Prokeš J, Trchová M. Reprotonation of polyaniline: A route to various conducting polymer materials. React Funct Polym 2008;68:1355–61. https://doi.org/10.1016/j.reactfunctpolym.2008.06.012.
[202] MacDiarmid AG, Epstein AJ. Secondary doping in polyaniline. Synth Met 1995;69:85–92. https://doi.org/10.1016/0379-6779(94)02374-8.
[203] Santos J, Goswami S, Calero N, Cidade MT. Electrorheological behaviour of suspensions in silicone oil of doped polyaniline nanostructures containing carbon nanoparticles. J Intell Mater Syst Struct 2019;30:755–63. https://doi.org/10.1177/1045389X18818776.
[204] Poussin D, Morgan H, Foot PJS. Thermal doping of polyaniline by sulfonic acids. Polym Int 2003;52:433–8. https://doi.org/10.1002/pi.1107.
[205] Choi YK, Kim HJ, Kim SR, Cho YM, Ahn DJ. Enhanced thermal stability of polyaniline with polymerizable dopants. Macromolecules 2017;50:3164–70. https://doi.org/10.1021/acs.macromol.6b02586.
[206] Stěnička M, Pavlínek V, Sáha P, Blinova NV, Stejskal J, Quadrat O. The electrorheological efficiency of polyaniline particles with various conductivities suspended in silicone oil. Colloid Polym Sci 2009;287:403–12. https://doi.org/10.1007/s00396-008-1977-9.
[207] Dong H, Prasad S, Nyame V, Jones WE. Sub-micrometer conducting polyaniline tubes prepared from polymer fiber templates. Chem Mater 2004;16:371–3. https://doi.org/10.1021/cm0347180.
[208] Wang J, Wang J, Wang Z, Zhang F. A template-free method toward urchin-like polyaniline microspheres. Macromol Rapid Commun 2009;30:604–8. https://doi.org/10.1002/marc.200800726.
[209] Yin J, Xia X, Xiang L, Qiao Y, Zhao X. The electrorheological effect of polyaniline nanofiber, nanoparticle and microparticle suspensions. Smart Mater Struct; 18; 2009. 10.1088/0964-1726/18/9/095007.
[210] Stejskal J, Sapurina I, Trchová M, Konyushenko EN. Oxidation of aniline: Polyaniline granules, nanotubes, and oligoaniline microspheres. Macromolecules 2008;41:3530–6. https://doi.org/10.1021/ma702601q.
[211] Stejskal J. Polymers of phenylenediamines. Prog Polym Sci 2015;41:1–31. https://doi.org/10.1016/j.progpolymsci.2014.10.007.
[212] Plachy T, Sedlacik M, Pavlinek V, Trchová M, Morávková Z, Stejskal J. Carbonization of aniline oligomers to electrically polarizable particles and their use in electrorheology. Chem Eng J 2014;256:398–406. https://doi.org/10.1016/j.cej.2014.07.010.
[213] Yin J, Wang X, Zhao X. Silicone-grafted carbonaceous nanotubes with enhanced dispersion stability and electrorheological efficiency. Nanotechnology 2015;26:065704. https://doi.org/10.1088/0957-4484/26/6/065704.
[214] Yin J, Xia X, Wang X, Zhao X. The electrorheological effect and dielectric properties of suspensions containing polyaniline@titania nanocable-like particles. Soft Matter 2011;7:10978. https://doi.org/10.1039/c1sm06059g.
[215] Lu J, Zhao X. Electrorheological properties of a polyaniline–montmorillonite clay nanocomposite suspension. J Mater Chem 2002;12:2603–5. https://doi.org/10.1039/B203921D.

[216] Li C, Chen Y, Wang L, Wang Z, Lin Y, Xiong K, et al. Electrorheological response behavior of PANI@MoS_2 core–shell nanocomposites. Adv Eng Mater 2023;25:2300029. https://doi.org/10.1002/adem.202300029.
[217] Sim B, Chae HS, Choi HJ. Fabrication of polyaniline coated iron oxide hybrid particles and their dual stimuli-response under electric and magnetic fields. Express Polym Lett 2015;9:736–43. https://doi.org/10.3144/expresspolymlett.2015.68.
[218] Tian X, He K, Wang B, Yu S, Hao C, Chen K, et al. Flower-like Fe_2O_3/polyaniline core/shell nanocomposite and its electroheological properties. Colloids Surf A Physicochem Eng Asp 2016;498:185–93. https://doi.org/10.1016/j.colsurfa.2016.03.054.
[219] Zhu X, Zhao Q, Zhang T, Pang X. Electrorheological response of novel polyaniline-Fe_2O_3 nanocomposite particles. Polym-Plast Technol Mater 2019;58:573–7. https://doi.org/10.1080/03602559.2018.1493118.
[220] Jeong JY, Kim S, Baek E, You CY, Choi HJ. Suspension rheology of polyaniline coated manganese ferrite particles under electric/magnetic fields. Colloids Surf A Physicochem Eng Asp 2023;656:130438. https://doi.org/10.1016/j.colsurfa.2022.130438.
[221] Kim JN, Dong YZ, Choi HJ. Pickering emulsion polymerized polyaniline/zinc-ferrite composite particles and their dual electrorheological and magnetorheological responses. ACS Omega 2020;5:7675–82. https://doi.org/10.1021/acsomega.0c00585.
[222] Kim HM, Kang SH, Choi HJ. Polyaniline coated $ZnFe_2O_4$ microsphere and its electrorheological and magnetorheological response. Colloids Surf A Physicochem Eng Asp 2021;626:127079. https://doi.org/10.1016/j.colsurfa.2021.127079.
[223] Kim TH, Choi HJ. Fabrication and shear response of conducting polymer-coated zinc ferrite particles under magnetic/electric field. IEEE Trans Magn 2022;58:1–5. https://doi.org/10.1109/TMAG.2021.3094805.
[224] Treasurer U, Filisko F, Radzilowski L. Polyelectrolytes as inclusions in electrorheologically active materials: effect of chemical characteristics on ER activity. J Rheol 1991;35:1051–68. https://doi.org/10.1122/1.550165.
[225] Filisko FE. Overview of ER technology. In: Havelka KO, Filisko FE, editors. Progress in Electrorheology: Science and Technology of Electrorheological Materials. Boston, MA: Springer; 1995. p. 3–18.
[226] Bloodworth R, Wendt E. Materials for ER fluids. Int J Mod Phys B 1996;10:2951–64. https://doi.org/10.1142/S0217979296001392.
[227] Krztoń-Maziopa A, Ciszewska M, Płocharski J. Polarization processes in electrorheological fluids based on conductive polymers. Polym Adv Technol 2006;17:37–40. https://doi.org/10.1002/pat.701.
[228] Dong Y, Yin J, Zhao X. Microwave-synthesized poly (ionic liquid) particles: a new material with high electrorheological activity. J Mater Chem A 2014;2:9812–9. https://doi.org/10.1039/C4TA00828F.
[229] Zhao J, Lei Q, He F, Zheng C, Zhao X, Yin J. Influence of geometry of mobile countercations on conductivity, polarization and electrorheological effect of polymeric anionic liquids at ice point temperature. Polymer 2020;205:122826. https://doi.org/10.1016/j.polymer.2020.122826.
[230] Minami H. Preparation and morphology control of poly (ionic liquid) particles. Langmuir 2020;36:8668–79. https://doi.org/10.1021/acs.langmuir.0c01182.
[231] Dong Y, Wang B, Xiang L, Liu Y, Zhao X, Yin J. Influence of side chain sizes on dielectric and electrorheological responses of poly (ionic liquid) s. J Phys Chem B 2017;121:6226–37. https://doi.org/10.1021/acs.jpcb.7b02366.
[232] He F, Wang B, Zhao J, Zhao X, Yin J. Influence of tethered ions on electric polarization and electrorheological property of polymerized ionic liquids. Molecules 2020;25:2896. https://doi.org/10.3390/molecules25122896.
[233] Wang Y, Ma R, Nie W, Zhao X, Yin J. Enhanced electrorheological performance of core–shell-structured polymerized ionic liquid@ doubly polymerized ionic liquid microspheres prepared via evaporation-assisted dispersion polymerization. Langmuir 2023;39:14006–14. https://doi.org/10.1021/acs.langmuir.3c01745.
[234] Bhat N, Geetha P, Pawde S. Preparation and characterization of composites of polypyrrole. Polym Eng Sci 1999;39:1517–24. https://doi.org/10.1002/pen.11544.
[235] Yang Y, Liu J, Wan M. Self-assembled conducting polypyrrole micro/nanotubes. Nanotechnology 2002;13:771. https://doi.org/10.1088/0957-4484/13/6/315.
[236] Kim YD, Song IC. Electrorheological and dielectric properties of polypyrrole dispersions. J Mater Sci 2002;37:5051–5. https://doi.org/10.1023/A:1021091700296.
[237] Temmer R, Must I, Kaasik F, Aabloo A, Tamm T. Combined chemical and electrochemical synthesis methods for metal-free polypyrrole actuators. Sens Actuators B 2012;166:411–8. https://doi.org/10.1016/j.snb.2012.01.075.
[238] Stejskal J, Sapurina I, Vilčáková J, Plachý T, Sedlačík M, Bubulinca C, et al. Conducting and magnetic composites polypyrrole nanotubes/magnetite nanoparticles: application in magnetorheology. React Funct Polym 2021;4:2247–56. https://doi.org/10.1021/acsanm.1c00063.
[239] Kang HC, Geckeler K. Enhanced electrical conductivity of polypyrrole prepared by chemical oxidative polymerization: effect of the preparation technique and polymer additive. Polymer 2000;41:6931–4. https://doi.org/10.1016/S0032-3861(00)00116-6.
[240] Pringle JM, Efthimiadis J, Howlett PC, Efthimiadis J, MacFarlane DR, Chaplin AB, et al. Electrochemical synthesis of polypyrrole in ionic liquids. Polymer 2004;45:1447–53. https://doi.org/10.1016/j.polymer.2004.01.006.
[241] Sapurina I, Li Y, Alekseeva E, Bober P, Trchová M, Morávková Z, et al. Polypyrrole nanotubes: the tuning of morphology and conductivity. Polymer 2017;113:247–58. https://doi.org/10.1016/j.polymer.2017.02.064.
[242] Xia X, Yin J, Qiang P, Zhao X. Electrorheological properties of thermo-oxidative polypyrrole nanofibers. Electrorheological properties of thermo-oxidative polypyrrole nanofibers 2011;52:786–92. https://doi.org/10.1016/j.polymer.2010.12.018.
[243] Almajdalawi S, Pavlinek V, Cheng Q, Saha P, Mrlik M, Stenicka M, et al. Electrorheological properties of suspensions of polypyrrole ribbon particles in silicone oil. In: AIP Conference Proceedings, Vol. 1375, No. 1. American Institute of Physics; 2011. p. 275–83. https://doi.org/10.1063/1.3604488.
[244] Seo YP, Han S, Kim J, Choi HJ, Seo Y. Analysis of the flow behavior of electrorheological fluids containing polypyrrole nanoparticles or polypyrrole/silica nanocomposite particles. Rheol Acta 2020;59:415–23. https://doi.org/10.1007/s00397-020-01205-9.
[245] Kim YDH, Gwang Gi. Electrorheological properties of polypyrrole-silica nanocomposite suspensions. Korean J Chem Eng 2012;29:964–8. https://doi.org/10.1007/s11814-011-0270-7.
[246] Mrlik M, Pavlinek V, Cheng Q, Saha P. Synthesis of titanate/polypyrrole composite rod-like particles and the role of conducting polymer on electrorheological efficiency. Int J Mod Phys B 2012;26:1250007. https://doi.org/10.1142/S0217979212500075.
[247] Chen P, Cheng Q, Wang L-M, Liu YD, Choi HJ. Fabrication of dual-coated graphene oxide nanosheets by polypyrrole and poly(ionic liquid) and their enhanced electrorheological responses. J Ind Eng Chem 2019;69:106–15. https://doi.org/10.1016/j.jiec.2018.09.022.
[248] Fang FF, Choi HJ, Ahn W-S. Electrorheology of a mesoporous silica having conducting polypyrrole inside expanded pores. Microporous Mesoporous Mater 2010;130:338–43. https://doi.org/10.1016/j.micromeso.2009.11.032.
[249] Kim J, Liu F, Choi H, Hong S, Joo J. Intercalated polypyrrole/Na+-montmorillonite nanocomposite via an inverted emulsion pathway method. Polymer 2003;44:289–93. https://doi.org/10.1016/S0032-3861(02)00749-8.
[250] Schwarz G, Maisch S, Ullrich S, Wagenhöfer J, Kurth DG. Electrorheological fluids based on metallo-supramolecular polyelectrolyte–silicate composites. ACS Appl Mater Interfaces 2013;5:4031–4. https://doi.org/10.1021/am401104d.
[251] Wysocka-Zolopa M, Zablocka I, Basa A, Winkler K. Formation and characterization of mesoporous silica MCM-48 and polypyrrole composite. Chem Heterocycl Compd 2017;53:78–86. https://doi.org/10.1007/s10593-017-2024-x.
[252] Gercek B, Yavuz M, Yilmaz H, Sari B, Unal HI. Comparison of electrorheological properties of some polyaniline derivatives. Colloids Surf A Physicochem Eng Asp 2007;299:124–32. https://doi.org/10.1016/j.colsurfa.2006.11.028.
[253] Yilmaz H, Unal HI, Sari B. Synthesis, characterization and electrorheological properties of poly(o-toluidine)/Zn conducting composites. J Appl Polym Sci 2007;103:1058–65. https://doi.org/10.1002/app.25310.
[254] Harima Y, Sanada K, Patil R, Ooyama Y, Mizota H, Yano J. Monodisperse and isolated microspheres of poly(N-methylaniline) prepared by dispersion polymerization. Eur Polym J 2010;46:1480–7. https://doi.org/10.1016/j.eurpolymj.2010.04.017.
[255] Moon I-JC, Hyoung core-shell-structured copolyaniline-coated polymeric nanoparticle suspension and its viscoelastic response under various electric fields. Materials; 8: 4932-42; 2015. 10.3390/ma8084932.

[256] Dong Y, Wang S, Choi HJ. Poly(N-methylaniline)/magnetite microsphere and its electrical and magnetic dual responses. Polymer 2022;240:124492. https://doi.org/10.1016/j.polymer.2021.124492.
[257] Lu Q, Esmaeilnezhad E, Choi HJ. Magnetite-embedded poly (2-methylaniline) hybrid particles and their smart responses under magnetic and electric fields. J Mol Liq 2021;340:117294. https://doi.org/10.1016/j.molliq.2021.117294.
[258] Kuramoto N, Takahashi Y, Nagai K, Koyama K. Electrorheological properties of poly(o-anisidine) and poly(o-anisidine)-coated silica suspensions. React Funct Polym 1996;30:367–73. https://doi.org/10.1016/1381-5148(95)00127-1.
[259] Lee CJ, Choi HJ. Fabrication of poly(o-anisidine) coated silica core-shell microspheres and their electrorheological response. Materials Research Express; 4; 2017. 10.1088/2053-1591/aa985c.
[260] Cataldo F. On the polymerization of p-phenylenediamine. Eur Polym J 1996;32:43–50. https://doi.org/10.1016/0014-3057(95)00118-2.
[261] Plachy T, Sedlacik M, Pavlinek V, Stejskal J. The observation of a conductivity threshold on the electrorheological effect of p-phenylenediamine oxidized with p-benzoquinone. J Mater Chem C 2015;3:9973–80. https://doi.org/10.1039/c5tc02119g.
[262] Trlica J, Saha P, Quadrat O, Stejskal J. Electrorheological activity of polyphenylenediamine suspensions in silicone oil. Physica A 2000;283:337–48. https://doi.org/10.1016/S0378-4371(00)00113-8.
[263] Plachy T, Sedlacik M, Pavlinek V, Morávková Z, Hajná M, Stejskal J. An effect of carbonization on the electrorheology of poly(p- phenylenediamine). Carbon 2013;63:187–95. https://doi.org/10.1016/j.carbon.2013.06.070.
[264] Cao Y, Choi HJ, Zhang WL, Wang B, Hao C, Liu J. Eco-friendly mass production of poly(p-phenylenediamine)/graphene oxide nanoplatelet composites and their electrorheological characteristics. Compos Sci Technol 2016;122:36–41. https://doi.org/10.1016/j.compscitech.2015.11.010.
[265] Zhang K, Li H, Dong YZ, Zhang H, Zhao W, Zhao S, et al. Jellyfish-shaped p-phenylenediamine functionalized graphene oxide-g-polyaniline fibers and their electrorheology. Polymer 2019;168:29–35. https://doi.org/10.1016/j.polymer.2019.02.007.
[266] Mackintosh JG, Redpath CR, Jones AC, Langridge-Smith PRR, Mount AR. The electropolymerization and characterization of 5-cyanoindole. J Electroanal Chem 1995;388:179–85. https://doi.org/10.1016/0022-0728(95)03875-H.
[267] Syed Abthagir P, Dhanalakshmi K, Saraswathi R. Thermal studies on polyindole and polycarbazole. Synth Met 1998;93:1–7. https://doi.org/10.1016/S0379-6779(98)80125-2.
[268] Phasuksom K, Sirivat A. Synthesis of nano-sized polyindole via emulsion polymerization and doping. Synth Met 2016;219:142–53. https://doi.org/10.1016/j.synthmet.2016.05.033.
[269] Park IH, Kwon SH, Choi HJ. Emulsion-polymerized polyindole nanoparticles and their electrorheology. J Appl Polym Sci 2018;135:46384. https://doi.org/10.1002/app.46384.
[270] Sari B, Yavas N, Makulogullari M, Erol O, Unal HI. Synthesis, electrorheology and creep behavior of polyindole/polyethylene composites. React Funct Polym 2009;69:808–15. https://doi.org/10.1016/j.reactfunctpolym.2009.07.002.
[271] Erol O, Unal HI, Sari B. Synthesis, electrorheology, and creep behaviors of in situ intercalated polyindole/organo-montmorillonite conducting nanocomposite. Polym Compos 2009;31:471–81. https://doi.org/10.1002/pc.20827.
[272] Kang SH, Choi HJ. Dynamic response of polyindole coated zinc ferrite particle suspension under an electric field. Materials 2021;15:101. https://doi.org/10.3390/ma15010101.
[273] Hong CH, Jang HS, Oh SJ, Fu Lh, Choi HJ. Electric and magnetic field-responsive suspension rheology of core/shell-shaped iron oxide/polyindole microspheres. Korea-Aust Rheol J 2023;35:95–103. https://doi.org/10.1007/s13367-023-00056-z.
[274] Krztoń-Maziopa A, Wyciślik H, Płocharski J. Study of electrorheological properties of poly(p-phenylene) dispersions. J Rheol 2005;49:1177–92. https://doi.org/10.1122/1.2048740.
[275] Uygun A, Sen S, Aytemiz N, Tilki T, Yavuz AG, Maslakci Z, et al. Some novel conducting polythiophene derivatives: theoretical analysis, synthesis, characterization and electroreological properties. J Macromol Sci Part A Pure Appl Chem 2010;47:435–44. https://doi.org/10.1080/10601321003659655.
[276] Gumus OY, Erol O, Unal HI. Polythiophene/borax conducting composite II: Electrorheology and industrial applications. Colloids Surf A Physicochem Eng Asp 2011;32:756–65. https://doi.org/10.1002/pc.21095.
[277] Hong J-Y, Kwon E, Jang J. Fabrication of silica/polythiophene core/shell nanospheres and their electrorheological fluid application. Soft Matter 2009;5:951. https://doi.org/10.1039/b821291k.
[278] Chai Y, Li X, Geng J, Pan J, Huang Y, Jing D. Mechanistic study of drag reduction in turbulent pipeline flow over anionic polymer and surfactant mixtures. Colloid Polym Sci 2019;297:1025–35. https://doi.org/10.1007/s00396-019-04525-2.
[279] Li X, Yang H, Jing D, Wang L, Xie Y, Hui B. Critical role of ionic properties on the turbulence drag reduction performance of various polyacrylamide polymers in liquid. Ind Eng Chem Res 2023;62:11712–22. https://doi.org/10.1021/acs.iecr.3c01285.
[280] Chun Y, Ko YG, Do T, Jung Y, Kim SW, Su CU. Spent coffee grounds: Massively supplied carbohydrate polymer applicable to electrorheology. Colloids Surf A Physicochem Eng Asp 2019;562:392–401. https://doi.org/10.1016/j.colsurfa.2018.11.005.
[281] Jeong JY, Choi K, Choi HJ. Novel post-treatment of removed fine dust particle: Electrorheological application. J Clean Prod; 368; 2022. 10.1016/j.jclepro.2022.133128.
[282] Kwon SH, Park IH, Vu CM, Choi HJ. Fabrication and electro-responsive electrorheological characteristics of rice husk-based nanosilica suspension. J Taiwan Inst Chem Eng 2019;95:432–7. https://doi.org/10.1016/j.jtice.2018.08.018.
[283] Bach Q-V, Vu CM, Vu HT, Nguyen DD. Suspension of poly(o-toluidine)-coated silica-based core–shell-structured composite in silicone oil: fabrication and rheological properties at different external electric field strengths. Polym Bull 2020;77:3563–76. https://doi.org/10.1007/s00289-019-02933-6.
[284] Sharma RK, Kumar R, Singh AP. Extraction of cellulose micro-whiskers from rice husk: a greener approach. J Nanosci Nanotechnol 2018;18:3702–8. https://doi.org/10.1166/jnn.2018.14676.
[285] Rosa MF, Medeiros ES, Malmonge JA, Gregorski KS, Wood DF, Mattoso LHC, et al. Cellulose nanowhiskers from coconut husk fibers: Effect of preparation conditions on their thermal and morphological behavior. Carbohydr Polym 2010;81:83–92. https://doi.org/10.1016/j.carbpol.2010.01.059.
[286] El Achaby M, Kassab Z, Aboulkas A, Gaillard C, Barakat A. Reuse of red algae waste for the production of cellulose nanocrystals and its application in polymer nanocomposites. Int J Biol Macromol 2018;106:681–91. https://doi.org/10.1016/j.ijbiomac.2017.08.067.
[287] Subbiah T, Bhat GS, Tock RW, Parameswaran S, Ramkumar SS. Electrospinning of nanofibers. J Appl Polym Sci 2005;96:557–69. https://doi.org/10.1002/app.21481.
[288] Beck-Candanedo S, Roman M, Gray DG. Effect of reaction conditions on the properties and behavior of wood cellulose nanocrystal suspensions. Biomacromolecules 2005;6:1048–54. https://doi.org/10.1021/bm049300p.
[289] Samyn P, Laborie M-P, Mathew AP, Airoudj A, Haidara H, Roucoules V. Metastable patterning of plasma nanocomposite films by incorporating cellulose nanowhiskers. Langmuir 2012;28:1427–38. https://doi.org/10.1021/la202503h.
[290] Heath L, Thielemans W. Cellulose nanowhisker aerogels. Green Chem 2010;12:1448. https://doi.org/10.1039/c0gc00035c.
[291] Liu Z, Zhao Z, Jin X, Wang L-M, Liu YD. Preparation of cellulose/laponite composite particles and their enhanced electrorheological responses. Molecules 2021;26:1482. https://doi.org/10.3390/molecules26051482.
[292] Sim B, Bae DH, Choi HJ, Choi K, Islam MS, Kao N. Fabrication and stimuli response of rice husk-based microcrystalline cellulose particle suspension under electric fields. Cellul 2016;23:185–97. https://doi.org/10.1007/s10570-015-0836-3.
[293] Bae DH, Choi HJ, Choi K, Nam JD, Islam MS, Kao N. Fabrication of phosphate microcrystalline rice husk based cellulose particles and their electrorheological response. Carbohydr Polym 2017;165:247–54. https://doi.org/10.1016/j.carbpol.2017.02.037.
[294] Choi K, Nam JD, Kwon SH, Choi HJ, Islam MS, Kao N. Microfibrillated cellulose suspension and its electrorheology. Polymers 2019;11:2119. https://doi.org/10.3390/polym11122119.
[295] Plachy T, Kutalkova E, Skoda D, Holcapkova P. Transformation of cellulose via two-step carbonization to conducting carbonaceous particles and their outstanding electrorheological performance. Int J Mol Sci 2022;23:5477. https://doi.org/10.3390/ijms23105477.

[296] Österberg M, Peresin MS, Johansson L-S, Tammelin T. Clean and reactive nanostructured cellulose surface. Cellul 2013;20:983–90. https://doi.org/10.1007/s10570-013-9920-8.
[297] Gracia-Fernández C, Gómez-Barreiro S, Álvarez-García A, López-Beceiro J, Artiaga R. Electrorheological behaviour of a starch-oil system. Rheol Acta 2014;53:655–61. https://doi.org/10.1007/s00397-014-0786-y.
[298] See H, Li F. Increase in shear stress of an electrorheological fluid after repeated application of electric field and shearing. Nihon Reoroji Gakkaishi 2010;38:73–80. https://doi.org/10.1678/rheology.38.73.
[299] Zhong F, Li Y, Ibáñez AMO, Hun M, McKenzie KS, Shoemaker C. The effect of rice variety and starch isolation method on the pasting and rheological properties of rice starch pastes. Food Hydrocoll 2009;23:406–14. https://doi.org/10.1016/j.foodhyd.2008.02.003.
[300] Zhang Y, Zhang G. Starch content and physicochemical properties of green wheat starch. Int J Food Prop 2019;22:1463–74. https://doi.org/10.1080/10942912.2019.1651739.
[301] Park DP, Sung JH, Kim CA, Choi HJ, Jhon MS. Synthesis and electrorheology of potato starch phosphate. J Appl Polym Sci 2004;91:1770–3. https://doi.org/10.1002/app.13288.
[302] Zhang K, Kim SY, Jariyasakoolroj P, Chirachanchai S, Choi HJ. Stimuli-response of chlorosilane-functionalized starch suspension under applied electric fields. Polym Bull 2017;74:823–37. https://doi.org/10.1007/s00289-016-1747-7.
[303] Saboktakin MR, Tabatabaie RM, Maharramov A, Ramazanov MA. Synthesis and characterization of new electrorheological fluids by carboxymethyl starch nanocomposites. Carbohydr Polym 2010;79:1113–6. https://doi.org/10.1016/j.carbpol.2009.10.052.
[304] Yavuz M, Tilki T, Karabacak C, Erol O, Ibrahim Unal H, Uluturk M, et al. Electrorheological behavior of biodegradable modified corn starch/corn oil suspensions. Carbohydr Polym 2010;79:318–24. https://doi.org/10.1016/j.carbpol.2009.08.008.
[305] Kuznetsov NM, Zagoskin YD, Vdovichenko AY, Bakirov AV, Kamyshinsky RA, Istomina AP, et al. Enhanced electrorheological activity of porous chitosan particles. Carbohydr Polym 2021;256:117530. https://doi.org/10.1016/j.carbpol.2020.117530.
[306] Sung JH, Choi HJ, Jhon MS. Electrorheological response of biocompatible chitosan particles in corn oil. Mater Chem Phys 2003;77:778–83. https://doi.org/10.1016/S0254-0584(02)00167-0.
[307] Ko YG, Shin SS, Choi US, Park YS, Woo JW. Gelation of chitin and chitosan dispersed suspensions under electric field: effect of degree of deacetylation. ACS Appl Mater Interfaces 2011;3:1289–98. https://doi.org/10.1021/am200091r.
[308] Cabuk M, Yavuz M, Unal HI, Erol O. Synthesis, characterization and electrorheological properties of biodegradable chitosan/bentonite composites. Clay Miner 2013;48:129–41. https://doi.org/10.1180/claymin.2013.048.4.09.
[309] Cabuk M, Alan Y, Unal HI. Enhanced electrokinetic properties and antimicrobial activities of biodegradable chitosan/organo-bentonite composites. Carbohydr Polym 2017;161:71–81. https://doi.org/10.1016/j.carbpol.2016.12.067.
[310] Kuznetsov NM, Kovaleva VV, Zagoskin YD, Vdovichenko AY, Malakhov SN, Yastremsky EV, et al. Specific features of the porous polymeric particle composites application as fillers for electrorheological fluids. Nanobiotechnol Rep 2021;16:840–6. https://doi.org/10.1134/S2635167621060148.
[311] Yaghi OM, O'Keeffe M, Ockwig NW, Chae HK, Eddaoudi M, Kim J. Reticular synthesis and the design of new materials. Nature 2003;423:705–14. https://doi.org/10.1038/nature01650.
[312] Li G, Xia L, Dong J, Chen Y, Li Y. Metal-organic frameworks. Solid-phase extraction: 285-309; 2020. 10.1016/B978-0-12-816906-3.00010-8.
[313] Wen Q, Ma L, Wang C, Wang B, Han R, Hao C, et al. Preparation of core–shell structured metal–organic framework@PANI nanocomposite and its electrorheological properties. RSC Adv 2019;9:14520–30. https://doi.org/10.1039/C9RA02268F.
[314] Wang L, Li C, Wang R, Lin Y, Xiong K, Wang B, et al. The preparation and smart electrorheological behavior of MOF-Ti@PANI core-shell nanoparticles. Journal of Molecular Liquids; 376; 2023. 10.1016/j.molliq.2023.121373.
[315] Sun W, Ma J, Xi Z, Lin Y, Wang B, Hao C. Titanium oxide-coated titanium-loaded metal organic framework (MOF-Ti) nanoparticles show improved electrorheological performance. Soft Matter 2020;16:9292–305. https://doi.org/10.1039/D0SM01147A.
[316] Wang L, Chen L, Yan H, Wang C, Lin Y, Wang B, et al. Synthesis and electrorheological behaviour of silica-coated porous metal-organic frameworks. Ceramics International; 50; 2024. 10.1016/j.ceramint.2024.01.033.
[317] Li C, Li Z, Li Q, Zhang Z, Dong S, Yin L. MOFs derived hierarchically porous TiO_2 as effective chemical and physical immobilizer for sulfur species as cathodes for high-performance lithium-sulfur batteries. Electrochim Acta 2016;215:689–98. https://doi.org/10.1016/j.electacta.2016.08.044.
[318] He K, Wen Q, Wang C, Wang B, Yu S, Hao C, et al. Porous TiO_2 nanoparticles derived from titanium metal–organic framework and its improved electrorheological performance. Ind Eng Chem Res 2018;57:6888–96. https://doi.org/10.1021/acs.iecr.8b00846.
[319] Liu YD, Kim J, Ahn W-S, Choi HJ. Novel electrorheological properties of a metal–organic framework $Cu_3(BTC)_2$. Chem Commun 2012;48:5635. https://doi.org/10.1039/c2cc30367a.
[320] Ma R, Nie W, Wang Y, Hu X, Zhao X, Yin J. Mixed ionic–electronic covalent organic frameworks as a platform for high-performance electro-responsive smart materials. Chem Mater 2024;36:6961–72. https://doi.org/10.1021/acs.chemmater.4c01052.
[321] Wen W, Huang X, Yang S, Lu K, Sheng P. The giant electrorheological effect in suspensions of nanoparticles. Nat Mater 2003;2:727–30. https://doi.org/10.1038/nmat993.
[322] Ma H, Wen W, Tam WY, Sheng P. Frequency dependent electrorheological properties: origin and bounds. PhysRevLett 1996;77:2499–502. https://doi.org/10.1103/PhysRevLett.77.2499.
[323] Kun-Quan L, Rong S, Xue-Zhao W, Gang S, Wei-Jia W, Ji-Xing L. Polar molecule dominated electrorheological effect. Chin Phys 2006;15:2476–80. https://doi.org/10.1088/1009-1963/15/11/002.
[324] Lu K, Shen R. The characteristics of polar molecule ER fluids and a new type of polar molecule ER fluid. Smart Mater Struct 2017;26:054005. https://doi.org/10.1088/1361-665X/aa5d38.
[325] Sun Y, Wu X, Lu B, Wang M, Ding J, Pu H, et al. Electrostatic layer jamming variable stiffness enhanced by giant electrorheological fluid. IEEE/ASME Trans Mechatron 2023;29:324–34. https://doi.org/10.1109/TMECH.2023.3275961.
[326] Sun Y, Chen C, Liao N, Jia W, Wang M, Ding J, et al. Parameter characterization of variable bending stiffness module with electrostatic layer jamming based on giant electrorheological fluid. Smart Mater Struct 2024;33:065032. https://doi.org/10.1088/1361-665X/ad49ee.
[327] Cao X, Zhao J, Mao L, Sun Z, Cao H, Luo J, et al. Investigation of a 2-DOF GER fluid damper in cut mode. Int J Mech Sci 2024;274:109258. https://doi.org/10.1016/j.ijmecsci.2024.109258.
[328] Pu H, Liu J, Wang M, Ding J, Luo J, Sun Y. Vibration control of giant electrorheological damper combining nonlinear fractional-order controller and extended state observer. Smart Mater Struct 2024;33:045016. https://doi.org/10.1088/1361-665X/ad2e38.
[329] Qiu H, Luo X, Wang J, Zhong X, Qi S. Synthesis and characterization of ternary polyaniline/barium ferrite/reduced graphene oxide composite as microwave-absorbing material. J Electron Mater 2019;48:4400–8. https://doi.org/10.1007/s11664-019-07220-8.
[330] Lu K, Shen R, Wang X, Wang D, Sun G. Polar-molecule-dominated electrorheological (PM-ER) fluids: the properties and evaluations. Int J Mod Phys B 2011;25:957–62. https://doi.org/10.1142/S021797921105850X.
[331] Qiu Z, Huang J, Shen R, Wang Y, Wu X, Lu K, et al. The role of adsorbed water on TiO_2 particles in the electrorheological effect. AIP Adv 2018;8:105319. https://doi.org/10.1063/1.5053165.
[332] Yang SH, Gao X, Li CX, Wang Q, Shen R, Sun G, et al. Composition analysis of the giant electrorheological fluids. Mod Phys Lett B 2012;26:1150023. https://doi.org/10.1142/S0217984911500230.
[333] Zhao H, Shen R, Lu K. The electric field and frequency responses of giant electrorheological fluids. Chin Phys B 2018;27:078301. https://doi.org/10.1088/1674-1056/27/7/078301.
[334] Wang X, Shen R, Sun G, Wen W, Lu K. The modified electrodes for the application of polar molecule dominated electrorheological (PM-ER) fluids. Int J Mod Phys B 2007;21:4940–4. https://doi.org/10.1142/S0217979207045864.
[335] Shen R, Wang XZ, Lu Y, Wen WJ, Sun G, Lu KQ. The methods for measuring shear stress of polar molecule dominated electrorheological fluids. J Appl Phys 2007;102:024106. https://doi.org/10.1063/1.2756515.

[336] Xu L, Tian WJ, Wu XF, Cao JG, Zhou LW, Huang JP, et al. Polar-molecules-driven enhanced colloidal electrostatic interactions and their applications in achieving high active electrorheological materials. J Mater Res 2008;23:409–17. https://doi.org/10.1557/JMR.2008.0057.
[337] Kimura H. Influence of alternating electric field on electrorheological effect of aqueous dispersions of stevensite. Appl Clay Sci 2024;254:107393. https://doi.org/10.1016/j.clay.2024.107393.
[338] Hao T, Yu H, Xu Y. The conductivity confined temperature dependence of water-free electrorheological fluids. J Colloid Interface Sci 1996;184:542–9. https://doi.org/10.1006/jcis.1996.0650.
[339] Ikazaki F, Kawai A, Uchida K, Kawakami T, Edamura K, Sakurai K, et al. Mechanisms of electrorheology: the effect of the dielectric property. J Phys D Appl Phys 1998;31:336. https://doi.org/10.1088/0022-3727/31/3/014.
[340] Yin J, Xia X, Xiang L, Zhao X. Conductivity and polarization of carbonaceous nanotubes derived from polyaniline nanotubes and their electrorheology when dispersed in silicone oil. Carbon 2010;48:2958–67. https://doi.org/10.1016/j.carbon.2010.04.035.
[341] Wang Z, Gong X, Yang F, Jiang W, Xuan S. Dielectric relaxation effect on flow behavior of electrorheological fluids. J Intell Mater Syst Struct 2015;26:1141–9. https://doi.org/10.1177/1045389X14536007.
[342] Choi H, Hong C, Jhon M. Cole-Cole analysis on dielectric spectra of electrorheological suspensions. Int J Mod Phys B 2007;21:4974–80. https://doi.org/10.1142/S0217979207045918.
[343] Havriliak S, Negami S. A complex plane representation of dielectric and mechanical relaxation processes in some polymers. Polymer 1967;8:161–210. https://doi.org/10.1016/0032-3861(67)90021-3.
[344] Dong YZ, Choi HJ. Electrorheological characteristics of poly (diphenylamine)/magnetite composite-based suspension. Materials 2019;12:2911. https://doi.org/10.3390/ma12182911.
[345] Chen Y, Sun W, Zheng H, Li C, Zhang B, Wang B, et al. The electrorheological response behavior of small coral-like $H_2Ti_2O_5$@ SiO_2 core-shell nanoparticles. J Taiwan Inst Chem Eng 2021;129:327–41. https://doi.org/10.1016/j.jtice.2021.09.028.
[346] Cole KS, Cole RH. Dispersion and absorption in dielectrics II. Direct current characteristics. J Chem Phys 1942;10:98–105. https://doi.org/10.1063/1.1723677.
[347] Cole KS, Cole RH. Dispersion and absorption in dielectrics I. Alternating current characteristics. J Chem Phys 1941;9:341–51. https://doi.org/10.1063/1.1750906.
[348] Mrlík M, Ilčíková M, Plachý T, Moučka R, Pavlínek V, Mosnáček J. Tunable electrorheological performance of silicone oil suspensions based on controllably reduced graphene oxide by surface initiated atom transfer radical polymerization of poly (glycidyl methacrylate). J Ind Eng Chem 2018;57:104–12. https://doi.org/10.1016/j.jiec.2017.08.013.
[349] Li C, He K, Sun W, Wang B, Yu S, Hao C, et al. Synthesis of hollow TiO2 nanobox with enhanced electrorheological activity. Ceram Int 2020;46:14573–82. https://doi.org/10.1016/j.ceramint.2020.02.257.
[350] Conrad H, Li Y, Chen Y. The temperature dependence of the electrorheology and related electrical properties of corn starch/corn oil suspensions. J Rheol 1995;39:1041–57. https://doi.org/10.1122/1.550616.
[351] Yin J, Zhao X. Temperature effect of rare earth-doped TiO2 electrorheological fluids. J Phys D Appl Phys 2001;34:2063. https://doi.org/10.1088/0022-3727/34/13/317.
[352] Yin J, Xia X, Xiang L, Zhao X. Temperature effect of electrorheological fluids based on polyaniline derived carbonaceous nanotubes. Smart Mater Struct 2010;20:015002. https://doi.org/10.1088/0964-1726/20/1/015002.
[353] Klingenberg DJ, Ulicny JC, Golden MA. Mason numbers for magnetorheology. J Rheol 2007;51:883–93. https://doi.org/10.1122/1.2764089.
[354] Saabome SM, Park Y-S, Ko YG. Designing particle size of aminated polyacrylonitrile spheres to enhance electrorheological performances of their suspensions. Powder Technol 2021;394:986–95. https://doi.org/10.1016/j.powtec.2021.08.096.
[355] Yuan J, Wang Y, Lei Q, Zhao X, Yin J. Influence of particle size on electrorheological effect of poly (ionic liquid) microsphere suspensions. Colloids Surf A Physicochem Eng Asp 2023;672:131745. https://doi.org/10.1016/j.colsurfa.2023.131745.
[356] Lengalova A, Pavlinek V, Saha P, Quadrat O, Stejskal J. The effect of dispersed particle size and shape on the electrorheological behaviour of suspensions. Colloids Surf A Physicochem Eng Asp 2003;227:1–8. https://doi.org/10.1016/S0927-7757(03)00348-0.
[357] Ko YG, Choi US, Chun YJ. Influence of particle size on shear behavior of amine-group-immobilized polyacrylonitrile dispersed suspension under electric field. J Colloid Interface Sci 2009;335:183–8. https://doi.org/10.1016/j.jcis.2009.03.032.
[358] Yuan J, Wang Y, Lei Q, Hou Q, Zhao X, Yin J. Electrorheological effect of suspensions containing mixed size of poly (ionic liquid) microspheres. Colloids Surf A Physicochem Eng Asp 2023;678:132528. https://doi.org/10.1016/j.colsurfa.2023.132528.
[359] See H, Kawai A, Ikazaki F. The effect of mixing particles of different size on the electrorheological response under steady shear flow. Rheol Acta 2002;41:55–60. https://doi.org/10.1007/s003970200005.
[360] Jun J-B, Uhm S-Y, Cho S-H, Suh K-D. Bidisperse electrorheological fluids using hydrolyzed styrene-acrylonitrile copolymer particles: synergistic effect of mixed particle size. Langmuir 2004;20:2429–34. https://doi.org/10.1021/la030248c.
[361] Morillas JR, Bombard AJ, de Vicente J. Enhancing magnetorheological effect using bimodal suspensions in the single-multidomain limit. Smart Mater Struct 2018;27:07LT1. https://doi.org/10.1088/1361-665X/aac8ae.
[362] Morillas JR, Bombard AJ, de Vicente J. Magnetorheology of bimodal fluids in the single–multidomain limit. Ind Eng Chem Res 2018;57:13427–36. https://doi.org/10.1021/acs.iecr.8b03438.
[363] Zhang K, Gao CY, Choi HJ, Yin J, Zhao X. Rheological analysis of titanium dioxide nano-whisker based electrorheological fluids. J Ind Eng Chem 2020;83:285–8. https://doi.org/10.1016/j.jiec.2019.11.040.
[364] Liu Z, Chen P, Liu YD, Wang L-M, Choi HJ. Electrorheological Responses of Acid-Hydrolyzed Cellulose Suspensions. Current Smart Materials 2018;3:58–67. https://doi.org/10.2174/2405465803666180627094551.
[365] Howard S, Akiko K, Fumikazu I. The effect of mixing particles of different size on the electrorheological response under steady shear flow. Rheol Acta 2002;41:55–60. https://doi.org/10.1007/s003970200005.
[366] Wu J, Song Z, Liu F, Guo J, Cheng Y, Ma S, et al. Giant electrorheological fluids with ultrahigh electrorheological efficiency based on a micro/nano hybrid calcium titanyl oxalate composite. NPG Asia Mater 2016;8:e322-e. https://doi.org/10.1038/am.2016.158.
[367] Liang Y, Yuan X, Wang L, Zhou X, Ren X, Huang Y, et al. Highly stable and efficient electrorheological suspensions with hydrophobic interaction. J Colloid Interface Sci 2020;564:381–91. https://doi.org/10.1016/j.jcis.2019.12.129.
[368] Yin J, Zhao X, Xiang L, Xia X, Zhang Z. Enhanced electrorheology of suspensions containing sea-urchin-like hierarchical Cr-doped titania particles. Soft Matter 2009;5:4687. https://doi.org/10.1039/b910274d.
[369] Lee BM, Kim JE, Fang FF, Choi HJ, Feller J-F. Rectangular-shaped polyaniline tubes covered with nanorods and their electrorheology. Macromol Chem Phys 2011;212:2300–7. https://doi.org/10.1002/macp.201100306.
[370] Li C, Wang Z, Wang L, Bai Q, Wang B, Hao C. Synthesis and electrorheological properties of $TiOF_2$@SiO_2 cubic-like core/shell nanocomposite. Journal of Molecular Liquids; 366; 2022. 10.1016/j.molliq.2022.120335.
[371] Sun W, Zheng H, Chen Y, Li C, Wang B, Hao C, et al. Preparation and electrorheological properties of peanut-like hollow core–shell structure TiO_2 @SiO_2 nanoparticles. Adv Eng Mater 2021;23:2001416. https://doi.org/10.1002/adem.202001416.
[372] Cheng Q, Pavlinek V, He Y, Yan Y, Li C, Saha P. Template-free synthesis of hollow poly(o-anisidine) microspheres and their electrorheological characteristics. Smart Mater Struct; 20; 2011. 10.1088/0964-1726/20/6/065014.
[373] Yin JB, Zhao XP. Giant electrorheological activity of high surface area mesoporous cerium-doped TiO_2 templated by block copolymer. Chem Phys Lett 2004;398:393–9. https://doi.org/10.1016/j.cplett.2004.09.098.
[374] Cabuk M. Electrorheological response of mesoporous expanded perlite particles. Microporous Mesoporous Mater 2017;247:60–5. https://doi.org/10.1016/j.micromeso.2017.03.044.

[375] Guo H-x, Zhao X-p, Guo H-l, Zhao Q. Preparation of porous SiO_2/Ni/TiO_2 multicoated microspheres responsive to electric and magnetic fields. Langmuir 2003; 19:9799–803. https://doi.org/10.1021/la034948t.
[376] Cheng Q, Pavlinek V, He Y, Lengalova A, Li C, Saha P. Structural and electrorheological properties of mesoporous silica modified with triethanolamine. Colloids Surf A Physicochem Eng Asp 2008;318:169–74. https://doi.org/10.1016/j.colsurfa.2007.12.044.
[377] Cho MS, Choi HJ, Kim KY, Ahn WS. Synthesis and characterization of polyaniline/mesoporous SBA-15 nanocomposite. Macromol Rapid Commun 2002;23: 713–6. https://doi.org/10.1002/1521-3927(20020801)23:12<713::AID-MARC713>3.0.CO;2-Y.
[378] Cho MS, Choi HJ, Ahn W-S. Enhanced electrorheology of conducting polyaniline confined in MCM-41 channels. Langmuir 2004;20:202–7. https://doi.org/10.1021/la035051z.
[379] Kwon SH, Piao SH, Choi HJ. Electric field-responsive mesoporous suspensions: A review. Nanomaterials 2015;5:2249–67. https://doi.org/10.3390/nano5042249.

Mgr. Lenka Munteanu (ORCID 0009-0001-6449-528X) is a Ph. D student at Tomas Bata University in Zlín (Czech Republic), planning to finish the doctoral studies in 2026. Prior to starting the doctoral program 'Nanotechnology and Advanced Materials' in 2022, she completed her master degree at University of Palacky in Olomouc (Czech Republic). Electrorheological fluids are the primal topic of her thesis and, in particular, the niche of her research revolves around smart suspensions (electrorheological or magnetorheological) based on anticorrosive protective paint pigment particles. So far, she has published two papers on this particular topic, following with two other papers exploring smart magnetorheological systems.

Dr. Andrei Munteanu (ORCID 0000-0001-7150-4028) obtained a B.Sc. and M.Sc. in material science (2018 and 2020) from the University of Crete (Greece) through the Institute of Electronic Structure in the Foundation of Research and Technology - Hellas. Graduated from the doctoral program 'Nanotechnology and Advanced Materials' at Tomas Bata University in Zlín (Czech Republic) in 2024 and continues at the university as a postdoc researcher. At this time, he has published 7 papers, a book chapter all of which related to electro and magnetorheology. In particular, his research is around functionalized particles used in composite materials with various applications related to their electric and magnetic properties.

Prof. Michal Sedlacik (ORCID 0000-0003-3918-5084) is a full professor at Tomas Bata University in Zlín (TBU), Czech Republic. He is currently the director of the University Institute. He studied materials engineering and obtained his Ph.D. degree in 2012 from TBU. From 2010, he works at Centre of Polymer Systems at TBU as a senior researcher. At the same time, since 2012, he works at Faculty of Technology, Department of Production Engineering at TBU. He obtained his prof. degree I surface engineering in 2023 from University of Pardubice, Czech Republic. He has published over 80 papers in leading international journals (approx. 1,900 citation and h-index=29 according to the Web of Science) and his scientific interests include smart magnetorheological and electrorheological systems, their application, electromagnetic shielding materials, and tribology.